Mónica Gaspar Simões, MSc

Quantification of the degree of Nano-Scale Contact and its effects on Surface Adhesion using FRET Methods

DOCTORAL THESIS

to achieve the university degree of

Doktor der technischen Wissenschaften

submitted to

Graz University of Technology

Supervisor

Univ.-Prof. Dipl.-Ing. Dr.techn. Ulrich Hirn

Institute of Bioproducts and Paper Technology

Graz University of Technology

Co-supervisor

Univ.-Prof. Mag. Dr.rer.nat. Robert Schennach

Institute of Solid-State Physics

Graz University of Technology

Graz, September 2021

AFFIDAVIT

I declare that I have authored this thesis independently, that I have not used other than the declared sources/resources, and that I have explicitly indicated all material which has been quoted either literally or by content from the sources used. The text document uploaded to TUGRAZonline is identical to the present doctoral thesis.

Date, Signature

ABSTRACT

This doctoral thesis investigates the role of nano-scale contact (NSC) on surface adhesion. For this, Förster Resonance Energy Transfer (FRET) is introduced as a unique experimental technique to measure the NSC between soft surfaces, which allows establishing a linear correlation between FRET intensity and separation energy (adhesion).

In Publication I a working FRET system was developed to measure the degree of NSC between bonded polymeric thin films using FRET spectroscopy and FRET microscopy in a distance detection range of 2.6-10.2 nm. From the fluorescence images FRET intensity maps were obtained which also allowed the local analysis of NSC over thin films bonded areas. And accordantly, the association between NSC, measured by FRET and separation energy/adhesion using bonded thin films with different degrees of NSC (films pressed under various loads). was demonstrated.

To improve the method's efficiency and sensitivity, Manuscript II introduces an entirely new FRET pair. The resultant FRET system, specifically designed and optimized to measure NSC, presents high quantum yields and a distance detection range of 0.6-2.2 nm, closer to the interaction range of the intermolecular forces (hydrogen bonds and Van der Waals forces) responsible for adhesion.

And in Manuscript III, the functionalization of the adhering surfaces with FRET-dye nanolayers formed by physical vapor deposition (PVD) is presented. Here, the dye molecules on which FRET depends are located only in the interface between the films, where NSC and intermolecular forces responsible for adhesion take place, reducing the noise coming from other dye molecules distributed throughout the entire polymeric matrix of the films. Therefore, with this approach, the method can be applied to estimate the degree of NSC on arbitrary transparent surfaces.

This work opens an entirely novel approach for the quantification (FRET spectroscopy) and imaging (FRET microscopy) of NSC between transparent adhering surfaces, representing a substantial advance in the study of solid materials contact mechanics and all fields where adhesion or NSC plays a role.

KURZFASSUNG

Diese Doktorarbeit untersucht die Rolle des Materialkontakts im Nano-Maßstab (*nano-scale contact* - NSC) bei Adhäsion. Dazu wird der Förster Resonance Energy Transfer (FRET) als einzigartige experimentelle Technik zur Messung des NSC zwischen weichen Oberflächen eingeführt, die es ermöglicht, eine lineare Korrelation zwischen FRET-Intensität und Trennenergie (Adhäsion) herzustellen.

In Publikation I wurde ein funktionierendes FRET-System entwickelt, um den Grad des NSC zwischen gebundenen Polymer-Dünnfilmen mittels FRET-Spektroskopie und FRET-Mikroskopie in einem Detektionsbereich von 2,6-10,2 nm zu messen. Aus den dabei erhaltenen Fluoreszenzbildern wurden FRET-Intensitätsdiagramme abgeleitet, die auch eine lokale Analyse des NSC in den Bindungsbereichen zwischen Dünnschichten ermöglichten. Dementsprechend konnte der Zusammenhang zwischen NSC (gemessen durch FRET) und Trennenergie/Adhäsion bei gebundenen Dünnschichten unterschiedlicher NSC-Grade (unter verschiedenen Lasten gepresst) gezeigt werden.

Um die Effizienz und Sensitivität der Methode zu verbessern, führt Manuskript II ein völlig neues FRET-Paar ein. Das resultierende FRET-System, das speziell für die Messung von NSC entwickelt und optimiert wurde, bietet hohe *Quantum Yields* und einen Detektionsbereich von 0,6-2,2 nm, näher am Wechselwirkungsbereich der intermolekularen Kräfte (Wasserstoffbrücken und Van-der-Waals-Kräfte), die für die Adhäsion verantwortlich sind.

In Manuskript III wird die Funktionalisierung der haftenden Oberflächen mit FRET-Farbstoff-Nanoschichten vorgestellt, die mittels physikalischer Gasphasenabscheidung (PVD) gebildet wurden. Hier befinden sich die Farbstoffmoleküle, von denen FRET abhängt, nur an der Grenzfläche zwischen den Filmen, also nur dort, wo NSC und intermolekulare Kräfte (für die Adhäsion verantwortlich) auftreten. Dadurch konnte das Messrauschen signifikant reduziert werden, welches in den vorangegangenen Experimenten aufgrund der über die gesamte Polymermatrix verteilten Farbstoffmoleküle entstand. Daher kann das Verfahren mit diesem Ansatz nun angewendet werden, um den Grad des NSC auf beliebigen transparenten Oberflächen abzuschätzen.

Diese Arbeit eröffnet einen völlig neuen Ansatz für die Quantifizierung (FRET-Spektroskopie) und Bildgebung (FRET-Mikroskopie) von NSC zwischen transparenten, adhäsiven Oberflächen, was einen wesentlichen Fortschritt in der Untersuchung der Kontaktmechanik von Festkörpermaterialien und allen Bereichen darstellt, in denen Adhäsion oder NSC eine Rolle spielen.

ACKNOWLEDGEMENTS

I would like to thank Professors Ulrich Hirn and Robert Schennach for this opportunity and for being the best bosses on the planet.
I also would like to thank all my dear colleagues for having made my work so enjoyable.
Finally, I want to thank my family and friends for all the unconditional love and support.

Without all of you, I wouldn't have gotten here.
And for that, thank you very much.

Research Project

This doctoral thesis was done in context of the FibreNet project, funded by the European Union's Horizon 2020 research and innovation program under the Marie Skłodowska-Curie grant agreement No 764713.

CONTENTS

List of Figures

List of Tables

List of Abbreviations

1. Introduction

1.1. Motivation

Adhesion can be found everywhere. It is present in nature, between organic and inorganic materials, any type of surface, fiber, cell or protein [1–3]. Adhesion is also highly relevant in man-made components, from tribology to sealants and adhesives, including basically all sorts of engineering applications [4–6]. Therefore, the role of interfacial adhesion between solid materials is essential in several fields of biology, science, and technology, such as cellular adhesion and contact mechanics [7,8]. Adhesion results from a network of intermolecular forces formed by hydrogen bonds and Van der Waals forces; that can only be developed if the adhering surfaces are in nano-scale contact (NSC), i.e. 0.1-0.4nm [9–13].

However, it is rare to have two surfaces in complete NSC. Instead, what we have is a mixture of bonded areas and open gaps (Figure 1); this can be problematic to measure NSC, since surfaces that appear to be in full contact at the micro-scale, end up revealing gaps when inspected at the nanometric length scale (Figure 1) [14–16]. Thus, to properly quantify the NSC and its influence on adhesion, it is essential to utilize a measurement method that works on the relevant length scale of the intermolecular forces (i.e. distance range of 0.1-0.4nm).

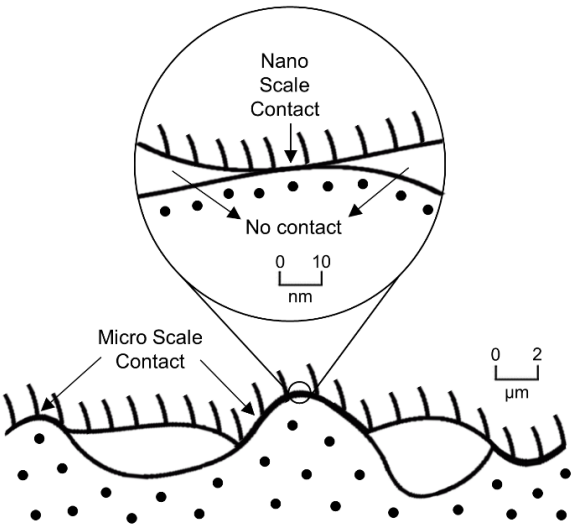

Figure 1 – Two surfaces in physical contact observed at micrometer and nanometer scale. Contact area decreases with increasing magnification.

Nevertheless, optical microscopy [17–23], force modulation with depth-sensing nanoindentation [23–25] and contact mechanics theories and simulations [5,12,26–28] have been used over the

last decades to estimate NSC and adhesion between solid materials. However, none of those studies offered an experimental technique to properly evaluate NSC and thus, cannot provide a complete investigation of the mechanisms responsible for adhesion at the nanometric scale.

This work is an attempt to improve the fundamental understanding of the role of NSC on adhesion using Förster Resonance Energy Transfer (FRET) methods. FRET is a technique capable to quantify the degree of close contact between two surfaces in a distance range of 0-20 nm. For that FRET needs two fluorescence molecules named Donor and Acceptor [29].

If the molecules are close enough to each other, i.e. within a distance range of 0-20 nm, and the Donor molecule is excited, a non-radiative energy is transferred to the Acceptor molecule and, a FRET signal can be detected; which is observed as an increase of the fluorescence Acceptor dye [30]. This signal can be used to determine the FRET efficiency (FRETeff) and the average distance between the Donor and Acceptor molecules due to the Förster Theory [31]. Hence, FRET can be employed to measure NSC between transparent surfaces. For this, each surface needs to be labelled with a dye molecule, one with Donor and one with Acceptor, which depending on the degree of NSC, will interact and provide FRET. The resulting FRET signal can be related to the adhesion forces between the surfaces. This approach opens an entirely novel method to quantify NSC and to study its influence on surface adhesion.

1.2. Aim of the work

This work was focused on providing a proof of concept for the measurement of NSC, and its interrelation with adhesion between soft surfaces using FRET methods. It can be divided into four main goals:

1) Develop a working FRET system to measure the degree of NSC between bonded polymeric thin films using FRET spectroscopy and FRET microscopy;
2) Validate the correlation between NSC, measured by FRET and adhesion (separation energy) using bonded thin films with different degrees of NSC (prepared by pressing the films under different loads);
3) Develop a new FRET pair/system with a low distance range detection (close to the interaction range of the intermolecular adhesion forces: hydrogen bonds and Van der Waals forces), specifically designed and optimized for the measurement of NSC and its influence on adhesion.

4) Measure NSC on arbitrary surfaces by functionalizing them with FRET-dye nanolayers formed via physical vapor deposition (PVD), to improve the overall sensitivity of the method; once the NSC and intermolecular forces responsible for adhesion only take place on the interfaces of the adhering surfaces.

1.3. Outline

This doctoral thesis is based on Publication I, and Manuscripts II and III. The following sections contain an introduction to adhesion, NSC, and FRET principles (Förster theory and FRET dyes). In addition, more details about the experimental methods used in the publication/manuscripts are given. These details are covering the selected fluorescence molecules, how to calculate FRET, and the computational evaluation of FRET signals using fluorescence microscopy.

Publication I presents FRET spectroscopy and FRET microscopy as experimental techniques to measure the degree of NSC between soft surfaces and its connection with adhesion force. For this, a well-known FRET pair was used with a distance detection range of 2.6-10.2nm. The primary focus was to develop a working FRET system using polymeric bonded thin films with different degrees of NSC; that later was correlated with its separation energy/adhesion. Publication I covers the aims of the work 1) and 2) as described in section 1.2.

Manuscript II introduces a new FRET pair/system for the measurement of NSC with FRET spectroscopy. The new FRET pair of compatible fluorescence molecules specifically developed for the proper quantification of NSC presents a high quantum yield and low FRET distance range of 0.6-2.2nm; which improved the sensitivity of the method and its accuracy to detect NSC, closer to the scale where the intermolecular forces responsible for adhesion forces occur. Manuscript II covers the aim of the work 3) as described in section 1.2.

Manuscript III provides a new approach to measure NSC with FRET methods using dye nanolayer films prepared by PVD. Once the NSC and FRET only take place on the interface, it is only necessary to have FRET dyes on the surface, which improves even further the method sensitivity. Moreover, this novel feature of the method allows the measurement of NSC between arbitrary surfaces. Manuscript III covers the aim of the work 4) as described in section 1.2.

2. Förster Resonance Energy Transfer

2.1. FRET principles and their relation to NSC

FRET is based on the Förster theory, presented in Theodor Förster's original papers, published between 1946 to 1965 [32]. By taking advantage of the fluorescence properties of certain molecules, FRET explores the non-radiative energy transferred between them to study their exact nanometric distance [31,33,34].

The fluorescence molecules, named Donor and Acceptor, interact as freely oscillating dipoles. As demonstrated in Figure 2A (blue lines), the Donor molecule absorbs an incoming photon and is excited to a high energy level. After reaching its higher excitation state, it relaxes and releases part of its energy to reach a lower excitation state (Figure 2A, blue lines). Afterwards, if no Acceptor molecule is close to it, the Donor molecule continues relaxing to reach its initial state (Figure 2A, blue lines), emitting standard fluorescence radiation in the process (Figure 2B, blue spectra) [35,36]. Alternatively, if there is an available Acceptor-compatible molecule close by (Figure 2A, green line), the energy released in the Donor relaxation processes can be non-radiatively incepted by the Acceptor, in a dipole-dipole interaction (Figure 2A, violet lines); followed by the Acceptor's emission of a photon, corresponding to the Acceptor fluorescence emission spectra (Figure 2b, green spectra), which only depends on the Donor and Acceptor properties, medium conditions and physical distance [37]. This non-radiative energy transfer from Donor to Acceptor is called FRET (Förster Resonance Energy Transfer) [31].

Accordantly, for Donor and Acceptor molecules to be compatible they need to have lined up energy bands, as shown in Figure 2A. In practice, they must present different, yet overlapping, Donor emission and Acceptor excitation spectra, see pink area in Figure 2B [31].

And therefore, a FRET signal (Figure 2C) is identified when in the presence of each other and in relation to their pure emission spectra (excited at the same wavelength), Donor intensity drops (from I_D to I_{DA}), and Acceptor intensity rises (from I_A to I_{AD}, observe arrows) due to the Donor → Acceptor energy transfer.

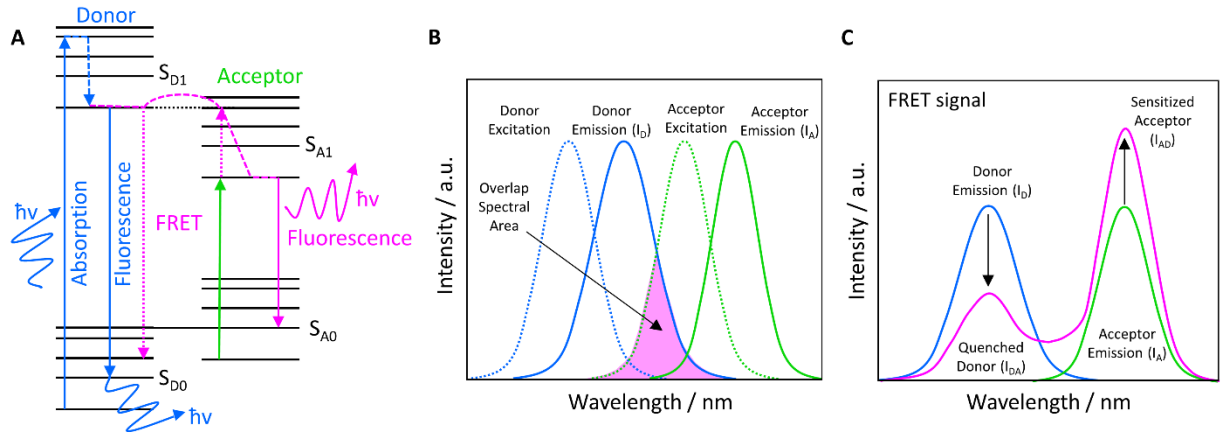

Figure 2 – (A) Jablonski diagram of fluorescence and non-radiative FRET between compatible Donor and Acceptor molecules; (B) Schematic representation of Donor and Acceptor excitation and emission spectra with spectral overlap (marked in pink), on which FRET depends; and (C) FRET signal: emission spectra of pure Donor (blue line), pure Acceptor (green line) and Donor-Acceptor interaction (pink line); when in the presence of each other and in relation to their pure spectra (see arrows), Donor intensity drops (from I_D to I_{DA}), and Acceptor intensity rises (from I_A to I_{AD}).

2.2. Förster Theory

The Förster theory allows us to explain the relationship between energy transfer, spectral overlap, and physical distance between compatible fluorescence molecules [31]. Therefore, if Donor and Acceptor molecules are close enough to each other, FRET (Donor → Acceptor energy transfer, Figure 3A) will occur and the FRET eff (%) can be calculated:

$$FRET\ eff = \frac{1}{1+(r/R_0)^6}\ [\%] \qquad (1)$$

where r [nm] is the distance between Donor and Acceptor and R_0 [nm] the Förster Radius. R_0 only relies on the properties and medium conditions of the selected Donor-Acceptor molecules and determines the FRET detection distance range of the system under study.

A FRET signal (Figure 3A) can only be properly detected within $0.5R_0$-$2R_0$ nm. Above $2R_0$, Donor and Acceptor molecules are simply too far apart from each other for FRET to be detected [31]. And below $0.5R_0$ it is possible to have orbital overlapping, which can result in electron exchange between the Donor and Acceptor molecules, and energy transfer in both directions: Donor → Acceptor and Acceptor → Donor [29,35,37,38]. This phenomenon is named as Dexter transfer, and can be recognized when in the presence of each other and in relation to their pure emission spectra (excited at the same wavelength), both Donor and Acceptor intensities increase (Figure 3B, observe arrows) due to the Donor ↔ Acceptor energy transfer.

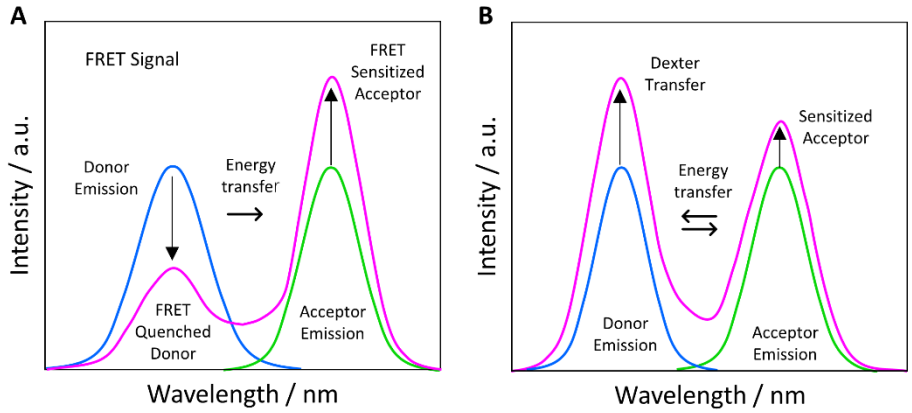

Figure 3 – (A) Standard FRET signal: when in the presence of each other and in relation to their pure spectra (see arrows), Donor intensity drops and Acceptor intensity rises due to the Donor → Acceptor energy transfer; and (B) Dexter transfer: when in the presence of each other and in relation to their pure spectra (see arrows), Donor and Acceptor intensities increase due to Donor ↔ Acceptor energy transfer, caused by dipole overlapping bellow $0.5R_0$.

Accordantly, Dexter transfer leads to false FRET intensities and is avoid by respecting the $0.5R_0$-$2R_0$ nm FRET distance range. For FRET systems that present Dexter transfer must be used a lower dye(s) molar concentration, which will reduce the number of molecules in the medium and therefore, increase the nanometric distance between them (preventing Donor-Acceptor orbital overlapping). To determine the FRET distance range, Following the instructions presented in the book from Medintz and Hildebrandt (chapter 5, pages 106-122)[30], R_0 can be written as:

$$R_0 = \left(\frac{9\ln(10)\,k^2 QY_{Donor}\,J}{128\,\pi^5 N_A n^4}\right)^{1/6} [\text{nm}] \qquad (2)$$

where N_A is Avogadro's constant [6.02 214 $\times 10^{23}$ mol^{-1}], n [-] the medium refractive index, QY_{Donor} the Donor quantum yield and k^2 [-] the orientation factor of the Donor-Acceptor dipoles. k^2 can vary from 0-4 but due to the complexity of its determination, most of the authors use the average of 2/3, since when the Donor-Acceptor dipoles orientation randomize during the excite state, the constant takes this value [39].

J [$nm^4.M^{-1}.cm^{-1}$] is the spectral overlap integral, on which FRET also depends [31] (Figure 1B). J can be calculated from:

$$J = \int f_D(\lambda)\,\epsilon_A(\lambda)\,\lambda^4\,d\lambda \qquad [\text{nm}^4.\text{M}^{-1}.\text{cm}^{-1}] \qquad (3)$$

where f_D is the Donor emission spectrum normalized to unity, ε_A the Acceptor molar attenuation coefficient [$M^{-1}.cm^{-1}$] and λ the wavelength [nm]. The Donor and Acceptor molar attenuation coefficients (ε) spectra are determined from the absorbance by Beer-Lambert's Law [35,40]:

$$Ab = \varepsilon\, c\, l \qquad (4)$$

where Ab is the absorbance defined as the negative decadic logarithm of the measured transmittance (by UV-Vis spectrometry), c is the molar concentration of the dye [M] and l is the length of the light path [cm].

Equations 1 to 3 are the basis of the Förster Theory, demonstrating the dependency of FRET eff on r and R_0, and how it is possible to properly calculate r having knowledge about the FRET pair (R_0) and the amount of energy being transferred (FRETeff).

Hence, FRET spectroscopy can be applied to study the degree of NSC between bonded films. For this, each surface is labelled with one of the dyes, Donor or Acceptor, and analyzed in the presence and absence of each other (Figure 4). In this case, the surfaces will present areas in full NSC and open gaps with higher nanometric distances separating them, due to roughness and/or flexibility of the films. Accordantly, in areas with no NSC above $2R_0$, FRET does not occur and no FRET signal can be sensed (Figure 4). On the contrary, in areas at NSC within $0.5R_0$-$2R_0$, FRET takes place and a FRET signal can be detected (Figure 4).

In this thesis, FRET spectroscopy was used to measure the average degree of NSC between bonded films from which adhesion depends, once the intermolecular forces responsible for it occur; allowing therefore, the direct correlation between FRET intensity and adhesion (bonded films separation energy).

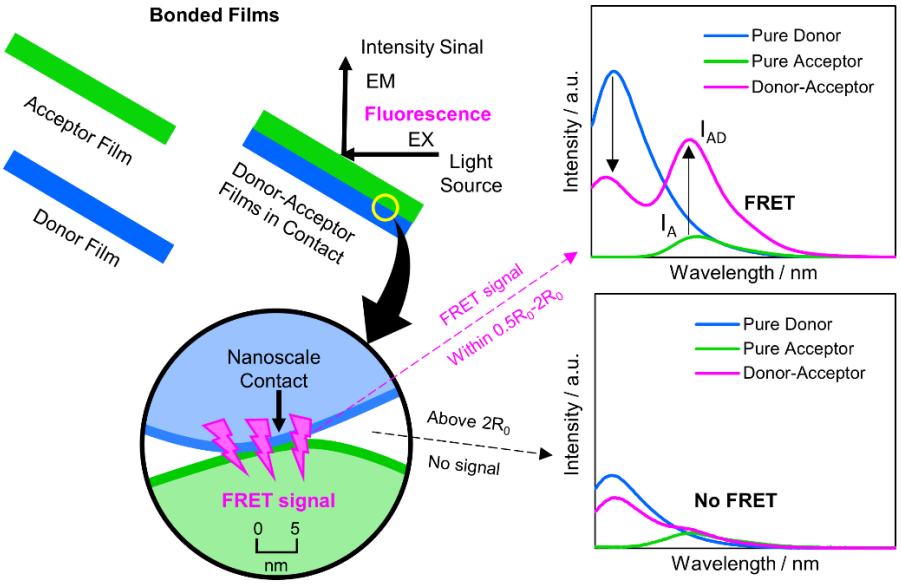

Figure 4 – Donor and Acceptor bonded films analyzed by FRET spectroscopy. At the nano-scale the films present areas in NSC ($0.5R_0$-$2R_0$), from witch a FRET signal can be detected, and open gaps (above $2R_0$) where no FRET occurs. The pure Donor, pure Acceptor and Donor-Acceptor in contact emission spectra on the right, represent both cases.

2.3. Design of a FRET pair

As demonstrated above, the choice of the FRET pair (Donor and Acceptor molecules) determines the capacity of the FRET system. For a couple of fluorescence molecules to be considered as a potential FRET pair, they need to [31]:

- Have an appropriate interaction range (Förster radius, R_0). The distance range of the FRET pair must fit the distance range of what is intended to be measured. Thus, only after knowing what is the nanometric distance range to be detected, a FRET pair with such sensitivity can be selected.
- Be spectroscopically compatible. To form a FRET pair, the molecules must present different, yet overlapping, Donor emission and Acceptor excitation spectra (Figure 2B), indicating lined-up energy bands (Figure 2A) on which FRET relies. Thanks to the spectral overlap, FRET utilizes the non-radiative energy transferred between Donor and Acceptor molecules to study their exact nanometric distance (Eq. 1). The area of the spectral overlap (J, Eq. 3) will determine the R_0 (Eq. 2) and the distance range of the FRET system ($0.5R_0$-$2R_0$). Larger overlap areas result in higher R_0, and accordantly, the contrary is also valid (Eq. 2 and 3).
- Present a high quantum yield (QY). The QY is the ratio between the number of photons emitted to the number of photons absorbed, indicating the capacity of the fluorescence dyes to absorb and emit light. Molecules with high QYs are easier to sense, which results in higher intensity signals. Therefore, lower QYs make FRET signals harder to be detected. This usually requires higher dye concentrations to overcome the low QY.

Besides this, it is also preferable to use molecules that are soluble in the same medium and molar concentration to enable further verification experiments. For example, the mixture of both dyes can be used as a positive FRET control (examples in section 2.4.3.).

2.4. Experimental

2.4.1. Fluorescence dyes

For the FRET experiments two pairs of compatible fluorescence molecules were used (Figure 5). The first pair has 7-(diethylamino)coumarin-3-carbohydrazide (DCCH) as the Donor dye and fluorescein-5-thiosemicarbazide (FTSC) as the Acceptor dye (Figure 5A). The DCCH/FTSC pair is FRET compatible (spectral overlap), soluble in the same solvent at the same molar concentration, acceptable QYs and an R_0 of 5.1 nm (Table 1). The selection of these molecules was based on the reported studies about the interaction between paper fibers realized by Thomson et al. [41,42]. A complete study about DCCH/FTSC performance in different solvents and pH can also be found in Urstöger et al. [43]; particularly relevant due to the strong dependency of FTSC on its surrounding environment [44], from which its fluorescence spectra can be significantly shifted as observed in Urstöger et al. [43]. Fortunately, such a phenomenon cannot be noticed when the dye molecule is entrapped in a polymeric matrix; as is the case for the poly(2-hydroxyethyl methacrylate) (pHema) thin films used for all the experiments realized in this work. Further details about the conditions utilized to employ the DCCH/FTSC pair in this thesis are described in Publication I [45].

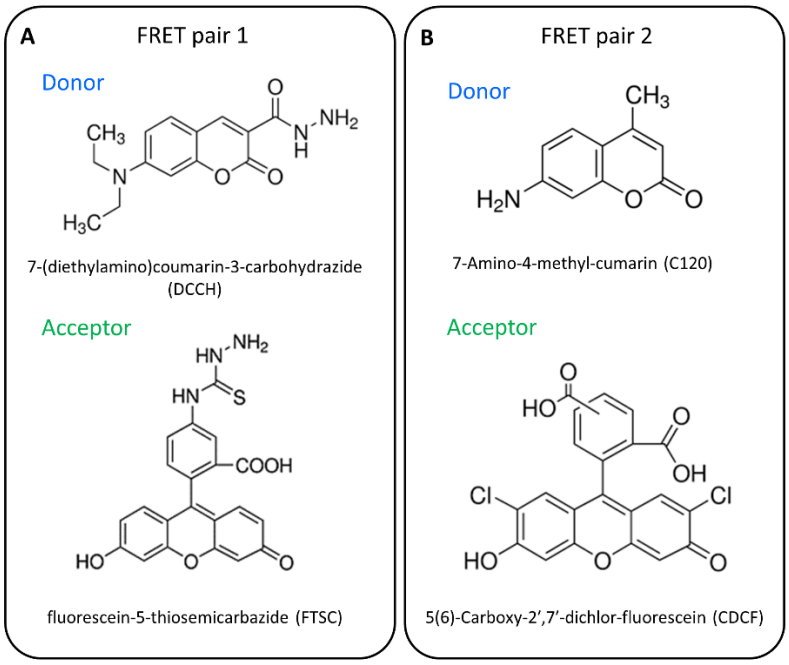

Figure 5 – Chemical structures of the fluorescence molecules: (A) – FRET pair 1 with DCCH and FTSC; and (B) – FRET pair 2 with C120 and CDCF as Donor and Acceptor dyes, respectively.

Table 1 – QY of the Donor and Acceptor molecules selected to form compatible FRET pairs and their correspondent solvent, R_o and FRET distance range at molar concentrations used in the FRET experiments.

FRET pair		QY	Solvent	Molar Concentration / mM	R_0 / nm	FRET distance range / nm
1	DCCH FTSC	0.14 0.12	Tetrahydrofuran	1.5	5.1	2.6-10.2
2	C120 CDCF	0.91 0.64	Ethanol	0.1	1.1	0.6-2.2

The second pair consisted of 7-Amino-4-methyl-cumarin (C120) as the Donor dye and 5(6)-carboxy-2′,7′-dichlor-fluorescein (CDCF) as the Acceptor dye (Figure 5B). On the contrary to the first pair of fluorophores, C120 and CDCF were carefully selected to form a new FRET pair/system specifically designed for the measurement of NSC. In comparison with DCCH/FTSC, the FRET compatible C120/CDCF pair demonstrates a smaller spectral overlap, which results in a smaller R_0 and distance detection range (i.e. 0.6-2.2 nm, Table 1) [31], closer to the distance range where the intermolecular forces responsible for adhesion occur; enhancing the accuracy of the FRET system for the measurement of NSC and its influence on adhesion. In addition, the C120/CDCF pair presents significantly higher QYs (Table 1), that positively contribute to the sensitivity of the method [36,46], which is particularly important for the analysis of non-uniformly bonded soft surfaces, as is the case in this work. And for last, the C120 and CDCF molecules also present a low vapor pressure, that allows us to form dye nanolayer films by PVD (according to the main goal number 4, section 1.2.); improving the overall precision of the method and its versatility. The conditions in which the C120 and CDCF molecules were used to develop the new FRET pair/system can be found in Manuscript II.

The dye labelling procedures, for both FRET pairs, are described in Publication I and Manuscripts II and III. In the following sections will give further explanations and examples about the experiments and calculations performed to develop both working FRET systems.

2.4.2. Ultraviolet–Visible (UV-Vis) Spectroscopy

UV-Vis spectroscopy is used to record the absorbance of the Donor and Acceptor molecules (Figure 6) and calculate the ε_D and ε_A (molar attenuation coefficients) spectra (Eq.4) [31]. The sample (e.g. a cuvette filled with a dye solution or a labelled thin film) is placed directly between the monochromatic light beam and the detector (Figure 6), and the equipment measures the amount of light absorbed by the sample with a certain or a range of wavelengths. To avoid inner filter effects or deviations from Beer-Lambert's law, the sample optical density should never exceed 0.5 in optical density [40].

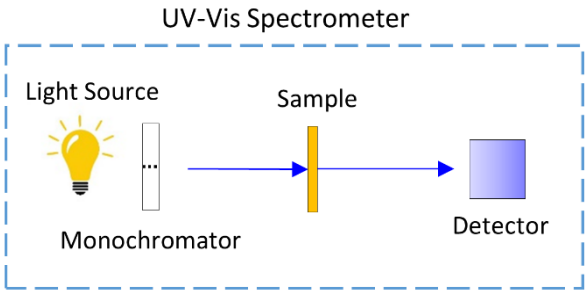

Figure 6 – Schematic representation of a UV-Vis spectrometer.

In Figure 7A and B one can see the ε_D and ε_A spectra (Eq. 4) of the DCCH/FTSC and C120/CDCF thin films prepared for this thesis, respectively (dye molar concentrations described in Table 1). These spectra indicate the capacity of the fluorescence molecules to capture light and the wavelength regions where both dyes can be excited simultaneously. For a correct FRET study, all measurements need to be performed using the same excitation wavelength [30]. It is appropriated to select a wavelength with high ε_D, as the Donor needs to receive enough light for himself and FRET (energy transfer to the Acceptor). On the contrary, ε_A should be lower, since during FRET the Acceptor receives extra energy from the Donor. Nevertheless, ε_A cannot be too low because the Acceptor also has to be excited for FRET (Figure 2A) [30]. Accordantly, all fluorescence spectra performed in this thesis were collected at the excitation wavelengths described in Table 2.

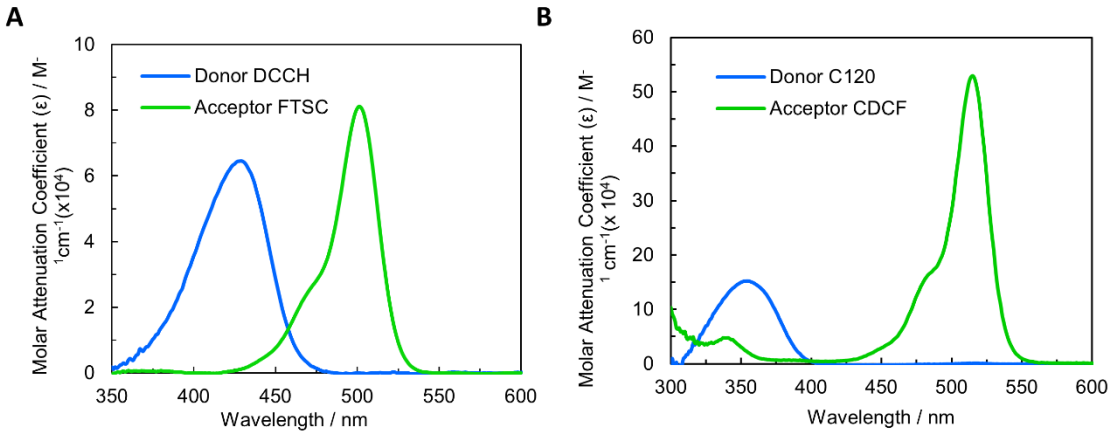

Figure 7 – Donor and Acceptor polymeric thin films ε spectra with: (A) FRET pair 1, DCCH and FTSC dye molecules and (B) FRET pair 2, C120 and CDCF dye molecules. Schematic representation of a UV-Vis spectrometer.

Table 2 – Selected measurement excitation wavelengths and correspondent $\varepsilon_A/\varepsilon_D$ ratios for FRET pair 1 and 2.

FRET pair	**Excitation Wavelength / nm**	**ε_D**	**ε_A**
DCCH/FTSC	440	5.2	0.4
C120/CDCF	330	9.1	3.8
	350	14.9	3.1

2.4.3. Fluorescence Spectroscopy

The fluorescence spectrometer, or just Fluorspectrometer, is the most common instrument used for FRET studies. And even when the main objective is to utilize other methods, e.g. Fluorescence Microscopy, at least the Donor emission spectrum needs to be recorded, to calculate the integral overlap (Eq. 3) of the selected FRET pair, on which R_0 depends (Eq. 2) [30,31].

Fluorescence spectroscopy is based on the same concept as UV-Vis. However, with a Fluorspectrometer the light is detected using a different angle than the incident beam (Figure 8), allowing to measure only the fluorescence emitted by the sample and not the direct light that passes through it. The sample can be, e.g., a cuvette filled with a dye solution or a labelled thin film, and the most frequently used angle for the measurements is 90º, as seen in Figure 8. The use of high dye concentrations can again lead to undesirable inner filter effects that reduce the intensity of the spectra or even disable its detection [40].

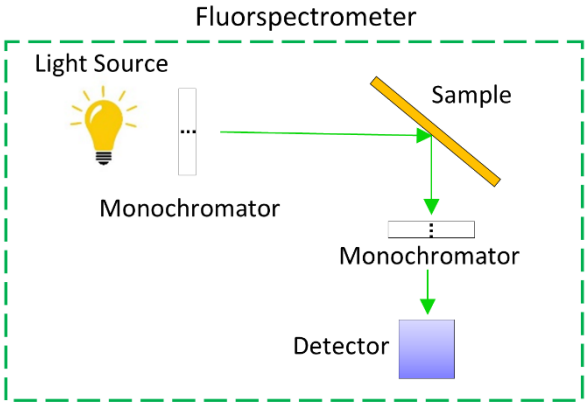

Figure 8 – Schematic representation of a Fluorspectrometer.

For FRET, in particular, another crucial aspect to pay attention to is the spectral bleed-through, which is characterized by the spectral overlap between the Donor and Acceptor emission spectra (Figure 9, marked in red). From the spectral bleed-through, light emitted from the Donor may be misinterpreted as Acceptor fluorescence, which can lead to false FRET results. Stressing that the spectral bleed-through does not take place in the spectral overlap between Donor emission and Acceptor excitation spectra (Figure 2B and Figure 9, marked in pink), on which FRET depends. Accordantly, it is preferable to select dyes with a minor bleed through overlap, and this is also the reason why in FRET studies, Donor and Acceptor dyes must always be analyzed in the presence and absence of each other, as the spectra might change.

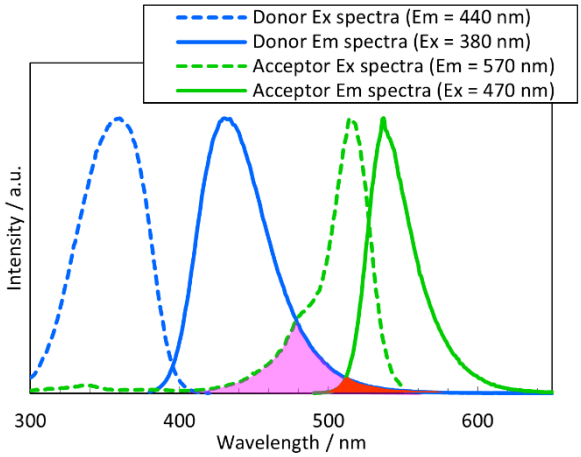

Figure 9 – Excitation and emission spectra of the FRET pair C120/CDCF in solution. The spectral overlap between the Donor emission and the Acceptor excitation spectra, on which FRET depends, is marked in pink. The bleed through region between the Donor and Acceptor emission spectra is marked in red.

Figure 10 depicts the fluorescence emission spectra of pure Donor, pure Acceptor and Donor-Acceptor mixed bonded thin films (at the same molar concentration), using the FRET

pairs/systems 1 and 2 (Figure 5). Here one can observe two examples of Donor → Acceptor FRET; characterized by the Donor peak intensity drop (from I_D to I_{DA}) and Acceptor peak intensity increase (from I_A to I_{AD}) from the mixed thin films in comparison to their pure spectra (see arrows, Figure 10A and B).

Since in the mixture thin films, both Donor and Acceptor molecules are entrapped in the same polymeric matrix, in close molecular contact, these FRET signals represent the maximum energy that can be transferred from the Donor to the Acceptor molecules, at the used molar concentrations (Table 1). Accordantly, these spectra were used as a reference/positive control in the experiments with the Donor/Acceptor bonded thin films further investigated in this thesis (Publication I and Manuscripts II and III).

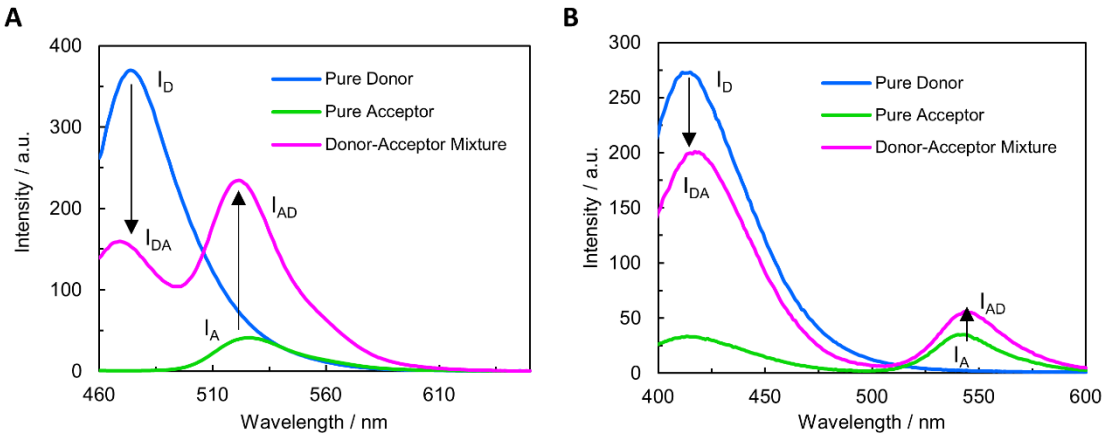

Figure 10 – Fluorescence emission spectra from pure Donor, pure Acceptor and Donor-Acceptor mixture thin films labelled with: (A) DCCH/FTSC, FRET pair 1 (1.5 mM) excited at 440 nm and (B) C120/CDCF, FRET pair 2 (0,1 mM) excited at 330 nm.

2.4.4. FRET efficiency (FRETeff)

FRETeff relates the R_0 (nm), r (D-A distance, nm) and the spectra of the Donor and Acceptor molecules in the presence and absence of each other. To calculate the FRETeff from a FRET signal several methods can be used such as Donor quenching, Acceptor sensitization and Donor/Acceptor photobleaching [30].

Donor quenching is related to the reduced emission from Donor molecules, occurring during FRET due to the energy transfer from the Donor to the Acceptor molecules. The ratio between the Donor luminescence in the presence (I_{DA}, FRET can occur) and absence (I_D, no FRET can occur) of the Acceptor can be used to calculate the FRETeff:

$$FRETeff_{Donor\ Quenching} = 1 - \frac{I_{DA}}{I_D} \quad (5)$$

However, Donor quenching does not only occur due to FRET (dynamic quenching). Several other quenching mechanisms, named static quenching (i.e. light, pressure, temperature or any type of reaction), can decrease the fluorescence capacity of Donor molecules. And thus, it is not recommended to use this method to determine FRETeff [30].,

In contrast, the Acceptor luminescence is only further excited when exposed to Donor FRET, which makes the Acceptor sensitization (Eq. 6) a much more reliable method.

$$FRETeff_{Acceptor\ Sensitization} = \left(\frac{I_{AD} - I_A}{I_A}\right)\left(\frac{\varepsilon_A}{\varepsilon_D}\right) \quad (6)$$

where I_{AD} and I_A stand for the Acceptor intensity (maximum peak value) in the presence and absence of the Donor, respectively. The direct excitation of the Acceptor at the Donor excitation wavelength must be considered; and thus, to achieve correct values of FRETeff, I_{AD}/ I_A is subtracted by I_A and multiplied by the ratio of ε_A and ε_D at the excitation wavelength used to collect the spectra during the FRET experiments (Table 2).

Furthermore, Donor and Acceptor photobleaching can also be used to calculate the FRETeff.

During photobleaching, the fluorophore is irreversibly damaged by photodegradation. In practice, the molecules are excited with a powerful light source until no luminescence can be emitted/detected. With the Donor photobleaching method, the time necessary to photobleach the Donor in the presence and absence of the Acceptor is used to determine the FRETeff [30]. In contrast, the Acceptor photobleaching method utilizes the luminescence of the Donor in the presence of the Acceptor, before and after the Acceptor photobleaching [30]; which means that it is only necessary to measure a single sample to calculate the FRETeff. This is quite useful in cases where it is difficult to control the concentration of the dyes, e.g., in protein or cell studies. Moreover, applying this method, due to the photodegradation of the Acceptor, the FRET path is also permanently demolished, and so for both methods, it is important to note that the samples cannot be used again. Depending on the type of study, this can or cannot be a suitable option to determine FRETeff [30].

For this thesis, the FRET experiments were conducted in bonded thin films, with known dye concentrations and uniform distribution, and therefore, to calculate the FRETeff the Acceptor sensitization method was employed (Eq. 6), which relies on the Acceptor performance and therefore, demonstrates true evidence of FRET [30]. Hence, were calculated the FRETeffs (Table

3 from FRET signals of the DCCH/FTSC and C120/CDCF pure and mixed thin films shown in Figure 10A and B.

Table 3 – Acceptor Sensitization FRETeff of the Donor-Acceptor mixture thin films.

FRET pair	Dye Molecules	Excitation Wavelength / nm	$\varepsilon_A/\varepsilon_D$	I_A	I_{AD}	FRETeff / %
1	DCCH/FTSC	440	0.07	41.3	234.3	32.7
2	C120/CDCF	330	0.41	35.0	55.7	24.2

2.4.5. Fluorescence Microscopy

In addition to the spectra, FRET signals can also be recorded and analyzed from fluorescence microscopy images, which allows the quantification and local analysis of FRET intensities [47–49]. For this fluorescence microscopy is used, which utilizes a light source to excite the sample and detects its re-emitted light in fluorescence images for further investigation [50].

As explained before, when using fluorescence spectroscopy, the fluorescence molecules are excited at a specific wavelength and the spectra are recorded using an emission wavelength interval. Accordantly, the fluorescence microscope utilizes filter cubes with defined and separated excitation and emission wavelength ranges [51]. For a FRET study it is necessary to equip the fluorescence microscope with a set of 3 different filters: Donor filter (D), Acceptor filter (A) and FRET filter (F); optimized to capture the Donor, Acceptor, and FRET fluorescence images. Each cube is formed by one excitation filter, a dichroic mirror and an emission filter, that corresponds to the particular fluorescence properties of the Donor and Acceptor molecules selected for the FRET measurements [41,50–52]. For this work, a fluorescence microscope was employed to study the NSC between crossed bonded thin films, labelled with the DCCH/FTSC FRET pair. Therefore, the filter cubes used for this purpose were specifically selected regarding the excitation and emission spectra of the DCCH and FTSC molecules, as can be observed in Figure 11 and Table 4.

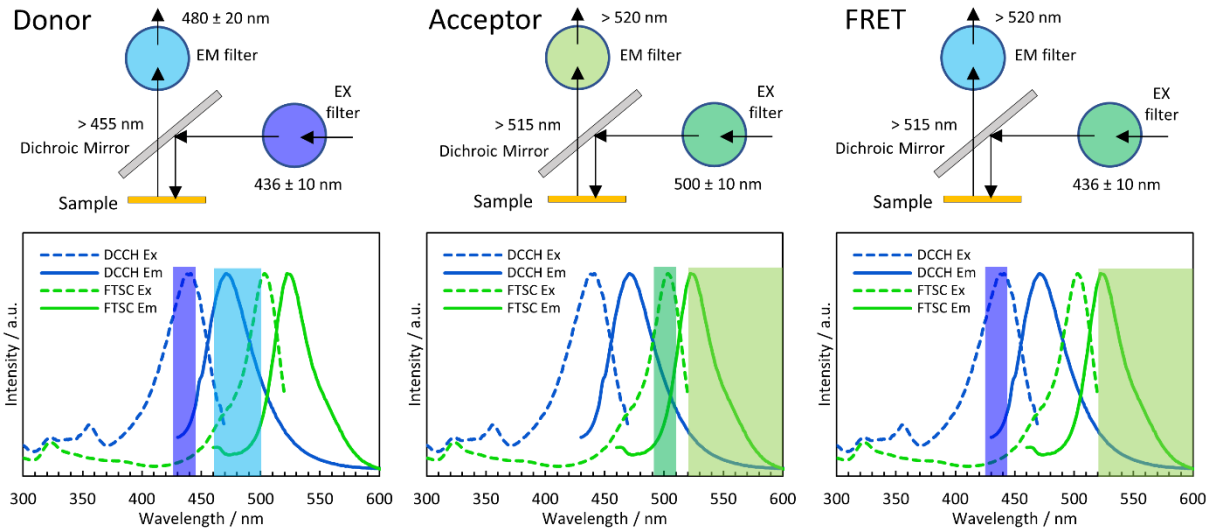

Figure 11 – Set of filter cubes used in this thesis to capture fluorescence images of the cross bonded thin films labeled with the DCCH/FTSC FRET pair. Donor, Acceptor and FRET filters correspond to the excitation and emission wavelength regions of the DCCH and FTSC thin films spectra.

Table 4 – Wavelength detection ranges of the fluorescence microscopy filter cubes sets used to study the crossed bonded thin films, labelled with the DCCH/FTSC FRET pair, and the respective c_{Lamp} (Eq. 7).

Filter cubes	Excitation / nm	Dichroic mirror / nm	Emission / nm	c_{Lamp}
Donor	436 ± 10	455 long pass	480 ± 20	4.41
Acceptor	500 ± 10	515 long pass	520 long pass	9.77
FRET	436 ± 10	515 long pass	520 long pass	-

First, the excitation filter selects the light coming from the light source according to the excitation wavelength of the molecules (Figure 11). The filtered light hits the dichroic mirror and the sample (Figure 11). Then, the fluorescence light emitted from the sample passes through the dichroic mirror, hits the emission filter (Figure 11) and is detected. Like the excitation filter, the emission filter just allows the wavelength range of interest to pass; reducing at the same time the potential spectral bleed through caused by the overlap between Donor and Acceptor emission spectra (Figure 9 and 11) [50].

As light sources lasers, light-emitting diodes (LEDs) or fluorescence lamps (i.e. halogen, xenon, mercury) can be used. Lasers and LEDs are efficient but also expensive and limited in terms of wavelength intervals. The fluorescence lamps are cheaper and more versatile since they provide a full wavelength spectrum [40] that later can be narrowed using adequate filter cubes, as demonstrated before. For all FRET microscopy experiments realized in this thesis, a 50W tungsten halogen lamp at 3200K was used. However, this lamp intensity shows a strong

dependency on the wavelength range used to excite the Donor and Acceptor molecules (Figure 11). Thus, it was necessary to calculate Donor and Acceptor lamp correction factors (c_{Lamp}) to employ them in the analysis of the fluorescence images. c_{Lamp} (Eq. 7) [51] can be described as the integral of the tungsten halogen lamp spectrum (I_{Lamp}) at 3200K between the upper ($f_{EX\ upper}$) and lower ($f_{EX\ lower}$) wavelength limits of the excitation filters (Table 3). For this thesis, the Donor and Acceptor c_{Lamp} are 4.41 and 9.77 (Table 4), respectively [51].

$$c_{Lamp} = \int_{f_{EX\ lower}}^{f_{EX\ upper}} I_{Lamp}(\lambda)d\lambda \tag{7}$$

Furthermore, the detector used in the experiments, a CMOS detector (optiMOS™ Scientific, QImaging, Canada) is also affected by the emission wavelength range of the molecules and correspondent filter cubes [51]. Therefore, it is also required to calculate Donor and Acceptor detector correction factors ($c_{Detector}$) for the Donor and Acceptor emission filters, using the following equation (Eq. 8):

$$c_{Detector} = \frac{\int_{f_{EM\ lower}}^{f_{EM\ upper}} QE(\lambda)\cdot I_{EM}(\lambda)d\lambda}{\int_{f_{EM\ lower}}^{f_{EM\ upper}} I_{EM}(\lambda)d\lambda} \tag{8}$$

where QE is the quantum efficiency of the CMOS detector, I_{EM} the Donor or Acceptor emission spectra and $f_{EM\ upper}$ and $f_{EM\ lower}$ the upper and lower wavelength limits of the emission filters [51]. The calculated Donor and Acceptor $c_{Detector}$ can be examined in Table 5. Each filter cube has two $c_{Detector}$, for the Donor and Acceptor emission spectra, which fortunately proved to be similar, simplifying the fluorescence images treatment and analysis [51].

Table 5 – Donor and Acceptor detector correction factors for the Donor and Acceptor emission filters.

Filter Cube	**$c_{Detector}$**	
	Donor	**Acceptor**
Donor	0.462	0.473
Acceptor	0.533	0.535

2.4.6. NFRET values

The fluorescence images acquired in the FRET experiments realized for this thesis were analyzed to obtain a local FRET intensity (NFRET) for each image pixel using algorithms provided e.g. by Gordon et al. and Xia et al. [53,54]. For every pixel, a dimensionless value (NFRET) was obtained indicating the local degree of FRET intensity [51,55], which can be converted in a map imaging the local variations of NSC between the interfaces over the examined sample area.
The fluorescence images were recorded with the three different filter cubes presented before (Figure 11), resulting in a total of three images of the cross bonded thin films (Figure 12) in the region of interest, containing in the same picture a pure Donor area (d), pure Acceptor area (a) and Donor-Acceptor bonded area (f, marked in pink), where FRET can occur.

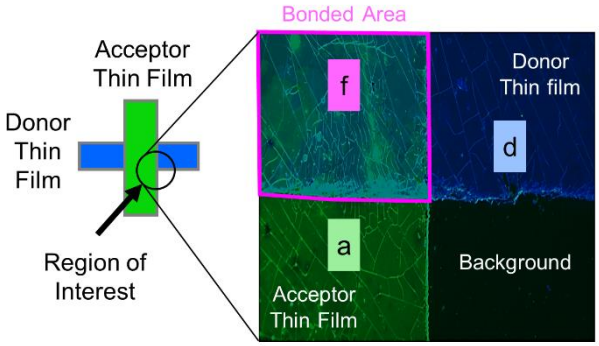

Figure 12 – False colour image of the cross bonded thin films taken with fluorescence microscopy, containing in the same picture a pure Donor (d), pure Acceptor (a) and Donor-Acceptor bonded (f, marked in pink) areas.

For this degree of analysis, the local pixel-to-pixel intensities are evaluated in the bonded region (Figure 12) where FRET is expected, together with average intensities of pure Donor and pure Acceptor fluorescence. Thus, calculating the level of FRET intensity NFRET in every pixel of the bonded thin films nine different values are needed (Figure 13). Six values are average intensities of pure Donor and pure Acceptor fluorescence in the different filter sets (areas lined in green, Figure 13). The other three values, the bonded regions are calculated for each pixel separately (areas lined in red, Figure 13). The regions to compute average fluorescence intensities were drawn manually in the respective images, as shown in Figure 13.

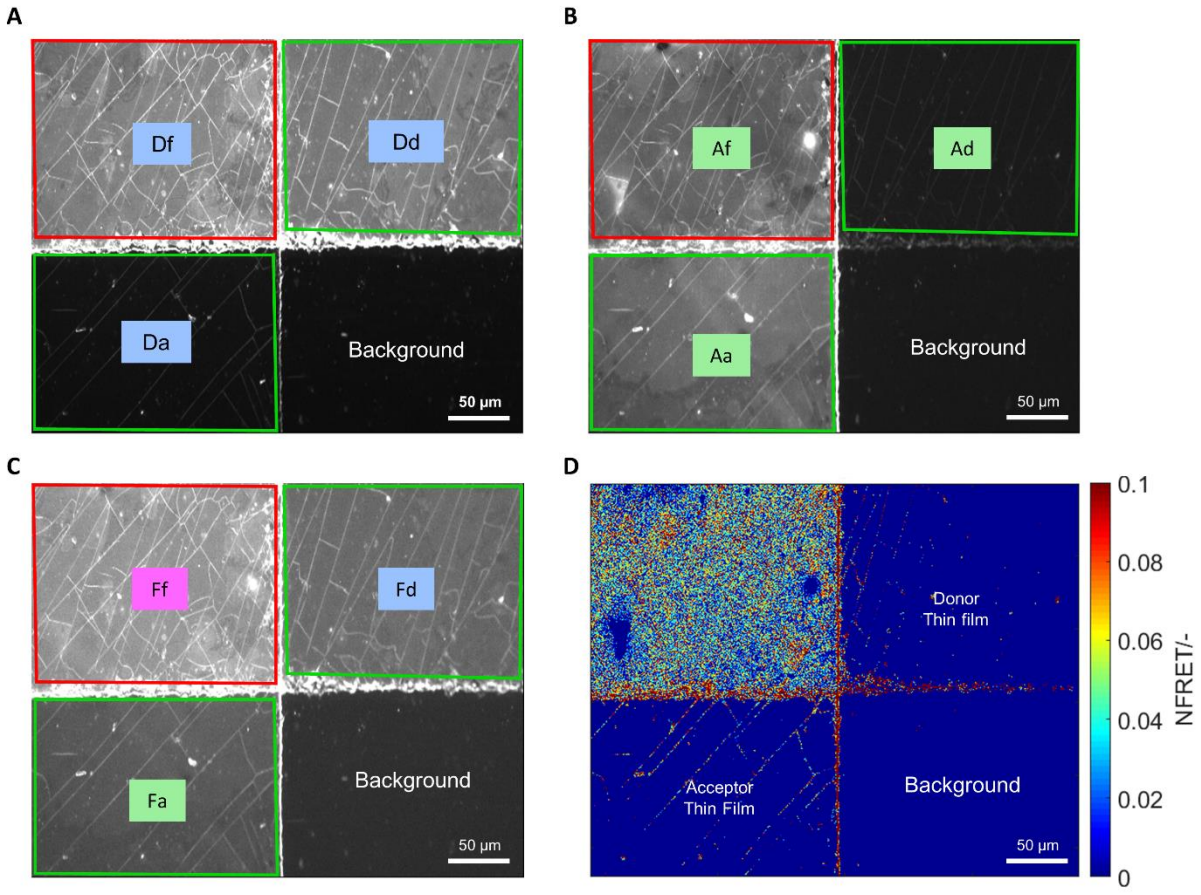

Figure 13 – Fluorescence images, of the cross bonded thin films captured with Donor (A), Acceptor (B) and FRET (C) filters cubes optimized for the DCCH/FTSC molecules used in the experiments. The first letter stands for the used filter cube (D = Donor filter, A = Acceptor filter, F = FRET filter) and the second for the investigated region (d = Donor only, a = Acceptor only, f = FRET bonded area). And (D) NFRET intensities maps resultant from the FRET microscope imagens analysis.

The first equations (Eq. 9-11) based on an algorithm developed by Gordon et al. [53] are used to calculate the correct FRET intensity considering all possible spectral bleed-through circumstances.

$$\overline{Afa} = \frac{Af - \left(\frac{Ad}{Fd}\right)Ff}{1 - \left(\frac{Fd}{Aa}\right)\left(\frac{Ad}{Fd}\right)} \tag{9}$$

$$FRET1 = \frac{\left(Ff - \left(\frac{Fd}{Dd}\right)Df - \overline{Afa}\left[\left(\frac{Fa}{Aa}\right) - \left(\frac{Fd}{Dd}\right)\left(\frac{Da}{Aa}\right)\right]\right)}{G\left[1 - \left(\frac{Da}{Fa}\right)\left(\frac{Fd}{Dd}\right)\right]} \tag{10}$$

$$\overline{Dfd} = Df + FRET1\left[1 - G\left(\frac{Da}{Aa}\right)\right] - \overline{Afa}\left(\frac{Da}{Aa}\right) \tag{11}$$

The equations consist of variables with two letters that represent the measured light intensities from the microscope images recorded in 16-bit grey values (Figure 13A-C and Eq. 9-11). The first letter stands for the used filter cube (D = Donor filter, A = Acceptor filter, F = FRET filter) and the second for the investigated sample (d = Donor only, a = Acceptor only, f = FRET bonded area) (Figure 13A-C). For instance, Df stands for the FRET region (bonded area) intensity inspected with the Donor filter. Afa refers to the Acceptor intensity in the bonded area, with the Acceptor filter, which means, without exciting the Acceptor (no FRET). Similarly, Dfd corresponds to the Donor intensity in the bonded area, with the Donor filter, without exciting the Acceptor (no FRET). G is a specific factor relating the loss of the Donor signal to the increase of the Acceptor signal. For DCCH/FTSC cross bonded thin films and the setup employed in this thesis, G is 0.758 [51].

Hence, equations 9 to 11 are used to calculate a FRET intensity normalized by the amount of Donor and Acceptor signal (FRET1, Eq. 10). To ensure accurate, normalized and dimensionless results, Xia and Liu used the Gordon algorithm to calculate NFRET values (Eq. 12) [54].

$$NFRET = \frac{FRET1}{\sqrt{\overline{Afa} * \overline{Dfd}}} \tag{12}$$

From this we get a NFRET intensity maps as can be observed in Figure 13D. In addition, a 5-pixel image erosion was applied to remove the edge of the drawn images, since they present high FRET intensities, which can lead to false-positive NFRET values.

In terms of NSC local variation analysis, Figure 14 gives two examples of NFRET intensity maps from cross bonded DCCH/FTSC thin films applying 50 and 100 bar. In the NFRET images one can notice bright areas in the bonded region which indicate NSC within $0.5R_0$-$2R_0$; and dark areas that correspond to open gaps (Figure 1 and 4) between the thin film interfaces. Moreover, from 50 (Figure 14A) to 100 bar (Figure 14B) it is clear that the open gaps get smaller and less dark; which indicates that the degree of NSC is increasing with the bonding pressure applied between the thin films. The NFRET ($2x10^2$) values from these maps are 8.1 (Figure 14A) and 8.7 (Figure 14B). These can then be compared with other maps from other cross bonded films under different pressures, FRETeffs from their corresponding FRET signals and separation energy (adhesion).

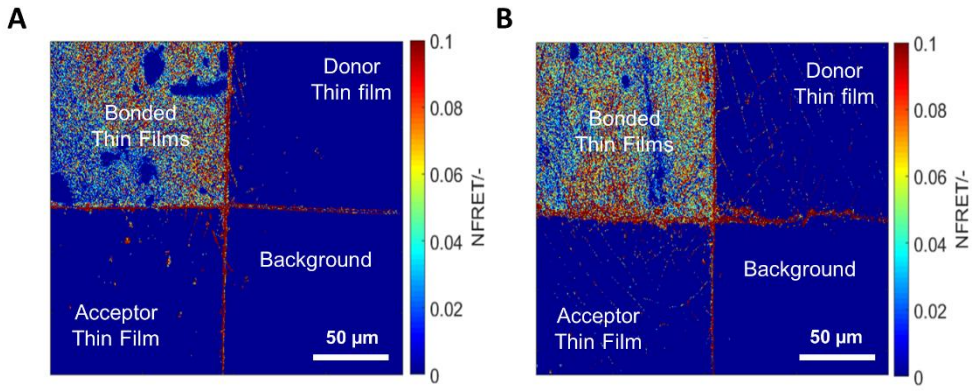

Figure 14 – NFRET intensity maps indicating the local variation in NSC between cross bonded thin films with (A) 50 and (B) 100 bar. Surface open gaps, can be noticed in the darker spots inside the bonded region, where no NSC or FRET occurs.

Further details from this part of this thesis work are described in Publication I. The MATLAB scripts used for the treatment and analysis of the fluorescence images were developed by Georg Urstöger [51] and can be found in in his PhD thesis.

REFERENCES

[1] M.P. Murphy, S. Kim, M. Sitti, Enhanced adhesion by gecko-inspired hierarchical fibrillar adhesives, ACS Appl. Mater. Interfaces. 1 (2009) 849–855. https://doi.org/10.1021/am8002439.

[2] B.N.J. Persson, On the mechanism of adhesion in biological systems, J. Chem. Phys. 118 (2003) 7614–7621. https://doi.org/10.1063/1.1562192.

[3] G.K. Dolan, B. Cartwright, M.R. Bonilla, M.J. Gidley, J.R. Stokes, G.E. Yakubov, Probing adhesion between nanoscale cellulose fibres using AFM lateral force spectroscopy: The effect of hemicelluloses on hydrogen bonding, Carbohydr. Polym. 208 (2019) 97–107. https://doi.org/10.1016/j.carbpol.2018.12.052.

[4] L.C. Bradley, N.D. Bade, L.M. Mariani, K.T. Turner, D. Lee, K.J. Stebe, Rough Adhesive Hydrogels (RAd gels) for Underwater Adhesion, ACS Appl. Mater. Interfaces. 9 (2017) 27409–27413. https://doi.org/10.1021/acsami.7b08916.

[5] B.N.J. Persson, Adhesion between an elastic body and a randomly rough hard surface, Eur. Phys. J. E. 8 (2002) 385–401. https://doi.org/10.1140/epje/i2002-10025-1.

[6] P. Monllor, L. Capablanca, J. Gisbert, P. Díaz, I. Montava, Á. Bonet, Improvement of Microcapsule Adhesion to Fabrics, Text. Res. J. (2010). https://doi.org/10.1177/0040517509346444.

[7] G. Lu, W. Hong, L. Tong, H. Bai, Y. Wei, G. Shi, Drying enhanced adhesion of polythiophene nanotubule arrays on smooth surfaces, ACS Nano. 2 (2008) 2342–2348. https://doi.org/10.1021/nn800443m.

[8] G. Le Saux, M.C. Wu, E. Toledo, Y.Q. Chen, Y.J. Fan, J.C. Kuo, M. Schvartzman, Cell-Cell Adhesion-Driven Contact Guidance and Its Effect on Human Mesenchymal Stem Cell Differentiation, ACS Appl. Mater. Interfaces. 12 (2020) 22399–22409. https://doi.org/10.1021/acsami.9b20939.

[9] P. Atkins, J. de Paula, Physical Chemistry for the Life Sciences, 1st ed., Oxford University Press, Oxford, 2006.

[10] U. Hirn, R. Schennach, Comprehensive analysis of individual pulp fiber bonds quantifies the mechanisms of fiber bonding in paper, Sci. Rep. 5 (2015) 10503. https://doi.org/10.1038/srep10503.

[11] G. Gong, C. Zhou, J. Wu, X. Jin, L. Jiang, Nanofibrous adhesion: The twin of gecko adhesion, ACS Nano. 9 (2015) 3721–3727. https://doi.org/10.1021/nn5063112.

[12] C. Yang, B.N.J. Persson, Molecular dynamics study of contact mechanics: Contact area and interfacial separation from small to full contact, Phys. Rev. Lett. 100 (2008) 1–4. https://doi.org/10.1103/PhysRevLett.100.024303.

[13] M.P. Murphy, S. Kim, M. Sitti, Enhanced adhesion by gecko-inspired hierarchical fibrillar adhesives, ACS Appl. Mater. Interfaces. 1 (2009) 849–855. https://doi.org/10.1021/am8002439.

[14] B.N.J. Persson, O. Albohr, U. Tartaglino, A.I. Volokitin, E. Tosatti, On the nature of surface roughness with application to contact mechanics, sealing, rubber friction and adhesion, J. Phys. Condens. Matter. 17 (2005) 1–62. https://doi.org/10.1088/0953-8984/17/1/R01.

[15] B.N.J. Persson, M. Scaraggi, Theory of adhesion: Role of surface roughness, J. Chem. Phys. 141 (2014) 1–14. https://doi.org/10.1063/1.4895789.

[16] M. Füllbrandt, D. Kesal, R. Von Klitzing, Multiscaling Approach for Non-Destructive Adhesion Studies of Metal/Polymer Composites, ACS Appl. Mater. Interfaces. 7 (2015) 16247–16256. https://doi.org/10.1021/acsami.5b01949.

[17] H.J. Kim, H.Y. Kim, H.D. Jeong, E.S. Lee, Y.J. Shin, Friction and thermal phenomena in chemical mechanical polishing, J. Mater. Process. Technol. 130–131 (2002) 334–338. https://doi.org/10.1016/S0924-0136(02)00820-8.

[18] I. Nitta, Measurements of real contact areas using PET films (thickness, 0.9 μm), Wear. 181–183 (1995) 844–849. https://doi.org/10.1016/0043-1648(95)90205-8.

[19] R.C. Bowen, L.P. Demejc, D.S. Rimai, A method of determining the contact area between a particle and substrate using scanning electron microscopy*, J. Adhes. 51 (1995) 191–199. https://doi.org/10.1080/00218469508009998.

[20] S. Asunmaa, B. Steenberg, Beaten pulps and the fibre-to-fibre bond in paper, Sven. Papperstidning. 61 (1958) 686–695.

[21] T. Kizuka, K. Yamada, S. Deguchi, M. Naruse, N. Tanaka, Cross-sectional time-resolved high-resolution transmission electron microscopy of atomic-scale contact and noncontact-type scannings on gold surfaces, Phys. Rev. B - Condens. Matter Mater. Phys. 55 (1997) R7398–R7401. https://doi.org/10.1103/PhysRevB.55.R7398.

[22] D.H. Alsem, S. Sood, N. Salmon, T.D.B. Jacobs, In situ electrical testing of device-relevant nanocontacts in the transmission electron microscope, Microsc. Microanal. 22 (2016) 818–819. https://doi.org/10.1017/s1431927616004943.

[23] T.D.B. Jacobs, A. Martini, Measuring and Understanding Contact Area at the Nanoscale: A Review, Appl. Mech. Rev. 69 (2017) 060802. https://doi.org/10.1115/1.4038130.

[24] S.A.S. Asif, K.J. Wahl, R.J. Colton, Mechanics Using Force Modulation, Mater. Res. 594 (1999) 471–476. https://doi.org/https://doi.org/10.1557/PROC-594-471.

[25] M. Benz, K.J. Rosenberg, E.J. Kramer, J.N. Israelachvili, The deformation and adhesion of randomly rough and patterned surfaces, J. Phys. Chem. B. 110 (2006) 11884–11893. https://doi.org/10.1021/jp0602880.

[26] B.N.J. Persson, O. Albohr, C. Creton, V. Peveri, Contact area between a viscoelastic solid and a hard, randomly rough, substrate, J. Chem. Phys. 120 (2004) 8779–8793. https://doi.org/10.1063/1.1697376.

[27] B.N.J. Persson, E. Tosatti, The effect of surface roughness on the adhesion of elastic solids, J. Chem. Phys. 115 (2001) 5597–5610. https://doi.org/10.1063/1.1398300.

[28] C. Yang, U. Tartaglino, B.N.J. Persson, A multiscale molecular dynamics approach to contact mechanics, Eur. Phys. J. E. 19 (2006) 47–58. https://doi.org/10.1140/epje/e2006-00004-9.

[29] D.L. Dexter, A theory of sensitized luminescence in solids, J. Chem. Phys. 21 (1953) 836–850. https://doi.org/10.1063/1.1699044.

[30] N. Hildebrandt, How to Apply FRET: From Experimental Design to Data Analysis, in: FRET – Förster Reson. Energy Transf., John Wiley & Sons, Ltd, 2013: pp. 105–163. https://doi.org/https://doi.org/10.1002/9783527656028.ch05.

[31] B.W. van der Meer, Förster Theory, in: FRET – Förster Reson. Energy Transf., John Wiley & Sons, Ltd, 2013: pp. 23–62. https://doi.org/https://doi.org/10.1002/9783527656028.ch03.

[32] T. Förster, Zwischenmolekulare Energiewanderung und Fluoreszenz, Ann. Phys. 437 (1948) 55–75. https://doi.org/https://doi.org/10.1002/andp.19484370105.

[33] H. Sahoo, Förster resonance energy transfer - A spectroscopic nanoruler: Principle and applications, J. Photochem. Photobiol. C Photochem. Rev. 12 (2011) 20–30. https://doi.org/10.1016/j.jphotochemrev.2011.05.001.

[34] P.M. Bendix, M.S. Pedersen, D. Stamou, Quantification of nano-scale intermembrane contact areas by using fluorescence resonance energy transfer, Proc. Natl. Acad. Sci. U. S. A. 106 (2009) 12341–12346. https://doi.org/10.1073/pnas.0903052106.

[35] B. Valeur, M.N. Berberan-Santos, Characteristics of Fluorescence Emission, in: B. Valeur (Ed.), Mol. Fluoresc. Princ. Appl., John Wiley & Sons, Ltd, 2012: pp. 53–74. https://doi.org/https://doi.org/10.1002/3527600248.ch3.

[36] T.K. Christopoulos, E.P. Diamandis, Chapter 14 - Fluorescence Immunoassays, in: E.P. Diamandis, T.K. Christopoulos (Eds.), Immunoassay, Academic Press, San Diego, 1996: pp. 309–335. https://doi.org/https://doi.org/10.1016/B978-012214730-2/50015-7.

[37] N.J. Turro, V. Ramamurthy, J.C. Scaiano, Modern Molecular Photochemistry of Organic Molecules, Angew. Chemie Int. Ed. 49 (2010) 6709–6710. https://doi.org/https://doi.org/10.1002/anie.201003826.

[38] B. Valeur, M.N. Berberan-Santos, Effects of Intermolecular Photophysical Processes on Fluorescence Emission, in: B. Valeur (Ed.), Mol. Fluoresc. Princ. Appl., John Wiley & Sons, Ltd, 2012: pp. 141–179. https://doi.org/https://doi.org/10.1002/3527600248.ch4.

[39] B.W. van der Meer, D.M. van der Meer, S.S. Vogel, Optimizing the Orientation Factor Kappa-Squared for More Accurate FRET Measurements, in: FRET – Förster Reson. Energy Transf., John Wiley & Sons, Ltd, 2013: pp. 63–104. https://doi.org/https://doi.org/10.1002/9783527656028.ch04.

[40] Joseph R. Lakowicz, Instrumentation for Fluorescence Spectroscopy, in: J.R. Lakowicz (Ed.), Princ. Fluoresc. Spectrosc., Springer US, Boston, MA, 2006: pp. 27–61. https://doi.org/10.1007/978-0-387-46312-4_2.

[41] C.I. Thomson, R.M. Lowe, A.J. Ragauskas, Imaging cellulose fibre interfaces with fluorescence microscopy and resonance energy transfer, Carbohydr. Polym. 69 (2007) 799–804. https://doi.org/10.1016/j.carbpol.2007.01.023.

[42] C.I. Thomson, R.M. Lowe, A.J. Ragauskas, First characterization of the development of bleached kraft softwood pulp fiber interfaces during drying and rewetting using FRET microscopy, Holzforschung. 62 (2008) 383–388. https://doi.org/10.1515/HF.2008.069.

[43] G. Urstöger, A. Steinegger, R. Schennach, U. Hirn, Spectroscopic investigation of DCCH and FTSC as a potential pair for förster resonance energy transfer in different solvents, PLoS One. 15 (2020) 1–13. https://doi.org/10.1371/journal.pone.0228543.

[44] R. Sjöback, J. Nygren, M. Kubista, Absorption and fluorescence properties of fluorescein, Spectrochim. Acta Part A Mol. Spectrosc. 51 (1995). https://doi.org/10.1016/0584-8539(95)01421-P.

[45] M.G. Simões, G. Urstöger, R. Schennach, U. Hirn, Quantification and Imaging of Nanoscale Contact with Förster Resonance Energy Transfer, ACS Appl. Mater. Interfaces. (2021). https://doi.org/10.1021/acsami.1c04226.

[46] J.C. Zwinkels, P.C. DeRose, J.E. Leland, Chapter 7 - Spectral Fluorescence Measurements, in: T.A. Germer, J.C. Zwinkels, B.K. Tsai (Eds.), Spectrophotometry, Academic Press, 2014: pp. 221–290. https://doi.org/https://doi.org/10.1016/B978-0-12-386022-4.00007-8.

[47] J.A. Broussard, B. Rappaz, D.J. Webb, C.M. Brown, Fluorescence resonance energy transfer microscopy as demonstrated by measuring the activation of the serine/threonine kinase Akt, Nat. Protoc. 8 (2013) 265. https://doi.org/10.1038/nprot.2012.147.

[48] M. Zammarano, P.H. Maupin, L.P. Sung, J.W. Gilman, E.D. McCarthy, Y.S. Kim, D.M. Fox, Revealing the interface in polymer nanocomposites, ACS Nano. 5 (2011) 3391–3399. https://doi.org/10.1021/nn102951n.

[49] T. Zal, N.R.J. Gascoigne, Using live FRET imaging to reveal early protein-protein interactions during T cell activation, Curr. Opin. Immunol. 16 (2004) 418–427. https://doi.org/10.1016/j.coi.2004.05.019.

[50] B. Valeur, M.N. Berberan-Santos, Fluorescence Microscopy, in: Mol. Fluoresc. Princ. Appl., John Wiley & Sons, Ltd, 2012: pp. 327–348. https://doi.org/https://doi.org/10.1002/9783527650002.ch11.

[51] G. Urstöger, M.G. Simoes, A. Steinegger, R. Schennach, U. Hirn, Evaluating the degree of molecular contact between cellulose fiber surfaces using FRET microscopy, Cellulose. 0123456789 (2019) 7037–7050. https://doi.org/10.1007/s10570-019-02575-x.

[52] M.J. Sanderson, I. Smith, I. Parker, M.D. Bootman, Fluorescence Microscopy, Cold Spring Harb Protoc. (2014) 1–36. https://doi.org/10.1101/pdb.top071795.Fluorescence.

[53] G.W. Gordon, G. Berry, X.H. Liang, B. Levine, B. Herman, Quantitative Fluorescence Resonance Energy Transfer Measurements Using Fluorescence Microscopy, Biophys. J. 74 (1998) 2702–2713.

[54] Z. Xia, Y. Liu, Reliable and global measurement of fluorescence resonance energy transfer using fluorescence microscopes, Biophys. J. 81 (2001) 2395–2402. https://doi.org/10.1016/S0006-3495(01)75886-9.

[55] C.I. Thomson, Probing the Nature of Cellulosic Fibre Interfaces with Fluorescence Resonance Energy Transfer Probing the Nature of Cellulosic Fibre Interfaces with Fluorescence Resonance Energy Transfer, Georgia Institute of Technology, 2007.

3. Publication I

Quantification and Imaging of Nanoscale Contact with Förster Resonance Energy Transfer

ACS APPLIED MATERIALS & INTERFACES

www.acsami.org

Research Article

Quantification and Imaging of Nanoscale Contact with Förster Resonance Energy Transfer

Mónica G. Simões, Georg Urstöger, Robert Schennach, and Ulrich Hirn*

Cite This: https://doi.org/10.1021/acsami.1c04226

Read Online

ACCESS | Metrics & More | Article Recommendations

ABSTRACT: Adhesion is caused by molecular interactions that only take place if the surfaces are in nanoscale contact (NSC); i.e., the distance between the surfaces is in the range of 0.1−0.4 nm. However, there are several difficulties measuring the NSC between surfaces, mainly because regions that appear to be in full contact at low magnification may show no NSC when observed at higher magnifications. Thus, the measurement area of NSC is very small with imaging techniques, and an experimental technique to evaluate NSC for large contact areas has not been available thus far. Here, we are proposing Förster resonance energy transfer (FRET) spectroscopy/microscopy for this purpose. We demonstrate that NSC in a distance range of 1−10 nm can be evaluated. Our experiments reveal that, for thin films pressed under different loads, NSC increases with the applied pressure, resulting in a higher FRET signal and a corresponding increase in adhesion force/energy when separating the films. Furthermore, we show that local variations in molecular contact can be visualized with FRET microscopy. Thus, we are introducing a spectroscopic technique for quantification (FRET spectroscopy) and imaging (FRET microscopy) of NSC between surfaces, demonstrated here for the application of surface adhesion. This could be of interest for all fields where adhesion or nanoscale surface contact are playing a role, for example, soft matter, biological materials, and polymers, but also engineering applications, like tribology, adhesives, and sealants.

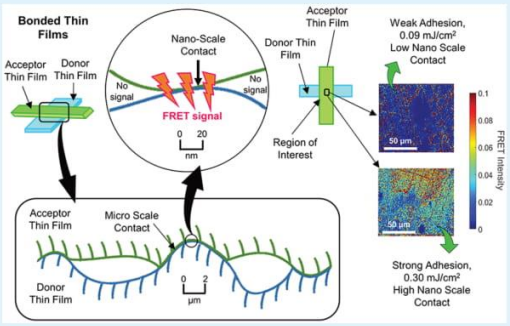

KEYWORDS: *nanoscale contact, adhesion, contact mechanics, Förster resonance energy transfer, polymer films, FRET spectroscopy, FRET microscopy*

INTRODUCTION

Adhesion between solid materials is crucial in several fields of biology, science, and technology, such as cellular adhesion and contact mechanics.[1−4] It is caused by intermolecular forces, like hydrogen bonding and van der Waals forces.[5] These mechanisms are taking place up to a distance of 0.1−0.4 nm[6,7] and, thus, require nanoscale contact (NSC) between the adhering surfaces.[8,9] As a result, an increase in nanoscale contact area (NSCA) leads to an increase in adhesion between surfaces.[10−12]

However, it is challenging to quantify the NSCA. Surfaces in close contact observed under lower resolution frequently reveal gaps when inspected at the atomic length scale (Figure 1).[13−15] Thus, the NSCA is usually lower (at maximum equal) than the contact observed at lower resolution.[16−18] In conclusion, direct observation of NSCA is only possible with imaging techniques having a resolution in the length scale of the interaction forces, i.e., around 1 nm. Nevertheless, optical microscopy is sometimes used to estimate the contact between materials with low roughness.[16,19] Also imaging of the contact area with scanning electron microscopy (SEM) resolution[17] can only reveal microscale contact. Transmission electron microscopy (TEM) is able to image surface contact on the relevant length scale.[20−23] However, high-resolution TEM is only suited for semi-quantitative inspection because the imaging area is below 1 μm^2, which makes it very hard to conduct a statistically meaningful quantitative analysis. Also, the sample preparation for TEM is delicate and laborious. In conclusion, direct imaging techniques with low magnification are systematically overestimating the NSCA, and high-resolution imaging techniques can only provide qualitative indications as a result of the extremely small imaging area.

Other groups use force modulation with depth-sensing nanoindentation, by mapping and comparing the surfaces before and after being in contact to estimate the NSCA.[23−25]

Received: March 5, 2021
Accepted: April 9, 2021

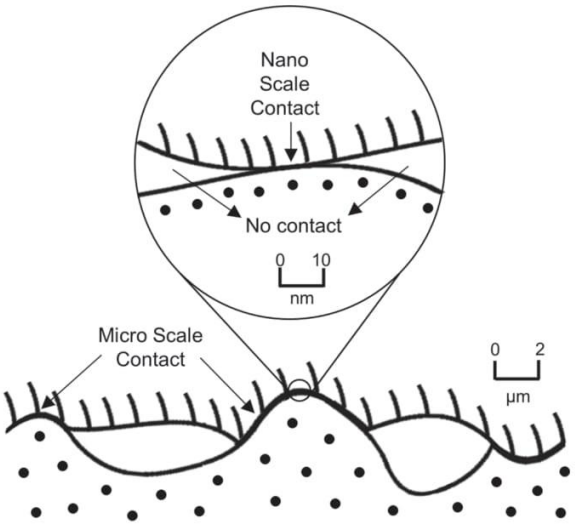

Figure 1. Two surfaces in physical contact observed at micro- and nanometer scales. The contact area decreases with increasing magnification.

However, this approach presents some disadvantages, e.g., the reduced sample size, low resolution, and possible recovery of the initial morphology/roughness of the material after it is no longer in contact. A key approach is contact mechanic simulations. Contact mechanic theories are used to study the NSCA dependence upon the scale of observation.[20,24,26−28] The influence of roughness on NSC, friction, and adhesion between elastic bodies is also modeled by multiscale molecular dynamics.[8,29] Modeling-based approaches are currently the best available techniques to estimate NSCA. To the best of our knowledge, no experimental technique is available to evaluate NSCA for an inspection area above the nanometer scale. In this work, we are proposing such a method, applicable up to the millimeter-scale sample area. We are employing Förster resonance energy transfer (FRET) spectroscopy for (a) quantification of NSC and (b) FRET microscopy for two-dimensional (2D) imaging of local variations in NSC. Such an experimental method to evaluate NSC could be useful to study adhesion between surfaces for soft matter and biological materials but also engineering applications, like tribology, adhesives, and polymers.

FRET is a technique capable of measuring the nanometric distance (0−20 nm) between surfaces in close contact.[30−32] For that, each surface is labeled with a fluorescence dye, donor or acceptor. FRET uses the non-radiative energy transferred between the donor and acceptor molecules to study their exact nanometric distance. The distance range of FRET depends upon the Förster radius (R_0) of the selected dye system. If the molecules are close enough to each other, i.e., below the critical distance of $2R_0$, a FRET signal can be detected.

FRET is commonly used in biological/biomedical applications to confirm NSC between molecules in studies related to, e.g., protein/cellular adhesion.[33−36] FRET microscopy and spectroscopy have also been used to study interdiffusion between polymeric materials.[30,37−39]

To apply FRET, donor and acceptor molecules must present different yet overlapping emission and excitation fluorescence spectra, respectively. By exciting them at the same excitation wavelength, the energy transfer can be observed.[40] Figure 2 shows a basic experiment to demonstrate FRET between a pair of one donor and one acceptor dye uniformly distributed in pHema thin films. First, their emission spectra are collected for the individual dyes (a) and then for a mixture of the dyes (b). Energy transfer between the dyes, i.e., a FRET signal, is identified when, in comparison to the spectra of the pure dyes, in the mixture, the intensity of the donor dye is dropping (left downward arrow) and the intensity of the acceptor dye is increasing (right arrow up from I_A to I_{AD}; see Figure 2C). Please note that the energy transfer between the dyes (in this case, FTSC and DCCH) can only take place between donor and acceptor molecules closer than $2R_0 < 10.2$ nm, which is obviously the case in the mixture (Figure 2B).

In this work, we are quantifying the degree of NSC between thin films bonded together. Therefore, one film is labeled with a FRET donor dye, and another film is labeled with a FRET acceptor dye (Figure 3). The degree of NSC between bonded films is evaluated by calculating the FRET energy transfer efficiency (FRET efficiency)[31] on the interface between two films, as seen in Figure 3. Then, the measured degree of NSC is correlated to the adhesion between the films, which have been bonded together with ascending pressure, thus leading to an increased degree of NSC and, as a consequence, to an increased adhesion between the films. By demonstrating the correlation between the FRET signal and the measured separation energy between the thin films, we are validating our approach to quantify NSC using FRET spectroscopy.

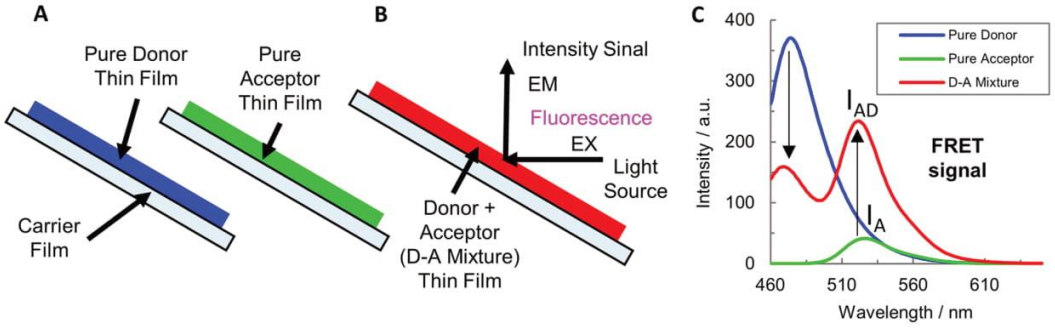

Figure 2. FRET signal: (A) donor and acceptor individual thin films, (B) donor−acceptor mixture thin film, and (C) pure donor, acceptor, and donor−acceptor mixture fluorescence spectra.

https://doi.org/10.1021/acsami.1c04226
ACS Appl. Mater. Interfaces XXXX, XXX, XXX−XXX

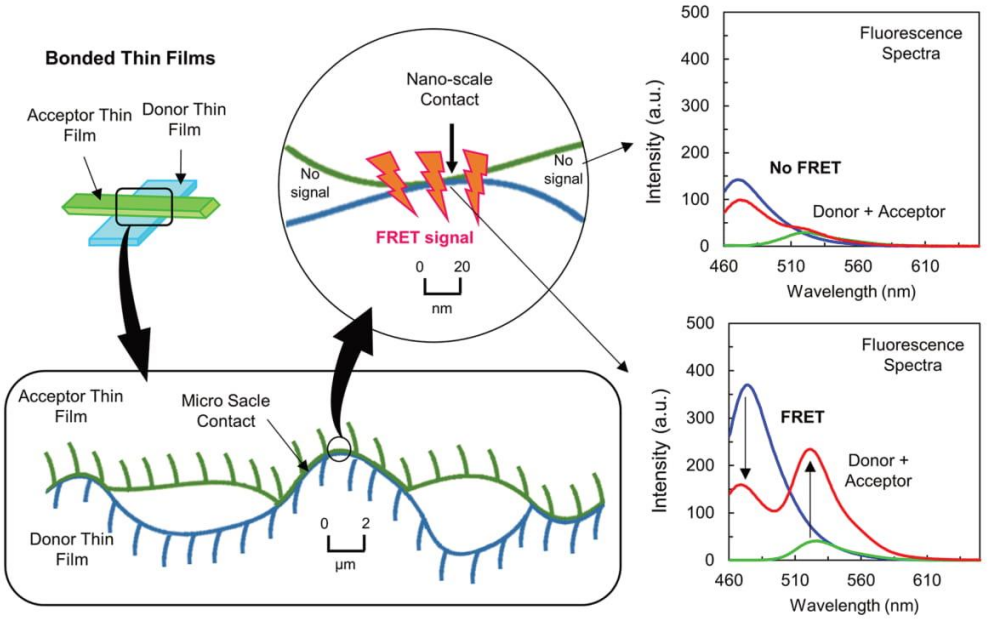

Figure 3. Donor- and acceptor-labeled thin films in close physical contact observed at micro- and nanometer scales. NSC decreases with increasing magnification. For NSC, a FRET signal can be observed between donor and acceptor surfaces and the signal does not occur for surfaces with a distance larger than 10 nm.

Finally, we are demonstrating that FRET microscopy can be used to image local variations in NSC between the bonded films. For FRET microscopy, the microscope is equipped with a set of fluorescence filters specific to the FRET dyes used. Images acquired with the different filter sets can be analyzed to obtain a local FRET intensity in every image pixel using FRET algorithms, as provided, e.g., by Gordon et al. and Xia et al.[41,42] For each image pixel, we obtain a dimensionless value (NFRET) indicating the local degree of NSC between the interfaces,[30,43] thus generating a map imaging the local variation of NSC over the sample area.

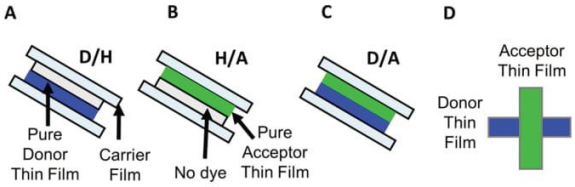

Figure 4. Thin films bonded by pressing with 1.5−150 bar: (A) donor/pHema (D/H), (B) pHema/acceptor (H/A), and (C) donor/acceptor (D/A) bonded thin films and (D) cross-bonded D/A thin films.

RESULTS AND DISCUSSION

For the FRET system, 7-(diethylamino)coumarin-3-carbohydrazide (DCCH, donor) and fluorescein-5-thiosemicarbazide (FTSC, acceptor) were selected as the fluorescence dyes.[44] At the dye concentration used in the experiments (see the Methods section), the DCCH/FTSC system presents a FRET distance range ($2R_0$) of 0−10.2 nm (R_0 = 5.1 nm), which allowed us to study NSC with this FRET pair. All thin films consisted of pHema and were produced by doctor blading. The dyes were mixed into pHema (Figures 2 and 4) at an equivalent molar concentration of 1.5 mM. The thickness (1.5 ± 0.1 μm) and low roughness (0.04 ± 0.01 μm) of the thin films show a uniform distribution of the dyes, which is of extreme importance for a correct FRET result.

The fluorescence spectra (Figure 5A) of the pure donor and acceptor thin films (Figure 2A) show the DCCH emission and FTSC excitation spectra overlapping area, which is necessary for FRET.[31,44] The spectra were measured on thin films bonded in the configuration shown in panels A and B of Figure 4.

The spectra (Figure 5B) of the molar attenuation coefficients (ε_D and ε_A) were calculated from the absorbance spectra of pure donor and pure acceptor thin films (eq 4). ε_D and ε_A spectra (Figure 5B) show how well the dyes absorb the light and the regions where both dyes can be analyzed at the same excitation wavelength. We chose to collect the fluorescence spectra and FRET measurements at 440 nm excitation, finding a ratio of $\varepsilon_A/\varepsilon_D$ = 0.07.

First, individual thin films of the pure donor, pure acceptor (Figure 2A), and a donor−acceptor (D−A) mixture (Figure 2B) are investigated as a positive control. In the D−A thin film both donor and acceptor dye are mixed, leading to short distances between the molecules in the thin-film polymeric matrix. Therefore, the D−A mixture thin film represents the maximum value of FRET efficiency that the system can reach, at this dye concentration. Figure 2C exhibits the fluorescence spectra where a strong FRET signal can be observed (drop in the donor intensity and an increase of the acceptor signal; see arrows). The FRET efficiency in acceptor sensitization measured for this system was FRETeff = 30.5%.

To validate FRET as a measurement for NSC between surfaces, we bonded dyed polymer thin films by pressing the surfaces together with a pressure from 1.5 to 150 bar.

The films were prepared by bonding pure donor (D), pure acceptor (A), and films with no dye (H) (panels A and B of

https://doi.org/10.1021/acsami.1c04226
ACS Appl. Mater. Interfaces XXXX, XXX, XXX−XXX

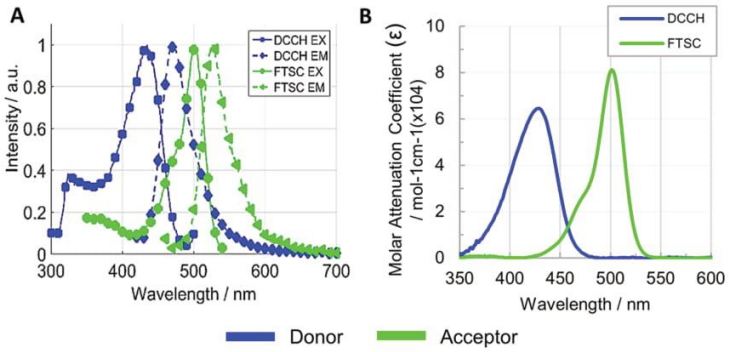

Figure 5. Donor (DCCH) and acceptor (FTSC) thin film fluorescence properties as a FRET pair: (A) excitation and emission florescence spectra and (B) molar attenuation coefficient spectra.

Figure 4). The arrangement of bonded thin films (panels C and D of Figure 4) was the same for all measurements, with the donor in the back position and acceptor in the front position. The left column of Figure 6 depicts the fluorescence spectra of the bonded thin films bonded with the lowest (1.5 bar) and highest (150 bar) pressure, as given in panels A and B of Figure 4.

FRET efficiencies were calculated by the acceptor sensitization method[30,31] (Table 1), which only relies on the acceptor performance (eq 3). The positive control (D−A mixture thin film) revealed a FRET efficiency of ∼30%. When the pressure to bond the thin films is increased, the FRET signals (left column of Figure 6) and their corresponding FRET efficiencies (Table 1) also increase accordingly. For the minimum bonding pressure of 1.5 bar, the measured FRET efficiency was 1.1%, and for the maximum bonding pressure of 150 bar, the FRET efficiency was 10%.

The thin films bonded at increasing pressure were also analyzed with FRET microscopy to demonstrate the capability to image local variations in NSC (middle and right columns of Figure 6) and validate FRET microscopy. For FRET microscopy, the efficiency of the energy transfer at the interface between the donor and acceptor thin films and, thus, the NSCA is measured by the NFRET value. For each image pixel, the local NFRET value indicates the degree of NSC in this image pixel. The donor−acceptor mixture thin film was again used as a reference, giving a maximum NFRET value of 125 (Table 1 and top row of Figure 6). For the remaining tests, the thin films were cross-bonded, and the images were captured in the region of interest (Figure 7). In the region of interest, only the top left part shows the bonded thin films; thus, only this part should show a NFRET signal. The other regions, showing donor film, acceptor film, and background, should not give a NFRET signal.

In the NFRET microscopy maps (right column of Figure 6), as expected, only the left top regions of the overlapping, bonded thin films exhibit a NFRET signal. Apart from some edge artifacts, the pure donor and acceptor films are showing no FRET signal, as expected. In the bonded regions, there is low NFRET intensity of the 1.5 bar thin films (second row of Figure 6), indicating very low NSC, and high intensity in the bonded area of the 150 bar thin films (bottom row of Figure 6), demonstrating high NSC between the donor and acceptor interfaces. Analyzing all bonded thin films (Figure 6), the same tendency observed before with the FRET spectroscopy experiments can be seen: when the pressure applied in the bonded thin films increases, the average NFRET values also increase accordingly (see the third column of Table 1). Both, FRET spectroscopy and FRET microscopy are thus able to correctly indicate the degree of NSC in the bonded polymer films.

Moreover, inspecting the FRET microscopy images, one can see that local variations in NSC, like, e.g., unbonded regions (right column, bottom row of Figure 6), can be identified. This indicates that FRET microscopy is indeed able to image NSC in the range of 1−10 nm for sample areas in the millimeter scale, bridging a scale difference in the order of 10^6.

Considering that donor and acceptor molecules are dissolved in the polymeric thin-film matrices, this could lead to migration of dye molecules into the opposing thin film, causing false FRET signals. Hence, the bonded thin films were analyzed by FRET spectroscopy over 16 weeks (Figure 8A). FRET efficiency has not significantly changed over time, which indicates no interdiffusion phenomena. Only NSC is responsible for the FRET signals.

Finally, the interrelation between NSC measured by FRET and surface adhesion was investigated. The bonded thin films were detached by *z*-directional tensile testing to measure the maximum adhesion force and separation energy of the films bonded with different pressures. The results show that maximum tensile force (Table 1) as well as separation energy are gradually increasing with increasing adhesion, i.e., separation force and separation energy (Figure 8B). The thin film separation energies per unit area were calculated by integrating the force−displacement curves of the tensile test and plotted in Figure 8C together with the FRET energy transfer efficiency between the bonded surfaces for FRET spectroscopy (FRET efficiency, red markers) and FRET microscopy (NFRET, green markers), as depicted in Figure 8B. With linearly increasing adhesion, the intensity of both FRET spectroscopy and FRET microscopy are also increasing linearly. The thin films are chemically and physically identical, and the differences in adhesion only descend from differences in NSC caused by increased pressing during the bonding. This proves that FRET spectroscopy and FRET microscopy are indeed a suitable approach to quantitatively investigate NSC between surfaces for millimeter-sized regions.

■ CONCLUSION

We have presented a proof of concept that FRET methods can be used to quantify the degree of NSC between surfaces. Our system of FRET dyes, DCCH and FTSC, indicates surface

https://doi.org/10.1021/acsami.1c04226
ACS Appl. Mater. Interfaces XXXX, XXX, XXX−XXX

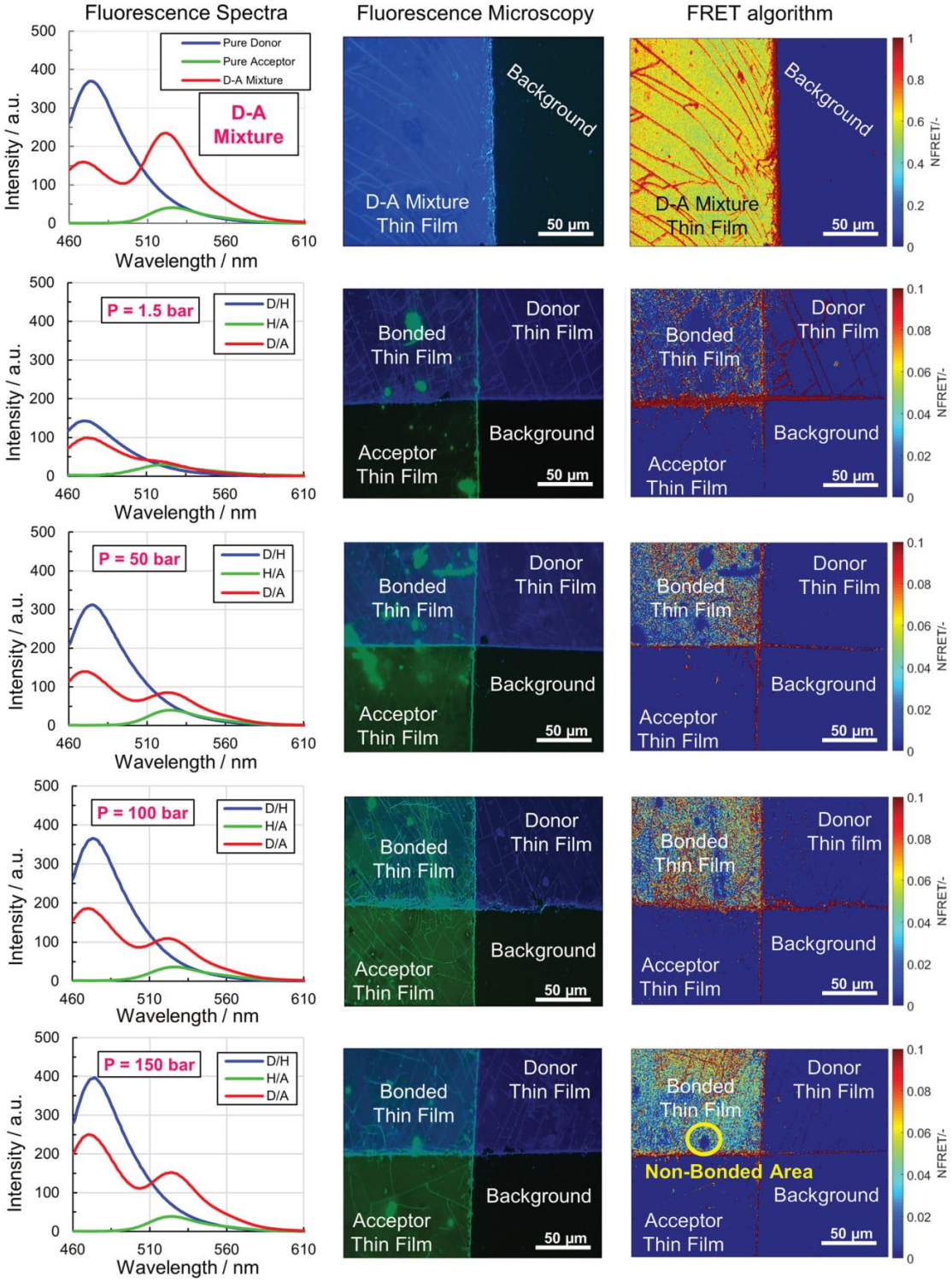

Figure 6. Maximum FRET signal in the positive control (top row), furthermore bonded thin films with increasing bonding pressure from 1.5 to 150 bar (other rows downward). Fluorescence spectra (left column). False color images of the thin films taken with fluorescence microscopy, with 50× magnification (middle column). NFRET intensity maps (right column) indicating the local variation in NSC between the surfaces; non-bonded regions (right column, bottom row) can also be identified.

https://doi.org/10.1021/acsami.1c04226
ACS Appl. Mater. Interfaces XXXX, XXX, XXX−XXX

Table 1. FRET Efficiency, NFRET, Maximum Tensile Force, and Separation Energy Per Unit Area of the Individual and Bonded Thin Films Prepared under Different Pressures[a]

sample	FRET efficiency (%)	NFRET (2×10^2)	maximum tensile force (N)	separation energy per unit area (mJ/cm^2)
D–A mixture	30.5 ± 1.1	125.0 ± 0.6		
D/A, 1.5 bar	1.2 ± 0.4	7.2 ± 0.04	18.7 ± 1.2	0.09 ± 0.02
D/A, 50 bar	3.6 ± 0.7	8.1 ± 0.01	25.1 ± 1.1	0.17 ± 0.01
D/A, 100 bar	7.1 ± 1.1	8.7 ± 0.11	32.6 ± 1.6	0.22 ± 0.01
D/A, 150 bar	9.7 ± 1.2	9.6 ± 0.06	41.8 ± 2.3	0.30 ± 0.03

[a]FRET efficiency was determined by acceptor sensitization (at 440 nm, $\varepsilon_A/\varepsilon_D = 0.07$; see Figure 5B). Values are the average ± 95% confidence interval ($n = 3$ for FRET efficiency; $n = 6$ for NFRET; and $n = 10$ for tensile force and separation energy).

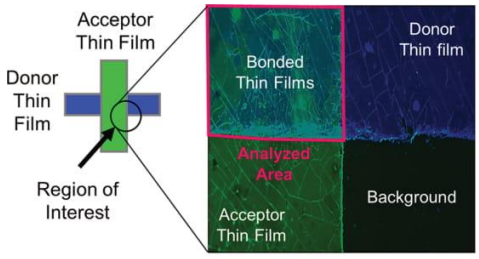

Figure 7. False color image of the bonded thin films taken with fluorescence microscopy, drawing the bonded area, region of interest, marked in magenta.

contact in the range of 1–10 nm or closer. The FRET efficiency measured by acceptor sensitization in FRET spectroscopy is corresponding to an increase in NSC and adhesion between polymeric thin films. Measurements of NFRET intensity with FRET microscopy are confirming this relation. An implementation of FRET microscopy furthermore enables spatially resolved analysis of NSC. We believe that this novel concept to quantify and image NSC contact for large surface contact areas using optical methods, namely, FRET spectroscopy and FRET microscopy, provides a useful experimental approach to study different kinds of phenomena related to nanoscale surface contact, like adhesion, friction, interdiffusion, and contact mechanics, in general. This could be of interest for all fields where nanoscale surface contact is playing a role, for example, soft matter, biological materials, and polymers, but also engineering applications, like tribology, adhesives, and sealants.

METHODS

Thin-Film Preparation. DCCH (SC-214392, Santa Cruz Biotechnology, Dallas, TX, U.S.A.), and FTSC (SC-211522, Santa Cruz Biotechnology, Dallas, TX, U.S.A.) were dissolved in tetrahydrofuran (3 mM). Donor–acceptor mixture solutions were prepared in a ratio of 1:1 (1.5 mM). A total of 100 μL of dye(s) solution was added to 500 μL of 10% (m/v) pHema (Mw 20 000 Da, CAS Registry Number 25249-16-5, Sigma-Aldrich, St. Louis, MO, U.S.A.) solution in an ethanol/Milli-Q water mixture 95:5 (v/v) and 5 μL of triethylamine, to ensure alkaline conditions.[44] The polymeric solutions were doctor-bladed over polyvinyl chloride carrier films using a bar film applicator (3M BYK-Gardner GmbH, Geretsried, Germany) and left at room temperature for the evaporation of the solvents and consolidation of the films.

Thin-Film Characterization. The thickness of the thin films was determined with a Bruker DekTak XT surface profiler. The scan length was set to 1000 μm over the time duration of 3 s with the hills and valleys scanning profile. The diamond stylus had a radius of 12.5 μm, and the employed force was 3 mg. The measured profile was then used to determine the thickness. Each layer thickness has been determined by averaging six measurements on three different spots on the thin films.

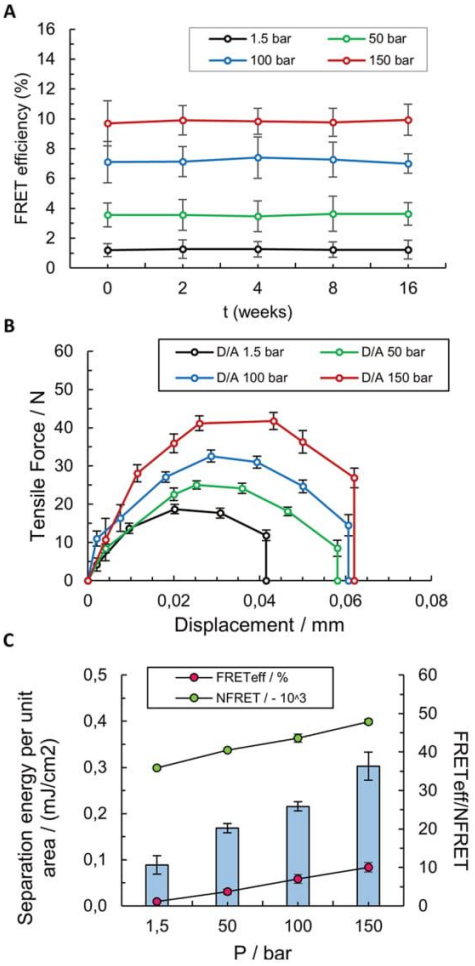

Figure 8. Thin films bonded by pressing with 1.5–150 bar, corresponding tensile force, FRET efficiency, and separation energy: (A) FRET efficiency of the D/A thin films bonded at different pressures over time, (B) separation force curves from bonded donor/acceptor thin films, and (C) FRET efficiency, NFRET, and separation energy per area of the D/A bonded thin films. The presented results refer to the mean average ± 95% confidence interval ($n = 3$).

Bonded Thin-Film Preparation. For FRET spectroscopy, the interface between the thin films was achieved by bonding 4 cm^2 of pure donor (D), pure acceptor (A), and/or pHema thin films without any dye (H), as demonstrated in panels A–C of Figure 4. For FRET microscopy the contact was obtained by cross bonding 0.5 cm of pure

https://doi.org/10.1021/acsami.1c04226
ACS Appl. Mater. Interfaces XXXX, XXX, XXX–XXX

donor and pure acceptor thin films, as shown in Figure 4D. For all samples, the thin films were pressed at 1.5, 50, 100, and 150 bar (hydraulic pressure PU30, V. Jessernigg & Urban, Graz, Austria) for 10 min at room temperature.

FRET Spectroscopy. Spectra measurements of the individual and bonded thin films (Figures 2 and 4) were recorded using a spectra fluorophotometer RF-5301PC (Shimadzu, Kyoto, Japan), at an excitation wavelength of 440 nm in a 45°/45° configuration, as demonstrated in Figure 2B.

FRET signals were detected from the individual/bonded thin films and analyzed by the Förster theory.[31] The dye system presents a FRET working range distance that corresponds to $2R_0$, where R_0 is the Förster radius (nm). It that can be calculated via eq 1

$$R_0 = \left(\frac{9\ln(10)k^2Q_{\text{donor}}J}{128\pi^5N_An^4}\right)^{1/6} \quad \text{(nm)} \tag{1}$$

where N_A is Avogadro's constant (6.02×10^{20} mM^{-1}), k^2 is the orientation factor ($^2/_3$), n is the refractive index (1.5 for the thin films), Q_{donor} is the donor quantum yield (measured by the absolute method, $Q_{donor} = 0.14$ and $Q_{acceptor} = 0.12$), and J (nm^4 M^{-1} cm^{-1}) is the spectral overlap integral calculated with eq 2

$$J = \int f_D(\lambda)\varepsilon_A(\lambda)\lambda^4\,d\lambda \quad (nm^4\,M^{-1}\,cm^{-1}) \tag{2}$$

where f_D is the donor emission spectrum normalized to unity (Figure 5A), ε_A is the attenuation coefficient of the acceptor ($\times 10^4$ M^{-1} cm^{-1}) (Figure 5B), and λ is the wavelength (cm^{-1}).

FRET efficiency (%) was calculated by the acceptor sensitization method[1] (eq 3). It is the ratio of the acceptor spectral intensity peak value in the presence (I_{AD}) and absence (I_A) of the donor (Figure 2C). To achieve appropriate FRET efficiency results, the direct luminescence of I_A is subtracted from I_{AD} and multiplied by the correct luminescence ratio of the acceptor and donor molar attenuation coefficients (ε_A and ε_D) at the excitation wavelength used for the FRET experiments (Figure 5B).

$$\text{FRETeff}_{(\text{acceptor sensitization})} = \left(\frac{I_{AD}}{I_A} - 1\right)\left(\frac{\varepsilon_A}{\varepsilon_D}\right) \quad (\%) \tag{3}$$

The molar attenuation coefficients ε ($\times 10^4$ M^{-1} cm^{-1}) (Figure 5B) are determined from the absorbance by Beer–Lambert's law (eq 4)

$$A = \varepsilon cl \tag{4}$$

where A is the absorbance defined as the negative decadic logarithm of the measured transmittance, c is the concentration of the dye in the polymeric matrix (mM), and l is the length of the light path, in this case, the thickness of the thin films (cm). Pure donor and pure acceptor thin film absorbance was measured with a Varian Cary ultraviolet–visible (UV–vis) spectrophotometer (Agilent Technologies, Santa Clara, CA, U.S.A.). To minimize the inner filter effect and deviations from Beer–Lambert's law, the optical density of the transmission measurements never exceeded 0.5 optical density (OD).

FRET Microscopy. Individual and bonded thin films were investigated using a wide field microscopy setup equipped with FRET filter sets (Table 2) customized to the dye excitation and emission spectra, operated with a 50 W tungsten halogen lamp. Images were taken with an optiMOS Scientific CMOS camera (QImaging, Canada) attached to the microscope via a C-mount interface.

Table 2. Fluorescence Microscopy Filter Sets Used to Study the Thin Films

filter set	excitation (nm)	dichroic mirror (nm)	emission (nm)
donor	436 ± 10	455 long pass	480 ± 20
acceptor	500 ± 10	515 long pass	520 long pass
FRET	436 ± 10	515 long pass	520 long pass

Both, the intensity of the lamp and the detector sensitivity show a dependency of the wavelength and were corrected by calculating correction factors from the lamp emission spectrum folded with the excitation filters, and the extinction coefficient and the detector sensitivity folded with the emission filters and the emission spectra.

Images were taken with an optiMOS Scientific CMOS camera (QImaging, Canada). All samples were investigated using a 50× magnification, and to minimize background noise, the microscope was operated in a dark space without ambient light.

The equations for the calculation of the FRET intensity are based on an algorithm developed by Gordon et al. (eqs 5–7).[41] The method makes use of images recorded with the three different filter sets (Table 2), resulting in nine pictures for the individual thin films (pure donor, pure acceptor, and donor–acceptor mixture thin films) and three images for the bonded thin films (that contain in the same region/picture pure donor, pure acceptor, and bonded area; Figure 7).

For a detailed description of the algorithm, please refer to the original paper. In brief, this method calculates the FRET intensity corrected for all possible spectral bleed-through scenarios according to the following equations:

$$\overline{\text{Afa}} = \frac{\text{Af} - \left(\frac{\text{Ad}}{\text{Fd}}\right)\text{Ff}}{1 - \left(\frac{\text{Fd}}{\text{Aa}}\right)\left(\frac{\text{Ad}}{\text{Fd}}\right)} \tag{5}$$

$$\text{FRET1} = \frac{\left(\text{Ff} - \left(\frac{\text{Fd}}{\text{Dd}}\right)\text{Df} - \overline{\text{Afa}}\left[\left(\frac{\text{Fa}}{\text{Aa}}\right) - \left(\frac{\text{Fd}}{\text{Dd}}\right)\left(\frac{\text{Da}}{\text{Aa}}\right)\right]\right)}{G\left[1 - \left(\frac{\text{Da}}{\text{Fa}}\right)\left(\frac{\text{Fd}}{\text{Dd}}\right)\right]} \tag{6}$$

$$\overline{\text{Dfd}} = \text{Df} + \text{FRET1}\left[1 - G\left(\frac{\text{Da}}{\text{Aa}}\right)\right] - \overline{\text{Afa}}\left(\frac{\text{Da}}{\text{Aa}}\right) \tag{7}$$

The equations consist of variables with two letters. The first letter stands for the used filter set (Table 2), and the second letter stands for the investigated sample (d = donor only, a = acceptor only, and f = FRET area). For example, Af therefore stands for the FRET region (bonded area) investigated with the acceptor filter set. The variables represent the measured light intensities from the aforementioned microscope images recorded as 16-bit gray values. Afa refers to the acceptor signal that would have been if no donor were present and, therefore, no FRET occurred. Similarly, Dfd refers to the donor signal that would have been if no acceptor were present and, therefore, no FRET occurred. eqs 5–7 are used to calculate a FRET intensity normalized by the amount of donor and acceptor signals. To ensure a properly normalized and dimensionless quantity, Xia and Liu used the Gordon algorithm to calculate the improved property NFRET (eq 8),[42] which we are using.

$$\text{NFRET} = \frac{\text{FRET1}}{\sqrt{\overline{\text{Afa}} \times \overline{\text{Dfd}}}} \tag{8}$$

The evaluation is performed pixelwise; i.e., for each pixel, an according NFRET value is calculated as the resulting NFRET intensity. G is an instrument and setup specific factor relating the loss of the donor signal to the increase of the acceptor signal. For thin films and the setup employed in this study, it amounted to 0.758.

To study NSC, a method was developed to select the appropriate area. The method consisted of manually drawing the bonded area (Figure 7, with regions of interest marked in magenta). Subsequently, we applied 5 pixel image erosion to remove the edge regions of the thin films, thus obtaining the eroded bonded area, which was then used for evaluation of FRET intensity. Removing the edge regions is necessary because regions of extreme NFRET intensity are appearing at the edges, which are a false-positive FRET signal.

Thin-Film Separation Energy. The z-direction tensile tests were performed in a ZwickRoell Z010 multipurpose tester (Kennesaw, GA, U.S.A.) equipped with two steel bars, in which only the upper steel bar moves, driven by a linear motor. The z-direction tensile tests were performed in a Zwick Roell Z010 (Kennesaw, GA, U.S.A.) equipped with lower and upper steel bars, in which the upper steel bar moves up

https://doi.org/10.1021/acsami.1c04226
ACS Appl. Mater. Interfaces XXXX, XXX, XXX–XXX

and down thanks to a linear motor. A double-sided adhesive tape is put on the upper and lower steel bars. After the sample is placed on the lower steel bar, the linear motor moves the upper steel bar down until it touches the sample. To guarantee good attachment of the sample at the steel bars, a defined compression force of 1.5 bar is applied. Then, the sample is pulled apart in the z direction until it fails between the two polymer thin films. The force F with respect to the separation distance x is recorded. The two main values for interpreting the tensile tests are the maximum tensile force and the separation energy. The separation energy is the integral of the force−distance curves.

AUTHOR INFORMATION

Corresponding Author

Ulrich Hirn − *Institute of Bioproducts and Paper Technology, 8010 Graz, Austria; CD Laboratory for Fiber Swelling and Paper Performance, 8010 Graz, Austria;* orcid.org/0000-0002-1376-9076; Phone: +43-0-316-873-30753; Email: ulrich.hirn@tugraz.at

Authors

Mónica G. Simões − *Institute of Bioproducts and Paper Technology, 8010 Graz, Austria; CD Laboratory for Fiber Swelling and Paper Performance, 8010 Graz, Austria*

Georg Urstöger − *Institute of Bioproducts and Paper Technology, 8010 Graz, Austria; CD Laboratory for Fiber Swelling and Paper Performance, 8010 Graz, Austria*

Robert Schennach − *CD Laboratory for Fiber Swelling and Paper Performance, 8010 Graz, Austria; Institute of Solid-State Physics, Graz University of Technology, 8010 Graz, Austria*

Complete contact information is available at: https://pubs.acs.org/10.1021/acsami.1c04226

Notes

The authors declare no competing financial interest.

ACKNOWLEDGMENTS

The authors thank the EU Horizon 2020 Program under Marie Sklodowska-Curie Grant Agreement 764713, ITN Project FibreNet. Furthermore, this research received funding from the Austrian Federal Ministry of Economy, Family and Youth and the Austrian National Foundation for Research, Technology and Development.

REFERENCES

(1) Lu, G.; Hong, W.; Tong, L.; Bai, H.; Wei, Y.; Shi, G. Drying Enhanced Adhesion of Polythiophene Nanotubule Arrays on Smooth Surfaces. *ACS Nano* **2008**, *2* (11), 2342−2348.

(2) Murphy, M. P.; Kim, S.; Sitti, M. Enhanced Adhesion by Gecko-Inspired Hierarchical Fibrillar Adhesives. *ACS Appl. Mater. Interfaces* **2009**, *1* (4), 849−855.

(3) Persson, B. N. J. On the Mechanism of Adhesion in Biological Systems. *J. Chem. Phys.* **2003**, *118* (16), 7614−7621.

(4) Le Saux, G.; Wu, M. C.; Toledo, E.; Chen, Y. Q.; Fan, Y. J.; Kuo, J. C.; Schvartzman, M. Cell-Cell Adhesion-Driven Contact Guidance and Its Effect on Human Mesenchymal Stem Cell Differentiation. *ACS Appl. Mater. Interfaces* **2020**, *12* (20), 22399−22409.

(5) Gong, G.; Zhou, C.; Wu, J.; Jin, X.; Jiang, L. Nanofibrous Adhesion: The Twin of Gecko Adhesion. *ACS Nano* **2015**, *9* (4), 3721−3727.

(6) Atkins, P.; de Paula, J. *Physical Chemistry for the Life Sciences*, 1st ed.; Oxford University Press: Oxford, U.K., 2006.

(7) Hirn, U.; Schennach, R. Comprehensive Analysis of Individual Pulp Fiber Bonds Quantifies the Mechanisms of Fiber Bonding in Paper. *Sci. Rep.* **2015**, *5* (July), 10503.

(8) Yang, C.; Persson, B. N. J. Molecular Dynamics Study of Contact Mechanics: Contact Area and Interfacial Separation from Small to Full Contact. *Phys. Rev. Lett.* **2008**, *100* (2), 1−4.

(9) Murphy, M. P.; Kim, S.; Sitti, M. Enhanced Adhesion by Gecko-Inspired Hierarchical Fibrillar Adhesives. *ACS Appl. Mater. Interfaces* **2009**, *1* (4), 849−855.

(10) Hu, S.; Xia, Z.; Gao, X. Strong Adhesion and Friction Coupling in Hierarchical Carbon Nanotube Arrays for Dry Adhesive Applications. *ACS Appl. Mater. Interfaces* **2012**, *4* (4), 1972−1980.

(11) Nolte, A. J.; Chung, J. Y.; Walker, M. L.; Stafford, C. M. In Situ Adhesion Measurements Utilizing Layer-by-Layer Functionalized Surfaces. *ACS Appl. Mater. Interfaces* **2009**, *1* (2), 373−380.

(12) Wang, Y.; Tian, H.; Shao, J.; Sameoto, D.; Li, X.; Wang, L.; Hu, H.; Ding, Y.; Lu, B. Switchable Dry Adhesion with Step-like Micropillars and Controllable Interfacial Contact. *ACS Appl. Mater. Interfaces* **2016**, *8* (15), 10029−10037.

(13) Persson, B. N. J.; Albohr, O.; Tartaglino, U.; Volokitin, A. I.; Tosatti, E. On the Nature of Surface Roughness with Application to Contact Mechanics, Sealing, Rubber Friction and Adhesion. *J. Phys.: Condens. Matter* **2005**, *17* (1), R1−R62.

(14) Persson, B. N. J.; Scaraggi, M. Theory of Adhesion: Role of Surface Roughness. *J. Chem. Phys.* **2014**, *141* (12), 124701.

(15) Füllbrandt, M.; Kesal, D.; Von Klitzing, R. Multiscaling Approach for Non-Destructive Adhesion Studies of Metal/Polymer Composites. *ACS Appl. Mater. Interfaces* **2015**, *7* (30), 16247−16256.

(16) Nitta, I. Measurements of Real Contact Areas Using PET Films (Thickness, 0.9 Mm). *Wear* **1995**, *181−183* (Part 2), 844−849.

(17) Bowen, R. C.; Demejo, L. P.; Rimai, D. S. A Method of Determining the Contact Area between a Particle and Substrate Using Scanning Electron Microscopy. *J. Adhes.* **1995**, *51* (1−4), 191−199.

(18) Pashazanusi, L.; Lwoya, B.; Oak, S.; Khosla, T.; Albert, J. N. L.; Tian, Y.; Bansal, G.; Kumar, N.; Pesika, N. S. Enhanced Adhesion of Mosquitoes to Rough Surfaces. *ACS Appl. Mater. Interfaces* **2017**, *9* (28), 24373−24380.

(19) Kim, H. J.; Kim, H. Y.; Jeong, H. D.; Lee, E. S.; Shin, Y. J. Friction and Thermal Phenomena in Chemical Mechanical Polishing. *J. Mater. Process. Technol.* **2002**, *130−131*, 334−338.

(20) Asunmaa, S.; Steenberg, B. Beaten Pulps and the Fibre-to-Fibre Bond in Paper. *Sven. Papperstidn.* **1958**, *61* (18B), 686−695.

(21) Kizuka, T.; Yamada, K.; Deguchi, S.; Naruse, M.; Tanaka, N. Cross-Sectional Time-Resolved High-Resolution Transmission Electron Microscopy of Atomic-Scale Contact and Noncontact-Type Scannings on Gold Surfaces. *Phys. Rev. B: Condens. Matter Mater. Phys.* **1997**, *55* (12), R7398−R7401.

(22) Alsem, D. H.; Sood, S.; Salmon, N.; Jacobs, T. D. B. In Situ Electrical Testing of Device-Relevant Nanocontacts in the Transmission Electron Microscope. *Microsc. Microanal.* **2016**, *22* (S3), 818−819.

(23) Jacobs, T. D. B.; Martini, A. Measuring and Understanding Contact Area at the Nanoscale: A Review. *Appl. Mech. Rev.* **2017**, *69* (6), No. 060802.

(24) Asif, S. A. S.; Wahl, K. J.; Colton, R. J. Mechanics Using Force Modulation. *Mater. Res.* **1999**, *594*, 471−476.

(25) Benz, M.; Rosenberg, K. J.; Kramer, E. J.; Israelachvili, J. N. The Deformation and Adhesion of Randomly Rough and Patterned Surfaces. *J. Phys. Chem. B* **2006**, *110* (24), 11884−11893.

(26) Persson, B. N. J.; Albohr, O.; Creton, C.; Peveri, V. Contact Area between a Viscoelastic Solid and a Hard, Randomly Rough, Substrate. *J. Chem. Phys.* **2004**, *120* (18), 8779−8793.

(27) Persson, B. N. J.; Tosatti, E. The Effect of Surface Roughness on the Adhesion of Elastic Solids. *J. Chem. Phys.* **2001**, *115* (12), 5597−5610.

(28) Persson, B. N. J. Adhesion between an Elastic Body and a Randomly Rough Hard Surface. *Eur. Phys. J. E: Soft Matter Biol. Phys.* **2002**, *8* (4), 385−401.

(29) Yang, C.; Tartaglino, U.; Persson, B. N. J. A Multiscale Molecular Dynamics Approach to Contact Mechanics. *Eur. Phys. J. E: Soft Matter Biol. Phys.* **2006**, *19* (1), 47−58.
(30) Urstöger, G.; Simoes, M. G.; Steinegger, A.; Schennach, R.; Hirn, U. Evaluating the Degree of Molecular Contact between Cellulose Fiber Surfaces Using FRET Microscopy. *Cellulose* **2019**, *26* (12), 7037−7050.
(31) Medintz, I.; Hildebrandt, N. *FRET—Föster Resonace Energy Tranfer*; Medintz, I., Hildebrandt, N., Eds.; Wiley-VCH Verlag: Weinheim, Germany, 2014.
(32) Wu, L.; Huang, C.; Emery, B. P.; Sedgwick, A. C.; Bull, S. D.; He, X. P.; Tian, H.; Yoon, J.; Sessler, J. L.; James, T. D. Förster Resonance Energy Transfer (FRET)-Based Small-Molecule Sensors and Imaging Agents. *Chem. Soc. Rev.* **2020**, *49* (15), 5110−5139.
(33) Shrestha, D.; Jenei, A.; Nagy, P.; Vereb, G.; Szöllősi, J. Understanding FRET as a Research Tool for Cellular Studies. *Int. J. Mol. Sci.* **2015**, *16* (4), 6718−6756.
(34) Sekar, R. B.; Periasamy, A. Fluorescence Resonance Energy Transfer (FRET) Microscopy Imaging of Live Cell Protein Localizations. *J. Cell Biol.* **2003**, *160* (5), 629−633.
(35) Zal, T.; Gascoigne, N. R. J. Using Live FRET Imaging to Reveal Early Protein-Protein Interactions during T Cell Activation. *Curr. Opin. Immunol.* **2004**, *16* (4), 418−427.
(36) Zhang, X.; Hu, Y.; Yang, X.; Tang, Y.; Han, S.; Kang, A.; Deng, H.; Chi, Y.; Zhu, D.; Lu, Y. FÖrster Resonance Energy Transfer (FRET)-Based Biosensors for Biological Applications. *Biosens. Bioelectron.* **2019**, *138* (April), 111314.
(37) Thomson, C.; Lowe, R.; Page, D.; Ragauskas, A. Exploring Fibre−Fibre Interfaces via FRET and Fluorescence Microscopy. *J. Pulp Pap. Sci.* **2008**, *33* (4), 113−120.
(38) Thomson, C. I.; Lowe, R. M.; Ragauskas, A. J. Imaging Cellulose Fibre Interfaces with Fluorescence Microscopy and Resonance Energy Transfer. *Carbohydr. Polym.* **2007**, *69* (4), 799−804.
(39) Thomson, C. I.; Lowe, R. M.; Ragauskas, A. J. First Characterization of the Development of Bleached Kraft Softwood Pulp Fiber Interfaces during Drying and Rewetting Using FRET Microscopy. *Holzforschung* **2008**, *62* (4), 383−388.
(40) Sahoo, H. Förster Resonance Energy Transfer—A Spectroscopic Nanoruler: Principle and Applications. *J. Photochem. Photobiol., C* **2011**, *12* (1), 20−30.
(41) Gordon, G. W.; Berry, G.; Liang, X. H.; Levine, B.; Herman, B. Quantitative Fluorescence Resonance Energy Transfer Measurements Using Fluorescence Microscopy. *Biophys. J.* **1998**, *74*, 2702−2713.
(42) Xia, Z.; Liu, Y. Reliable and Global Measurement of Fluorescence Resonance Energy Transfer Using Fluorescence Microscopes. *Biophys. J.* **2001**, *81* (4), 2395−2402.
(43) Thomson, C. I. Probing the Nature of Cellulosic Fibre Interfaces with Fluorescence Resonance Energy Transfer Probing the Nature of Cellulosic Fibre Interfaces with Fluorescence Resonance Energy Transfer. Ph.D. Thesis, Georgia Institute of Technology, Atlanta, GA, 2007.
(44) Urstöger, G.; Steinegger, A.; Schennach, R.; Hirn, U. Spectroscopic Investigation of DCCH and FTSC as a Potential Pair for Förster Resonance Energy Transfer in Different Solvents. *PLoS One* **2020**, *15* (2), e0228543.

https://doi.org/10.1021/acsami.1c04226
ACS Appl. Mater. Interfaces XXXX, XXX, XXX−XXX

4. Manuscript II

A system of FRET dyes designed to measure nano-scale contact between surfaces and its application to adhesion

A system of FRET dyes designed to measure nano-scale contact between surfaces and its application to adhesion

Mónica Gaspar Simões[a], Robert Schennach[b] and Ulrich Hirn[a,c]*

a – Institute of Bioproducts and Paper Technology, Inffeldgasse 23/EG, 8010 Graz, Austria.
b – Institute of Solid-State Physics, Graz University of Technology, Petersgasse 16, 8010 Graz, Austria.
c – CD Laboratory for Fiber Swelling and Paper Performance, Inffeldgasse 23/EG, 8010 Graz, Austria.
(*) corresponding author: Ulrich Hirn; Full postal address: Institute of Bioproducts and Paper Technology, Inffeldgasse 23/EG, 8010 Graz, Austria; Phone number: +43 (0)316 873-30753; Email address: ***ulrich.hirn@tugraz.at***

ABSTRACT

Adhesion is caused by intermolecular forces that only occur between surfaces at nano-scale contact (NSC) i.e., 0.1-0.4nm. To evaluate NSC and its influence on adhesion, Förster resonance energy transfer (FRET) spectroscopy has been used. FRET is a technique capable to measure nanometric distances between surfaces by taking advantage of the interaction amid some specific fluorescence molecules, named Donor and Acceptor. The Förster radius (R_0) of the FRET pair indicates the distance detection range ($0.5R_0$-$2R_0$) of the system and, must be selected considering the final purpose of each study.

Here, we propose a new FRET pair: 7-Amino-4-methyl-cumarin (C120) and 5(6)-Carboxy-2′,7′-dichlor-fluorescein (CDCF) with high quantum yield (QY, QY_{C120}=0.91 and QY_{CDCF}=0.64) and a distance range of 0.6-2.2nm (0.1 mM) specifically developed to measure NSC between soft surfaces. For this, polymeric thin films were bonded using different loads, from 1.5 to 150 bar, to create different degrees of NSC, analyzed by FRET spectroscopy, and later pulled apart to measure their interfacial separation energy/adhesion. Our experiments showed that NSC increases with the applied pressure in the bonded thin films, leading to higher FRET intensity and adhesion/separation energy. Thus, we have introduced a new FRET pair, suitable to measure the degree of NSC between surfaces and establish a linear relationship between FRET and adhesion; which can be of interest for any type of study with soft materials interfaces that include NSC and its influence on adhesion.

GRAPHICAL ABSTRACT

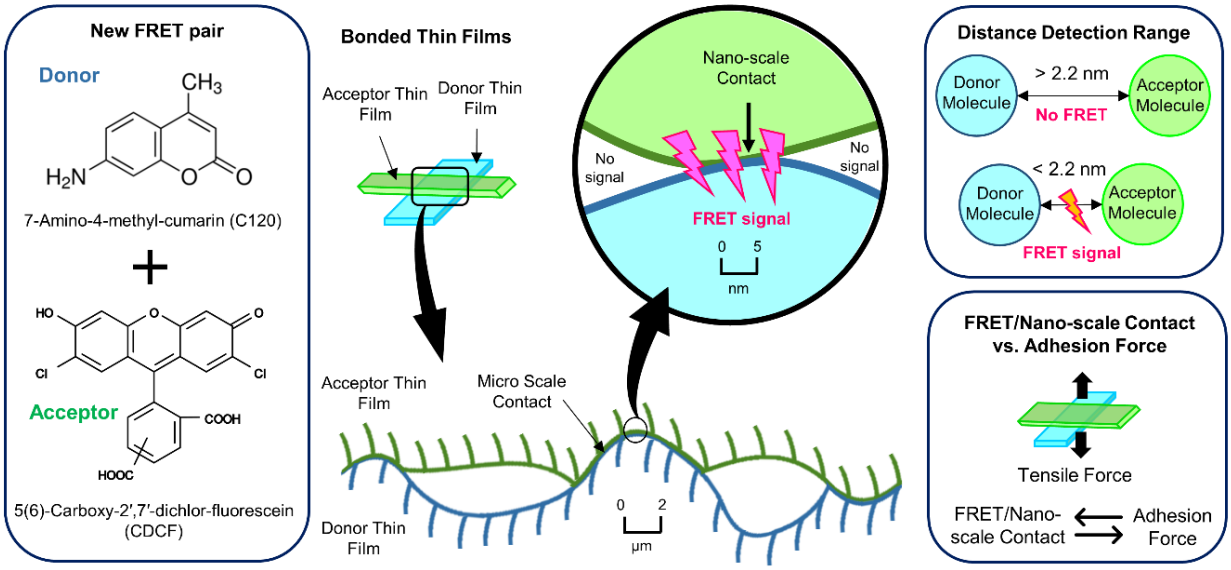

Keywords: nano-scale contact; adhesion force; fluorescence molecules; sensitive FRET pair; FRET spectroscopy; FRET distance range.

1. INTRODUCTION

The role of adhesion between soft surfaces is relevant in several areas of science, biology, and technology like e.g. contact mechanics and cellular adhesion [1–5]. It is created by intermolecular forces, as van der Waals and hydrogen bonding, that require nanometric scale among the adhering surfaces [6,7]. Thus, adhesion only occurs when the surfaces are in nano-scale contact (NSC) and it is directly influenced by the degree of NSC; since an increase in NSC improves adhesion [8–10].

Accordantly, NSC can only be properly evaluated using nano-scale working methods, as e.g., Förster Resonance Energy Transfer (FRET) spectroscopy, an experimental technique that can be used to measure the precise nanometric distance (0-20 nm) between surfaces in contact within that range [11–13]; commonly utilized in biomedical and biological applications to verify molecular contact in researches related to e.g. cellular or protein adhesion [14–17] and interdiffusion among polymeric materials [11].

Recently, it has been proposed to utilize FRET as a quantitative method to evaluate the degree of NSC [18], which can be applied to all kinds of research where adhesion or NSC are playing a role, for instance soft matter, lubricants, adhesives, or optical sensors for contact between soft interfaces .To study the interaction between surfaces in NSC, FRET uses a pair of compatible fluorescence dyes named Donor and Acceptor. The FRET distance detection range relies on the Förster Radius (R_0) of the dye system. Thus, between Donor and Acceptor labelled surfaces in NSC within 0.5 R_0-2 R_0, a non-radiative transfer of energy occurs from the Donor to the Acceptor molecules, and a FRET signal can be identified [18,19]. Figure 1 shows a schematic FRET spectroscopy experiment of the fluorescence emission spectra, collected for the dye surfaces alone (Figure 1A) and at NSC (Figure 1B) using the same excitation wavelength.

The FRET signal (Figure 1C) can be noticed when comparing the spectra of the individual dye surfaces with the spectrum of Donor-Acceptor surfaces in NSC, Donor intensity decreases, and Acceptor intensity increases (from I_A to I_{AD}). Through a FRET signal, it is possible to calculate the FRET efficiency (FRETeff) [19], which indicates the degree of NSC. Accordingly, this approach can also be applied between bonded thin films, Figure 2.

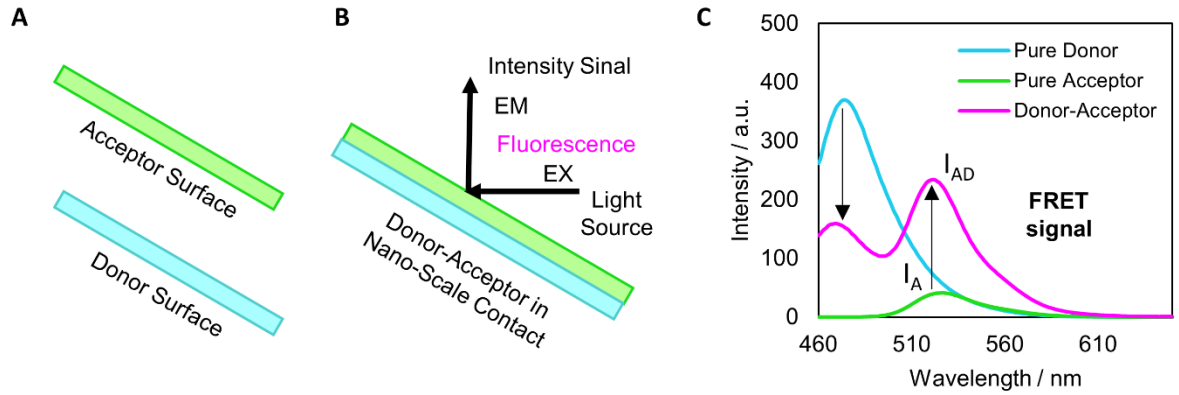

Figure 1 – FRET spectroscopy applied to surfaces in NSC: (A) Donor and Acceptor surfaces; (B) Donor and Acceptor surfaces in NSC (C) FRET signal with the pure Donor, Acceptor, and Donor−Acceptor in NSC fluorescence spectra, where Donor intensity drops and Acceptor intensity rises (from I_A to I_{AD}, see arrows) due to the Donor-Acceptor energy transfer.

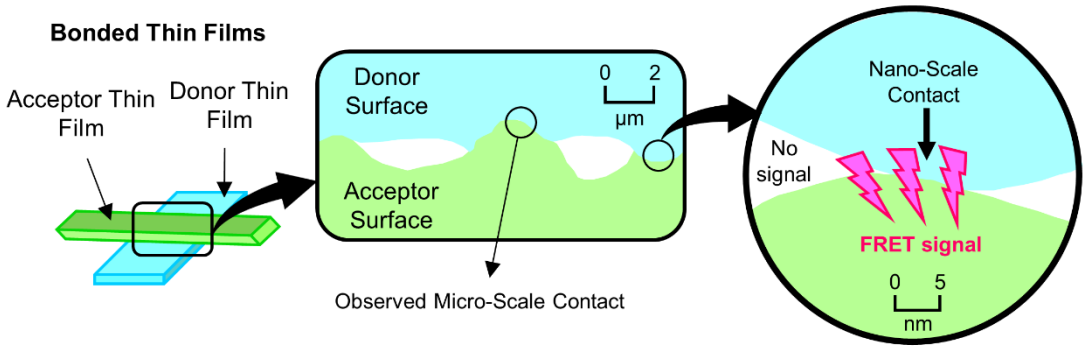

Figure 2 – Donor and Acceptor thin films in contact analyzed at micro- and nanometer scales. NSC decreases with higher magnification. For areas in NSC, a FRET signal can be detected. Above the FRET distance range of the system the transfer of energy does not occur, no FRET signal.

In that case, areas that look to be in complete contact at the micro-scale end up demonstrating no NSC when analyzed at the nanometric scale, and accordantly, in these zones, no FRET occurs (Figure 2). In the remaining areas where the surfaces are in NSC (0.5 R_0-2 R_0), it is possible to transfer energy from the Donor to the Acceptor molecules and detect a FRET signal.

Only very recently it has been shown that the NSC measured with FRET can be related to the adhesion force between soft materials [18]. The study revealed that for thin films pressed under different loads, the FRETeff and adhesion force increase with the applied pressure, caused by the correspondent increase of the degree of NSC [18]. Thus, FRET provides a suitable technique to quantify the degree of NSC on large - i.e. mm to cm-scale – measurement areas and for the correlation between FRET and adhesion in bonded surfaces, of any roughness, on statistically representative size scales. Additionally, it was demonstrated that FRET microscopy can not only be utilized for the same purpose but also for imaging NSC local variations [18].

1.1. Aim of the work

However, the FRET system applied in this initial work [18] was not designed to evaluate NSC, which brought up two issues: (1) the FRET interaction range was quite large, R_0=5.1nm. As the intermolecular forces (Van der Waals and hydrogen bonding) have an interaction range below 1nm, the FRET interaction distance should possibly be in this range when studying adhesion and (2) the poor sensitivity of the FRET pair of dyes employed in [18].

Therefore, a more suitable FRET system, optimized to study NSC and adhesion should present: (1) a Förster radius limited to the interaction range of hydrogen bonds and Van der Waals forces, i.e. 0.1-0.4nm [20,21], which is the range of intermolecular forces responsible for adhesion; and (2) a FRET pair of fluorescence dyes with high quantum yields (QYs) for higher FRET intensities, leading to a better signal to noise ratio, which is crucial to correctly evaluate the degree of NSC.

In this work, a new pair of FRET dyes with a low Förster radius, R_0=1.1nm (interaction range of 0.6 to 2.2nm), and an enhanced sensitivity (high quantum yield) has been developed. The suitability of the new FRET system for the measurement of NSC is demonstrated. Soft polymeric thin films are bonded together with increasing pressure, thus generating increasing degrees of NSC, and resulting adhesion. Therefore, a model system is created, where the degree of NSC is the only possible reason for variations in adhesion. By relating the NSC measured with FRET to the adhesion between the thin films (by evaluating the separation energy in tensile testing) we are demonstrating the expected relation between adhesion and NSC measured by FRET, thus presenting a new

system of FRET dyes particularly designed and optimized for evaluating NSC.

2. MATERIALS AND METHODS

2.1.*Förster theory.* The Förster theory was developed by Theodor Förster and presented in his original papers published from 1946 to 1965. The resume of his entire contribution to resonance energy transfer can be found in Igor Medintz and Niko Hildebrandt FRET handbook [22]. Briefly, the Förster theory allow us to explain the relationship between energy transfer, spectral overlap, and physical distance between compatible fluorescence molecules[22]. Hence, if the Donor and Acceptor molecules are close enough to each other, FRET will occur and FRET efficiency (FRETeff, %) can be calculated:

$$FRETeff = \frac{1}{1+(r/R_0)^6}\ (\%) \qquad (1)$$

where r (nm) is the Donor-Acceptor distance and R_0 (nm) the Förster Radius. R_0 only relies on the properties/medium conditions of the selected Donor-Acceptor molecules and determines the FRET detection distance range ($0.5R_0$-$2R_0$) of the system under study. A FRET signal can only be detected within $0.5R_0$-$2R_0$ nm, outside of this range Donor and Acceptor molecules are too close or too far apart for FRET to be detected. Following the instructions presented in the book by Medintz and Hildebrandt (chapter 5, pages 106-122)[19], R_0 can be written as:

$$R_0 = \left(\frac{9\ln(10)\,k^2 QY_{Donor}\,J}{128\,\pi^5 N_A n^4}\right)^{1/6} \quad (\text{nm}) \qquad (2)$$

where k is the orientation factor of the Donor-Acceptor dipoles (2/3), QY_{Donor} the Donor quantum yield, N_A is Avogadro's constant (6.02 214
$\times 10^{23}$ mol^{-1}), n the medium refractive index, and J the spectral overlap integral, on which FRET also depends. J can be calculated from:

$$J = \int f_D(\lambda)\,\epsilon_A(\lambda)\,\lambda^4\,d\lambda\ (\text{nm}^4\,\text{M}^{-1}\,\text{cm}^{-1}) \qquad (3)$$

where f_D is the normalized Donor emission spectrum, λ the wavelength (nm) and ε_A the Acceptor attenuation coefficient (M^{-1} cm^{-1}).
Equations 1 to 3 are the basis of the Förster Theory, demonstrating the dependency of FRETeff on r and R_0, and how it is possible to properly calculate r having knowledge about the FRET pair (R_0) and the amount of energy being transferred (FRETeff).

2.2.*Design of the FRET system.* The selection of the FRET pair (Donor and Acceptor fluorescence molecules) determines the performance of the FRET system. For a couple of fluorescence molecules to be considered as a FRET pair, they need to:

1) Have an appropriate interaction range (Förster radius R_0). The distance range of the FRET pair must fit the distance range of what is intended to be measured. For this work, it was desirable to find a FRET pair with low distance range sensitivity ($0.5R_0$-$2R_0$) as the intermolecular forces responsible for adhesion take place below 1nm.

2) Be spectroscopically compatible. For the design of a FRET pair, the fluorescence molecules must have lined-up energy bands, which means different, yet overlapping, Donor emission and Acceptor excitation spectra. Thanks to this spectral overlap, it is possible to study the molecules exact nanometric distance using the non-radiative energy transferred between them (Eq. 1). The area of the spectral overlap (J) will determine the R_0 (Eq. 2) and the distance range of the FRET system ($2R_0$). Larger overlap areas result in higher R_0, and accordantly, the contrary is also valid (Eq. 2 and 3). Here, we looked for a smaller spectral overlap area to attain a shorter and lower detection limit, more appropriated to estimate the degree of NSC amid bonded soft surfaces.

3) Present a high quantum yield (QY). The QY is the ratio between the number of photons emitted to the number of photons absorbed [23,24], indicating the capacity of the fluorescence dyes to absorb and emit light. Molecules with high QYs are easier to sense,

which results in higher intensity signals. Therefore, lower QYs make FRET signals (Figure 1) harder to be detected, which usually requires higher dye concentrations to overcome it. Therefore, in this study, a compatible pair of Donor and Acceptor molecules with high QYs was also preferable; especially considering that FRET was used to measure the NSC between non-even bonded thin films (Figure 2) pressed under different loads.

In addition, Donor and Acceptor molecules must be soluble in the same medium at the same molar concentration to allow some specific experiments of the method, for example, the mixture of both dyes in one thin film, used as a positive control.

For this study, and considering all aspects mentioned before, 7-Amino-4-methyl-cumarin (C120) and 5(6)-Carboxy-2′,7′-dichlor-fluorescein (CDCF) were selected as Donor and Acceptor molecules, respectively [25] (Figure 3). This FRET pair presents high QYs (QY_{Donor}=0.91 and $QY_{Acceptor}$=0.64), small spectra overlap area and thus, a low FRET distance range of 0.6-2.2nm (R_0=1.1nm, at the molar concentration of 0.1mM).

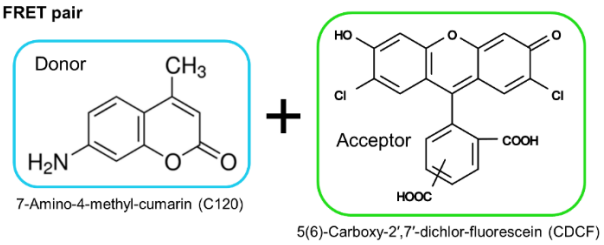

Figure 3 – FRET pair, Donor (7-Amino-4-methyl-cumarin, C120) and Acceptor (5(6)-Carboxy-2′,7′-dichlor-fluorescein, CDCF) chemical structures selected to evaluate NSC.

2.3.*Dye solutions and thin films preparation.* The FRET pair (Figure 3) fluorescence molecules C120 (Sigma-Aldrich, CAS:26093-31-2, USA) and CDCF (Sigma-Aldrich, CAS:111843-78-8, Switzerland) were dissolved in ethanol to prepare 0.1 mM Donor, Acceptor and mixed Donor-Acceptor (ratio of 1:1) solutions. Then, 100 µL of dye(s) solution was added to 500 µL of 10 % (m/v) pHema (Sigma-Aldrich, Mw 20 000 Da, CAS:25249-16-5, USA) solution in an ethanol/water-milliQ 95:5 (v/v). The polymer-dye solutions were doctor bladed over polyvinyl chloride carrier substrates with a bar film applicator (3M BYK-Gardner GmbH, Geretsried, Germany) [17] to form 1.5 µm thin films. [18]. To protect the dyes from unwanted quenching mechanisms or any other kind of light degradation, the dye solutions and thin films were prepared and handled in the dark and later protected in aluminum foil during the entire processes and experiments.

2.4.*Bonded Thin Films preparation.* For FRET spectroscopy the thin films were bonded by pressing 4 cm^2 of the pure Donor (D), pure Acceptor (A) and/or no dye/clean pHema thin films (H), as illustrated in Figure 4, at 1.5, 50, 100 and 150 bar for 10 min.

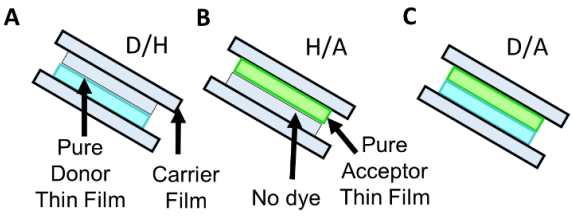

Figure 4 – Bonded thin films: (A) Donor/pHema (D/H), (B) pHema/Acceptor (H/A), and (C) Donor/Acceptor (D/A).

2.5.*FRET spectroscopy.* The thin films spectra were recorded with a Spectra Fluorophotometer RF-5301PC (Shimadzu, Kyoto, Japan) at 330 nm (excitation wavelength) in a 45°/45° configuration as shown in Figure 1B. The individual and bonded thin films spectra were analyzed for FRET signals and the FRETeff (%) was calculated using the Acceptor Sensitization method [18,22] (Eq. 4).

$$FRETeff = \left(\frac{I_{AD}}{I_A} - 1\right)\left(\frac{\varepsilon_A}{\varepsilon_D}\right) \quad (\%) \qquad (4)$$

where I_{AD} and I_A are the intensity peak values of the Acceptor in the presence and absence of the Donor, respectively (Figure 1C). For correct FRETeff results, the direct luminescence of I_A is

subtracted from I_{AD} and multiplied by the luminescence ratio of the Acceptor and Donor molar attenuation coefficients (ε_A and ε_D, $mol^{-1}.cm^{-1}.10^4$) at the excitation wavelength used for the FRET experiments (330 nm) [18,22]. ε_A and ε_D spectra (Figure 5B) were determined from the absorbance by Beer Lambert's Law (Eq. 5):

$$A = \varepsilon\, c\, l \quad (5)$$

where A is the absorbance, c the dye concentration (mM) and l the light path length (cm). For the absorbance spectra a Varian Cary, UV-vis spectrophotometer (Agilent Technologies, California, USA) was used.

2.6.*Thin film separation energy.* The tensile tests were performed in a ZwickRoell Z010 multi-purpose tester (Georgia, USA) as shown in Figure 5 and described in [18]. From each experiment a force-distance curve was recorded, from which the maximum tensile force can be identified. And finally, the separation energy per unit area of the bonded thin films was calculated using the integral of the corresponding curves.

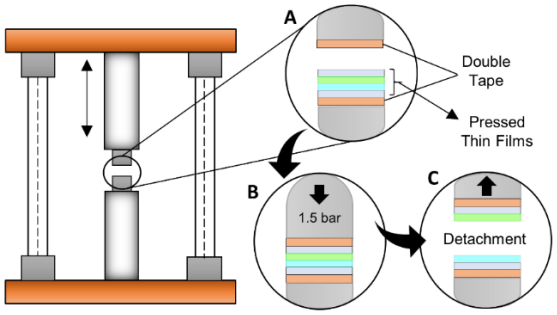

Figure 5 – Separation energy (adhesion intensity) tensile tests on the Donor-Acceptor bonded thin films: (A) – a double-sided adhesive tape is put on the upper and the lower steel bars of the equipment and the sample is placed on the lower steel bar; (B) – the linear motor moves the upper steel bar down until it touches the sample, (C) – the sample is pulled apart in z-direction until failure amid the two bonded thin films.

3. RESULTS AND DISCUSSION

To study the influence of NSC on adhesion force, we used bonded thin films pressed under different loads. The goal was to observe an increase in FRET intensity and adhesion force with NSC caused by the increased pressure applied on the bonded thin films.
First, the selected fluorescence molecules were studied as a potentially suitable FRET pair to detect NSC. Then, the performance of the FRET pair was tested as a FRET system in individual thin films (positive control). The final validation was done by testing the new FRET system with the bonded thin films.

3.1. Characterization of the FRET System

The FRET system not only depends on the FRET pair of fluorescence dyes but also, on the conditions in which it is used [18,22]. Thus, before doing the experiments with the bonded thin films, it was necessary to analyze the dyes as a FRET pair and the resulting thin films as a viable FRET system [11,18].
For the FRET pair, 7-Amino-4-methyl-cumarin (C120, Donor) and 5(6)-Carboxy-2′,7′-dichlor-fluorescein (CDCF, Acceptor) were the selected fluorescence dyes (Figure 3). The Donor C120 and the Acceptor CDCF present a QY of 0.91 and 0.64, respectively, which are considered high [23,24] and suitable QYs for a FRET study [22], especially to evaluate adhesion between bonded thin films that include non-uniform NSC areas (Figure 2).
For the fluorescence spectra, the FRET pair was analyzed in 2.5 µL ethanol solutions (Figure 6A) and in pHema thin films produced by doctor blading at 0.1mM (Figure 1 and 6B).

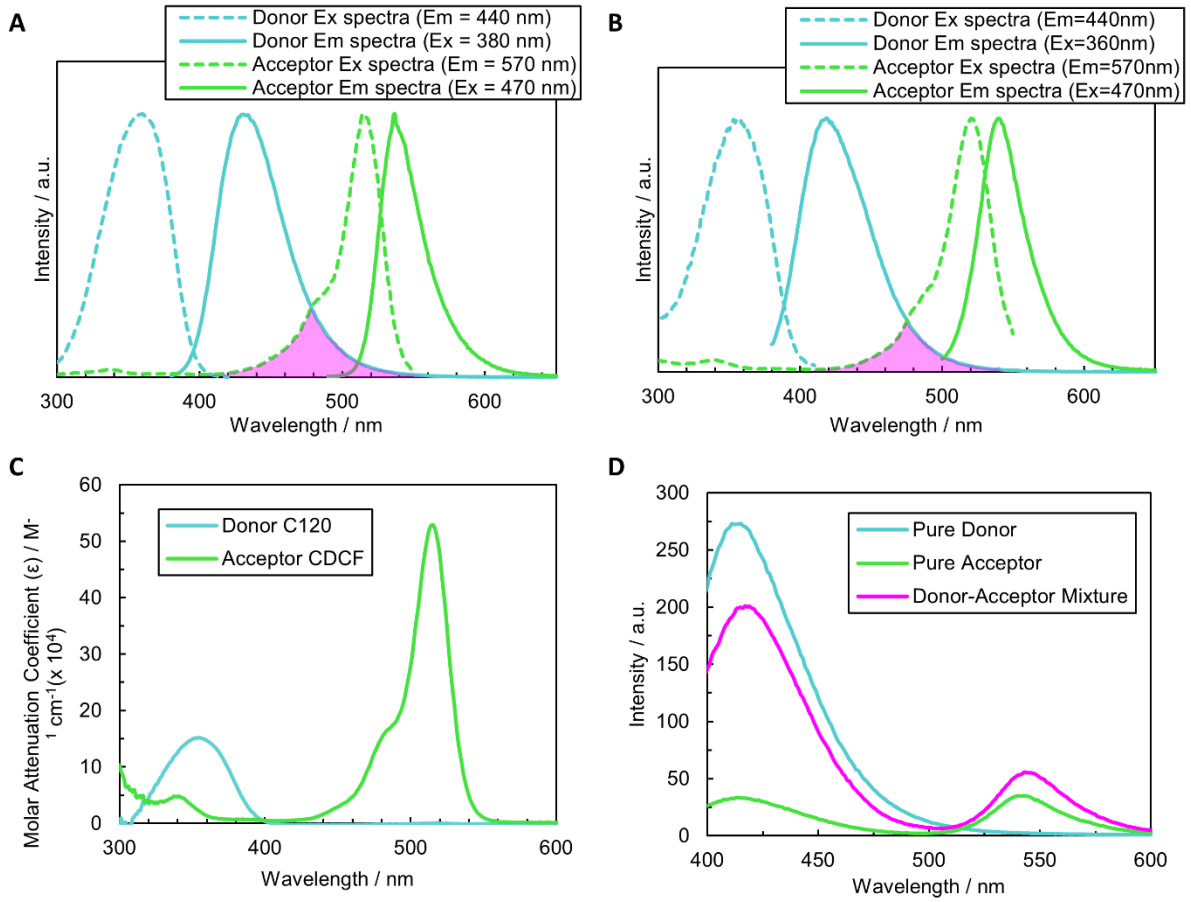

Figure 6 – Donor (C120) and Acceptor (CDCF) as a FRET pair: (A) fluorescence emission and excitation spectra of the dyes in ethanol at 2.5 µM (spectra overlap marked in violet); (B) fluorescence emission and excitation spectra of the (0.1mM) thin films (spectra overlap marked in violet); (C) molar attenuation coefficient spectra and (D) pure Donor, pure Acceptor, and Donor-Acceptor mixture thin films emission fluorescence spectra (Ex = 330 nm, $\varepsilon_A/\varepsilon_D$ = 0.41).

When compared, a slight variation between the emission and excitation spectra of the Acceptor in solution and the polymeric thin films can be noticed (Figure 6A and 6B). Such changes between the same molecules in different environments, influenced by the medium, concentration and thickness (light path), are expected. In this case, the thin films end up presenting a slightly smaller spectral overlap (Figure 6A and 6B, violet marked areas) than the ethanol solution. Nevertheless, in both cases, the overlap between the Donor emission and Acceptor excitation spectra, on which FRET depends, was confirmed. Moreover, both spectral overlap areas are not large, which indicates a small Förster Radius (R_0) and FRET distance range ($0.5R_0$-$2R_0$), as intended.

The ε_D and ε_A spectra (Figure 6C), determined from the Donor and Acceptor absorbance spectra (Eq. 5), indicate the dyes ability to absorb the light and the intervals where both dyes can be investigated using the same excitation wavelength.

At the C120/CDCF molar concentration of 0.1mM, the results showed a FRET distance range ($0.5R_0$-$2R_0$) [22] of 0.6-2.2 nm (R_0 = 1.1 nm, Eq. 2), which allowed us to improve our method to study the degree of NSC by reducing its detection limit and getting closer to the range of interaction of the intermolecular forces responsible for adhesion force.

As a reference/positive control we produced a Donor-Acceptor mixed thin film, where it was possible to make sure that both molecules are

entrapped in the same polymeric matrix, at nanometric distances. [11,18]. Therefore, this thin film represents the minimum distance between the molecules and the maximum FRETeff the system can reach at 0.1mM.

The fluorescence spectra were collected at 330 nm excitation, $\varepsilon A/\varepsilon D = 0.41$, where both can absorb light (Figure 6C). And Figure 6D depicts the pure Donor, pure Acceptor, and Donor-Acceptor mixed thin films spectra, where a FRET signal can be observed (Donor intensity drops and Acceptor intensity rises). From which the maximum FRETeff of the new FRET system was calculated by the Acceptor sensitization method (Eq.4), which yielded 24.5%. A high signal intensity, beside the low molar concentration of the dyes (0,1 mM), demonstrates that the high QYs of the chosen FRET pair molecules has led to an expected improvement in the FRET intensity of the dyes.

3.2. Validation of NSC measurement with FRET

To validate FRET as an experimental technique to measure NSC between soft surfaces, bonded dyed polymeric thin films were pressed together with several loads, from 1.5 to 150 bar. Pressing the thin films leads to an increase in NSC and a consequent increase in adhesion (i.e., separation energy), which later can be used to correlate FRET intensity with adhesion and demonstrate that the new FRET system works for NSC measurements.

The samples were produced by bonding pure Donor (D), pure Acceptor (A), and no dye/clean polymeric (H) thin films, as demonstrated in Figure 4 with the Donor in the back and Acceptor in the front position, in every experiment. Where D/H, H/A and D/A are the Donor-pHema, Acceptor-pHema, and Donor-Acceptor thin films combinations, respectively (Figure 4). Figure 7 depicts the bonded thin films fluorescence spectra pressed from 1.5 to 150 bar. To calculate the FRETeffs (Table 1) we used the Acceptor sensitization method (Eq.4) [11,22], which only relies on the Acceptor response to the nanometric presence and proximity of the Donor. Analyzing the fluorescence spectra, FRET signals (Figure 7) and FRETeffs (Table 1) altogether, our experiments reveal that when the pressure during bonding of the thin films increases, the FRET signals (Figure 7), and their relative FRETeffs (Table 1) also increase accordingly. For 1.5 bar the measured FRETeff was 0 %, indicating no NSC within $0.5R_0$-$2R_0$ (0.6-2.2 nm), and for 150 bar (maximum bonding pressure) the FRETeff was 12.4 % (Table 1). Moreover, all bonded thin films FRETeffs are lower than the positive control (Donor-Acceptor mixture thin film, with a FRETeff of ~ 25 %), since for the bonded surfaces there are no molecules mixed in the polymeric matrix. Furthermore no dye migration or interdiffusion at these pressure/temperature conditions is observed [11,18], so the transfer of energy only occurs on the interface between the thin films, and the FRET signals derive exclusively from their proximity, i.e. nanoscale contact.

Table 1 - FRETeff, maximum tensile force and separation energy per unit area of the positive control and bonded thin films. Values are average ± 95 % confidence interval (n=3 for FRETeff and n=10 for tensile force and separation energy).

Sample	FRETeff (%)	Maximum Tensile Force (N)	Separation energy per unit area (mJ/cm^2)
D-A Mixture	24.5 ± 0.9	-	-
D/A 1.5 bar	0.0 ± 0.0	18.7 ± 1.2	0.09 ± 0.02
D/A 50 bar	2.1 ± 0.5	25.1 ± 1.1	0.17 ± 0.01
D/A 100 bar	8.3 ± 1.6	32.6 ± 1.6	0.22 ± 0.01
D/A 150 bar	12.4 ± 1.4	41.8 ± 2.3	0.30 0.03

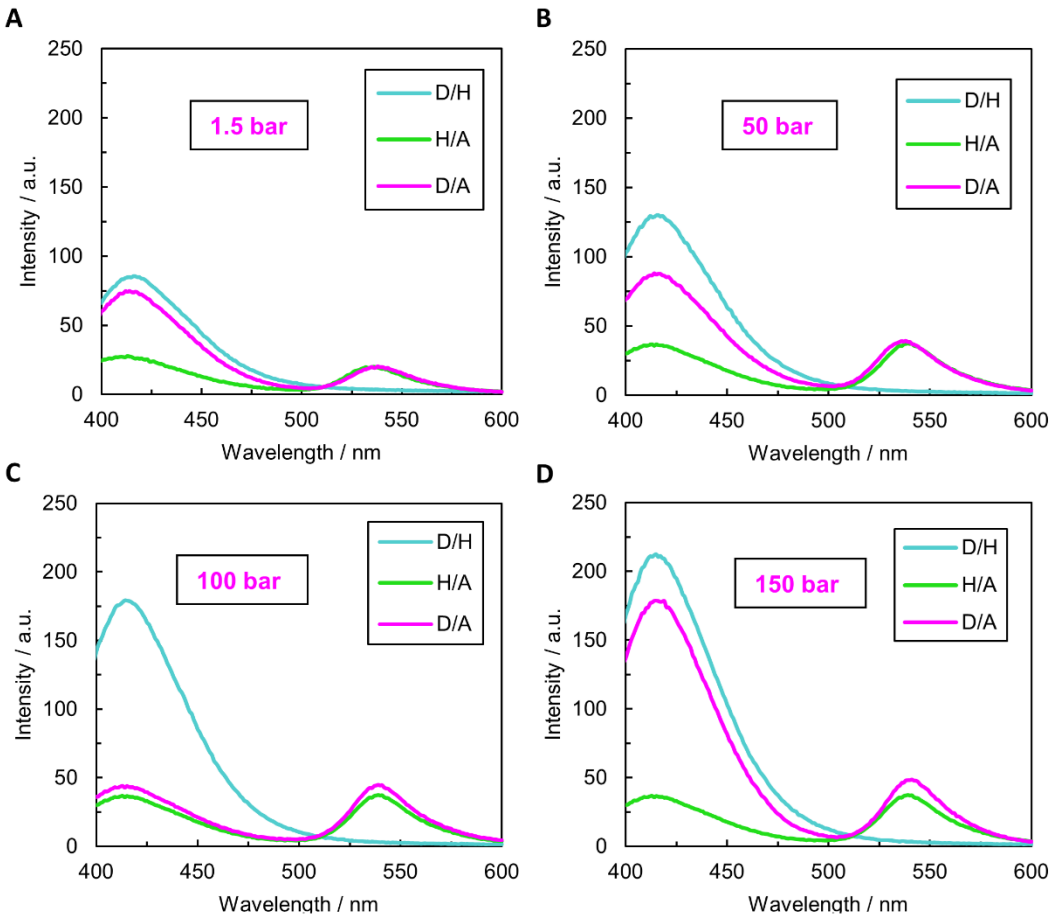

Figure 7 – Emission fluorescence spectra of the Donor (C120) and Acceptor (CDCF) 0.1 mM bonded thin films with increasing bonding pressure of (A) 1.5 bar, (B) 50 bar, (C) 100 bar and (D) 150 bar (Ex = 330 nm, $\varepsilon_A/\varepsilon_B$ = 0.41).

Finally, the influence of NSC on surface adhesion, measured by FRET spectroscopy was analyzed. First, the bonded thin films were separated by z-directional tensile testing to determine the separation energy and maximum adhesion force. The results showed that both parameters increase, with the increasing pressure applied to bonded thin films (Table 1), due to a higher degree of NSC and adhesion force. The separation energy per unit area was calculated by the integral of the tensile test force-displacement curves (Figure 8A) [18]. The bonded surfaces FRETeffs and correspondent adhesion force (separation energy per unit area) were plotted together in Figure 8B. The adhesion force linearly increases with the increase of FRETeff, Figure 8, demonstrating that the new pair of FRET dyes is appropriate for our FRET system/method to study and quantify NSC surface adhesion.

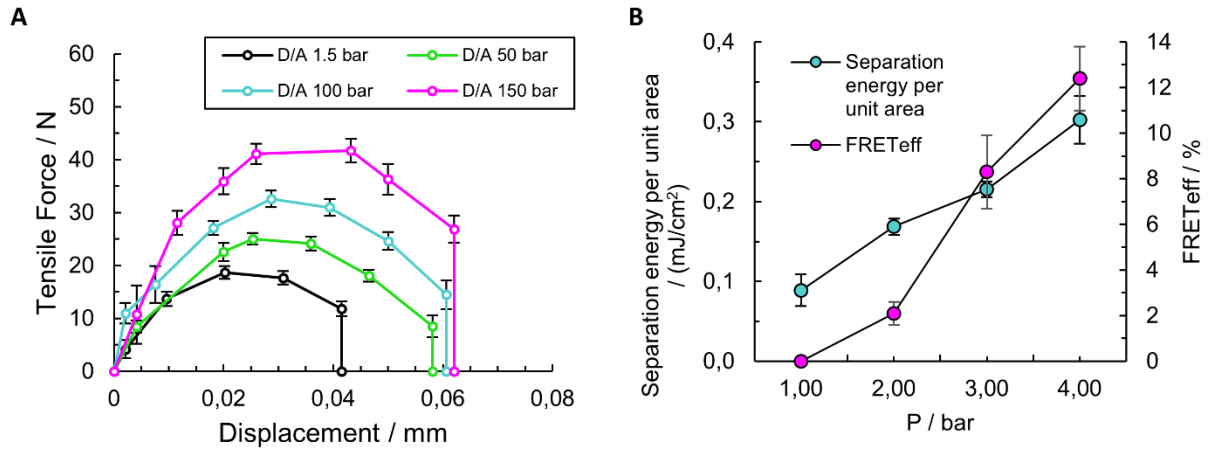

Figure 8 - FRETeff and separation energy per unit area of the Donor/Acceptor bonded thin films pressed with 1.5 to 150 bar. The presented results refer to mean average ± 95 % confidence interval, n=3.

4. CONCLUSIONS

In this work we have introduced a new system of FRET dyes (C120 and CDCF) specifically designed and optimized to quantify the degree of nanoscale contact between surfaces. The novel FRET system is characterized by a Förster radius of 1.1nm, enabling it to detect NSC between surfaces for an interaction distance of 0.6-2.2nm. Moreover, the chosen FRET dyes have a high quantum yield, which permits the use of lower dye concentrations and improves the method's sensitivity.

For its validation as a viable FRET system to quantify NSC, we used polymer thin films bonded with several loads (from 1.5 to 150 bar). The results showed a linear increase in FRET intensity and adhesion (dissipated energy to separate the films) with the pressure applied to bond the thin films. Both, increasing adhesion and increasing FRET signal, are caused by increasing NSC due to the pressing, revealing a direct correlation between NSC, measured by FRET, and adhesion.

Our findings are presenting a refined and optimized experimental approach to study nanoscale contact between soft surfaces using FRET. It can be used to study NSC and its impact on diverse contact mechanics phenomena (adhesion, friction and interdiffusion), which might be useful for applications like e.g. tribology, natural and synthetic adhesives, sealants and optical pressure sensors.

5. FUNDING

This work was supported by the EU Horizon 2020 program under Marie Sklodowska-Curie Grant Agreement No. 764713, ITN Project FibreNet.

6. REFERENCES

[1] G. Lu, W. Hong, L. Tong, H. Bai, Y. Wei, G. Shi, Drying enhanced adhesion of polythiophene nanotubule arrays on smooth surfaces, ACS Nano. 2 (2008) 2342–2348. https://doi.org/10.1021/nn800443m.

[2] M.P. Murphy, S. Kim, M. Sitti, Enhanced adhesion by gecko-inspired hierarchical fibrillar adhesives, ACS Appl. Mater. Interfaces. 1 (2009) 849–855. https://doi.org/10.1021/am8002439.

[3] B.N.J. Persson, On the mechanism of adhesion in biological systems, J. Chem. Phys. 118 (2003) 7614–7621. https://doi.org/10.1063/1.1562192.

[4] G. Le Saux, M.C. Wu, E. Toledo, Y.Q. Chen, Y.J. Fan, J.C. Kuo, M. Schvartzman, Cell-Cell Adhesion-Driven Contact Guidance and Its Effect on Human Mesenchymal Stem Cell Differentiation, ACS Appl. Mater. Interfaces. 12 (2020) 22399–22409.

https://doi.org/10.1021/acsami.9b20939.

[5] R. Ungai-Salánki, B. Csippa, T. Gerecsei, B. Péter, R. Horvath, B. Szabó, Nanonewton scale adhesion force measurements on biotinylated microbeads with a robotic micropipette, J. Colloid Interface Sci. 602 (2021) 291–299. https://doi.org/10.1016/j.jcis.2021.05.180.

[6] M. Raftari, Z.J. Zhang, S.R. Carter, G.J. Leggett, M. Geoghegan, Nanoscale Contact Mechanics between Two Grafted Polyelectrolyte Surfaces, Macromolecules. 48 (2015) 6272–6279. https://doi.org/10.1021/acs.macromol.5b01540.

[7] M. Benz, K.J. Rosenberg, E.J. Kramer, J.N. Israelachvili, The deformation and adhesion of randomly rough and patterned surfaces, J. Phys. Chem. B. 110 (2006) 11884–11893. https://doi.org/10.1021/jp0602880.

[8] S. Hu, Z. Xia, X. Gao, Strong adhesion and friction coupling in hierarchical carbon nanotube arrays for dry adhesive applications, ACS Appl. Mater. Interfaces. 4 (2012) 1972–1980. https://doi.org/10.1021/am201796k.

[9] A.J. Nolte, J.Y. Chung, M.L. Walker, C.M. Stafford, In situ adhesion measurements utilizing layer-by-layer functionalized surfaces, ACS Appl. Mater. Interfaces. 1 (2009) 373–380. https://doi.org/10.1021/am8000874.

[10] Y. Wang, H. Tian, J. Shao, D. Sameoto, X. Li, L. Wang, H. Hu, Y. Ding, B. Lu, Switchable Dry Adhesion with Step-like Micropillars and Controllable Interfacial Contact, ACS Appl. Mater. Interfaces. 8 (2016) 10029–10037. https://doi.org/10.1021/acsami.6b01434.

[11] G. Urstöger, M.G. Simoes, A. Steinegger, R. Schennach, U. Hirn, Evaluating the degree of molecular contact between cellulose fiber surfaces using FRET microscopy, Cellulose. 0123456789 (2019) 7037–7050. https://doi.org/10.1007/s10570-019-02575-x.

[12] L. Wu, C. Huang, B.P. Emery, A.C. Sedgwick, S.D. Bull, X.P. He, H. Tian, J. Yoon, J.L. Sessler, T.D. James, Förster resonance energy transfer (FRET)-based small-molecule sensors and imaging agents, Chem. Soc. Rev. 49 (2020) 5110–5139. https://doi.org/10.1039/c9cs00318e.

[13] B.W. van der Meer, Förster Theory, in: FRET – Förster Reson. Energy Transf., John Wiley & Sons, Ltd, 2013: pp. 23–62. https://doi.org/https://doi.org/10.1002/9783527656028.ch03.

[14] D. Shrestha, A. Jenei, P. Nagy, G. Vereb, J. Szöllősi, Understanding FRET as a research tool for cellular studies, Int. J. Mol. Sci. 16 (2015) 6718–6756. https://doi.org/10.3390/ijms16046718.

[15] R.B. Sekar, A. Periasamy, Fluorescence resonance energy transfer (FRET) microscopy imaging of live cell protein localizations, J. Cell Biol. 160 (2003) 629–633. https://doi.org/10.1083/jcb.200210140.

[16] T. Zal, N.R.J. Gascoigne, Using live FRET imaging to reveal early protein-protein interactions during T cell activation, Curr. Opin. Immunol. 16 (2004) 418–427. https://doi.org/10.1016/j.coi.2004.05.019.

[17] X. Zhang, Y. Hu, X. Yang, Y. Tang, S. Han, A. Kang, H. Deng, Y. Chi, D. Zhu, Y. Lu, FÖrster resonance energy transfer (FRET)-based biosensors for biological applications, Biosens. Bioelectron. 138 (2019) 111314. https://doi.org/10.1016/j.bios.2019.05.019.

[18] M.G. Simões, G. Urstöger, R. Schennach, U. Hirn, Quantification and Imaging of Nanoscale Contact with Förster Resonance Energy Transfer, ACS Appl. Mater. Interfaces. (2021). https://doi.org/10.1021/acsami.1c04226.

[19] N. Hildebrandt, How to Apply FRET: From Experimental Design to Data Analysis, in: FRET – Förster Reson. Energy Transf., John Wiley & Sons,

Ltd, 2013: pp. 105–163. https://doi.org/https://doi.org/10.1002/9783527656028.ch05.

[20] P. Atkins, J. de Paula, Physical Chemistry for the Life Sciences, 1st ed., Oxford University Press, Oxford, 2006.

[21] U. Hirn, R. Schennach, Comprehensive analysis of individual pulp fiber bonds quantifies the mechanisms of fiber bonding in paper, Sci. Rep. 5 (2015) 10503. https://doi.org/10.1038/srep10503.

[22] I. Medintz, N. Hildebrandt, FRET - Föster Resonace Energy Tranfer: From Theory to Applications, 1st ed., WILEY-VCH Verlag, Weinheim, Germany, 2014.

[23] J.C. Zwinkels, P.C. DeRose, J.E. Leland, Chapter 7 - Spectral Fluorescence Measurements, in: T.A. Germer, J.C. Zwinkels, B.K. Tsai (Eds.), Spectrophotometry, Academic Press, 2014: pp. 221–290. https://doi.org/https://doi.org/10.1016/B978-0-12-386022-4.00007-8.

[24] T.K. Christopoulos, E.P. Diamandis, Chapter 14 - Fluorescence Immunoassays, in: E.P. Diamandis, T.K. Christopoulos (Eds.), Immunoassay, Academic Press, San Diego, 1996: pp. 309–335. https://doi.org/https://doi.org/10.1016/B978-012214730-2/50015-7.

[25] G.Y. Wiederschain, The Molecular Probes handbook. A guide to fluorescent probes and labeling technologies, Biochem. 76 (2011) 1276. https://doi.org/10.1134/S0006297911110101.

5. Manuscript III

Functionalizing Surfaces by Physical Vapor Deposition to Measure Nano-Scale Contact using FRET

Functionalizing Surfaces by Physical Vapor Deposition to Measure Nano-Scale Contact using FRET

Mónica Gaspar Simões, Katrin Unger, Anna Maria Coclite, Robert Schennach and Ulrich Hirn*

Authors information

Mónica G. Simões - Institute of Bioproducts and Paper Technology, Inffeldgasse 23, 8010 Graz, Austria
Katrin Unger - Institute of Solid-State Physics, Graz University of Technology, Petersgasse 16, 8010 Graz, Austria
Anna Maria Coclite - Institute of Solid-State Physics, Graz University of Technology, Petersgasse 16, 8010 Graz, Austria
Robert Schennach - CD Laboratory for Fiber Swelling and Paper Performance, Inffeldgasse 23, 8010 Graz, Austria and Institute of Solid-State Physics, Graz University of Technology, Petersgasse 16, 8010 Graz, Austria
Corresponding Author (*) Ulrich Hirn - Institute of Bioproducts and Paper Technology and CD Laboratory for Fiber Swelling and Paper Performance, Inffeldgasse 23, 8010 Graz, Austria; Phone: +43 (0)316 873-30753; Email: ***ulrich.hirn@tugraz.at***

GRAPHICAL ABSTRACT

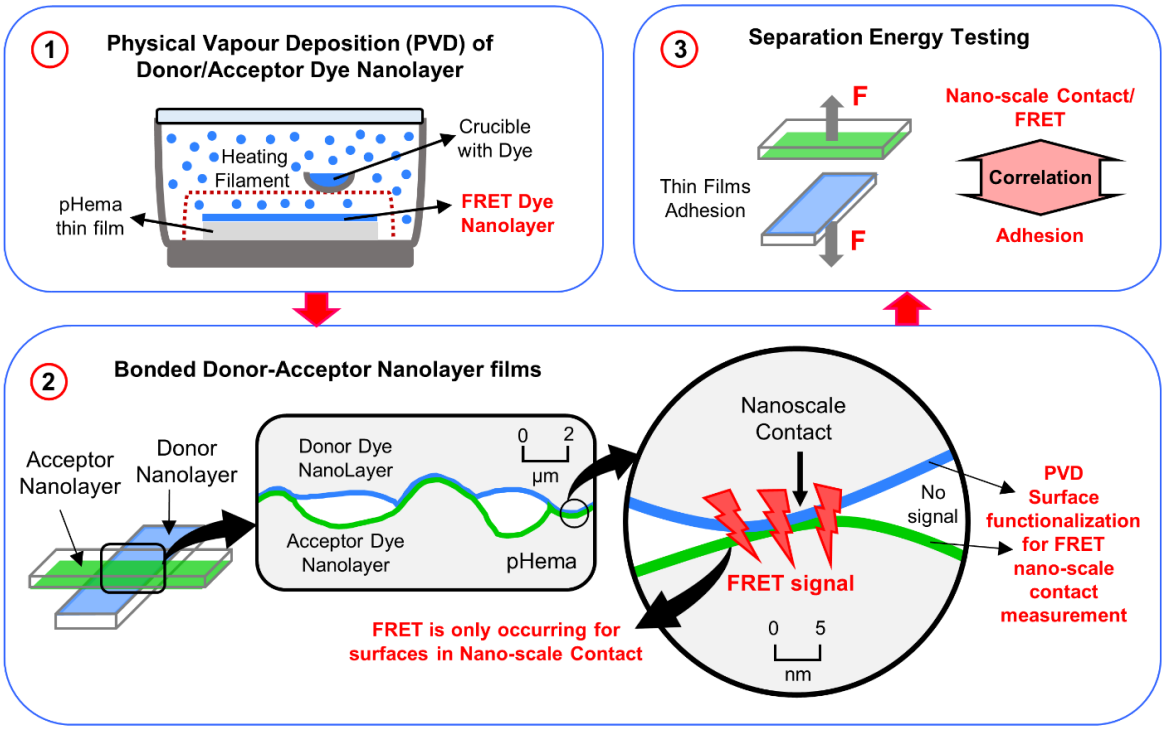

KEYWORDS: adhesion; nano-scale contact; FRET spectroscopy; physical vapor deposition; dye-nanolayer; FRET-adhesion correlation.

ABSTRACT

Adhesion between solid materials is caused by a network of intermolecular forces, like hydrogen bonds and Van der Waals interactions, that only take place if the adhering surfaces are at nano-scale contact (NSC) i.e. 0.1-0.4 nm. To study adhesion, NSC can be evaluated with Förster Resonance Energy Transfer (FRET). FRET uses the interaction of compatible fluorescence molecules to measure the nanometric distance between bonded surfaces. For this, each surface is labeled with one fluorescence dye, named Donor or Acceptor. If these molecules are close enough to each other i.e. in NSC, a non-radiative Donor-Acceptor energy transfer will occur and can be detected using FRET spectroscopy. Here, we introduce a new concept of a FRET-based NSC measurement employing dye-nanolayer films prepared by physical vapor deposition (PVD).

The dye nanolayers were prepared by PVD from the vaporization of the Donor and Acceptor molecules separately. The selected molecules, 7-Amino-4-methyl-cumarin (C120) and 5(6)-Carboxy-2′,7′-dichlor-fluorescein (CDCF) present high quantum yields (QY, QY_D=0.91 and QY_A=0.64) and a low FRET distance range of 0.6-2.2 nm, adequate for the study of NSC. The produced dye-nanolayer films exhibit a uniform dye distribution (verified by AFM) and suitable fluorescence intensities.

For the validation of the NSC measurements, FRET spectroscopy experiments were performed with bonded dye-nanolayer films prepared under different loads (from 1.5 to 140 bar), thus creating different degrees of NSC. The results show an increase of FRET intensity (R^2 = 0.95) with the respective adhesion energy between the films, which is directly related to the degree of NSC.

This work represents a novel concept to establish FRET as an experimental technique for the measurement of NSC, and its relation to surface adhesion. Most importantly, with the FRET dye nanolayer approach, the method can be employed on arbitrary surfaces. Essentially, any sufficiently transparent substrate can be functionalized with FRET compatible dyes to evaluate NSC, which represents a breakthrough in contact mechanics investigations on soft and hard solid materials.

INTRODUCTION

Measurement of NSC between Surfaces using FRET

Surface adhesion is essential in several engineering applications, contact mechanics, and biological systems[1–3]. It is caused by intermolecular forces, like hydrogen bonds and Van der Waals interactions, that only take place if the adhering surfaces are in nano-scale contact (NSC) i.e. 0.1-0.4 nm[4–8]. Therefore, the adhesion between two surfaces is proportional to its degree of NSC, and can only be properly investigated if the associated NSC is correctly evaluated[9].

Förster Resonance Energy Transfer (FRET) has recently been introduced as an experimental technique for the measurement of NSC between soft surfaces[10]. FRET takes advantage of the fluorescence properties of specific compatible molecules to determine their exact nanometric distance (0-20 nm)[11]. Thus, if these molecules, named Donor and Acceptor, are in NSC, a non-radiative Donor → Acceptor energy transfer will occur and, a FRET intensity can be detected[12,13]. The FRET distance range depends on the Förster Radius (R_0) of the FRET system under study and can only be properly sensed between $0.5R_0$ and $2R_0$[12]. Above $2R_0$, the Donor and Acceptor molecules are simply too distant for FRET interaction. And bellow $0.5R_0$ the dyes are too close to each other, which can lead to orbital overlapping and electron exchange (Dexter transfer)[14]. Resulting in an energy transfer in both directions: Donor ↔ Acceptor; which invalidates any FRET measurement[13,14].

To employ this technique between surfaces in NSC, each interface needs to be labeled with the Donor or Acceptor dye (Figure S1)[10]. Due to the natural roughness of any surface, the NSC is not complete[15]. Instead, areas that look to be in full contact at the micro-scale end up revealing opens gaps at the nanometric scale[16]. Thus, the areas in NSC are usually overestimated (Figure S1). However, with FRET only within areas in NSC ($0.5R_0$-$2R_0$) a FRET signal can be detected[13]. And for the open gaps, above $2R_0$, no FRET (Figure S1) can be noticed. In practice, the surfaces in NSC can be analyzed by FRET spectroscopy to follow the spectral effect of FRET on the Donor and Acceptor molecules. A FRET signal (Figure 1) can be identified when, comparing the spectra of the individual dye surfaces with the spectrum of Donor-Acceptor surfaces in NSC, Donor intensity decreases (from I_D to I_{DA}), and Acceptor intensity increases (from I_A to I_{AD}) due to the Donor → Acceptor energy transfer. Through a FRET signal, it is possible to calculate the FRET efficiency (FRETeff)[12,13], which indicates the degree of NSC.

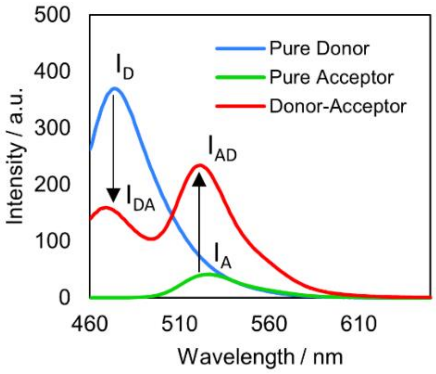

Figure 1 – FRET signal with the pure Donor (I_D) and Acceptor (I_A) without NSC between the dye. In case of NSC Donor intensity drops (from I_D to I_{DA}) and Acceptor intensity rises (from I_A to I_{AD}) due to the Donor-Acceptor energy transfer (see arrows).

Recently it was demonstrated that the NSC measured with FRET correlates to the adhesion between soft materials[10]. The studies showed that for bonded thin films pressed under different loads, the FRETeff and adhesion increase with the applied pressure, caused by the correspondent increase of the degree of NSC[10]. Introducing FRET as a proper technique to quantify the degree of NSC and establish a relation between FRET and adhesion in bonded films.

PVD of FRET-Dye Nanolayers to measure NSC between Arbitrary Surfaces

In the original approach, the dyes were mixed in soft thin films, which allow us to produce uniform and well distributed dye films, use exact dye concentrations, and study/develop different FRET systems for the measurement of NSC. However, to do this both fluorescence molecules must be soluble in the same solvent and miscible in polymeric solution at the same molar concentration[10]. A group of requirements that reduces the applicability of several FRET pairs and the method itself. Moreover, utilizing these films the dye molecules were not only present in the interface between the thin films, where FRET can occur within $0.5R_0$-$2R_0$, but through the entire polymeric matrix of the thin films (Figure 2A); causing noise and hurting the detected FRET signals (low signal to noise ratio)[17], due to the excess of luminescence/noise from all the molecules present in the system that are not involved in FRET, but still captured in the fluorescence measurements.

Therefore, one most suitable system should only have Donor and Acceptor molecules on the interface of the films, to reduce the noise from the polymeric matrix of the films. To increase the signal-to-noise ratio, making it easier to detect smaller FRET signals and thus, enhance the sensitivity of the method[18] for the measurement of NSC and associated adhesion.

In this work was develop a new FRET system with dye-nanolayer films, prepared by physical vapor deposition (PVD). PVD is a coating technique mostly utilized in nanoscience for the fabrication of functional nanolayers; where the molecules are vaporized and condensate over a substrate at the atomic level employing a combination of high vacuum and temperatures[19–21]. It can be used to form single-crystalline Si layers on glass substrates[22], metal monolayers for semiconductors[23] or biosensors, and surface modifications[24].

For this research, the Donor and Acceptor molecules are separately vaporized and deposited over clean polymeric thin films. By functionalizing the films with this approach all dye molecules are concentrated at the surface and noise from the bulk will not occur (Figure 2B). Moreover, any Donor and Acceptor molecules with low saturation pressure can be deposited over other types of transparent films/substrates, enhancing the applicability of the method.

For the experiments we used a FRET pair, specially designed by us for the measurement of NSC. The FRET pair is composed of 7-Amino-4-methyl-cumarin (C120, Figure 3A) as the Donor dye and 5(6)-Carboxy-2′,7′-dichlor-fluorescein (CDCF, Figure 3B) as the Acceptor dye.

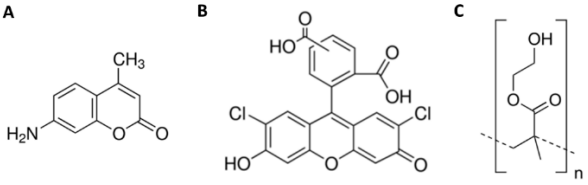

Figure 3 – (A) Donor, C120; (B) Acceptor, CDCF and (C) pHema (thin films material) chemical structures.

Both molecules present high quantum yields (QY, QY_D=0.91 and QY_A=0.64) and a FRET distance range from 0.6 to 2.2 nm (at 0.1 mM); suitable for the study of NSC and adhesion caused by intermolecular forces that only occur at low nanometric distances (bellow 1nm). The C120 and CDCF nanolayers are deposited over poly(2-hydroxyethyl methacrylate) (pHema, Figure 3C) thin films by PVD. The Donor- and Acceptor-nanolayer films are bonded with increasing pressure, creating increasing degrees of NSC, and subsequent adhesion. Therefore, the degree of NSC is the only driving force for adhesion. Linking the NSC measured with FRET to the adhesion between the dye-nanolayer films (by evaluating the separation energy in tensile testing) we are proving the expected relation between FRET and adhesion; employing a new FRET system specially developed to evaluate surface interactions at short nanometric distances with high precision.

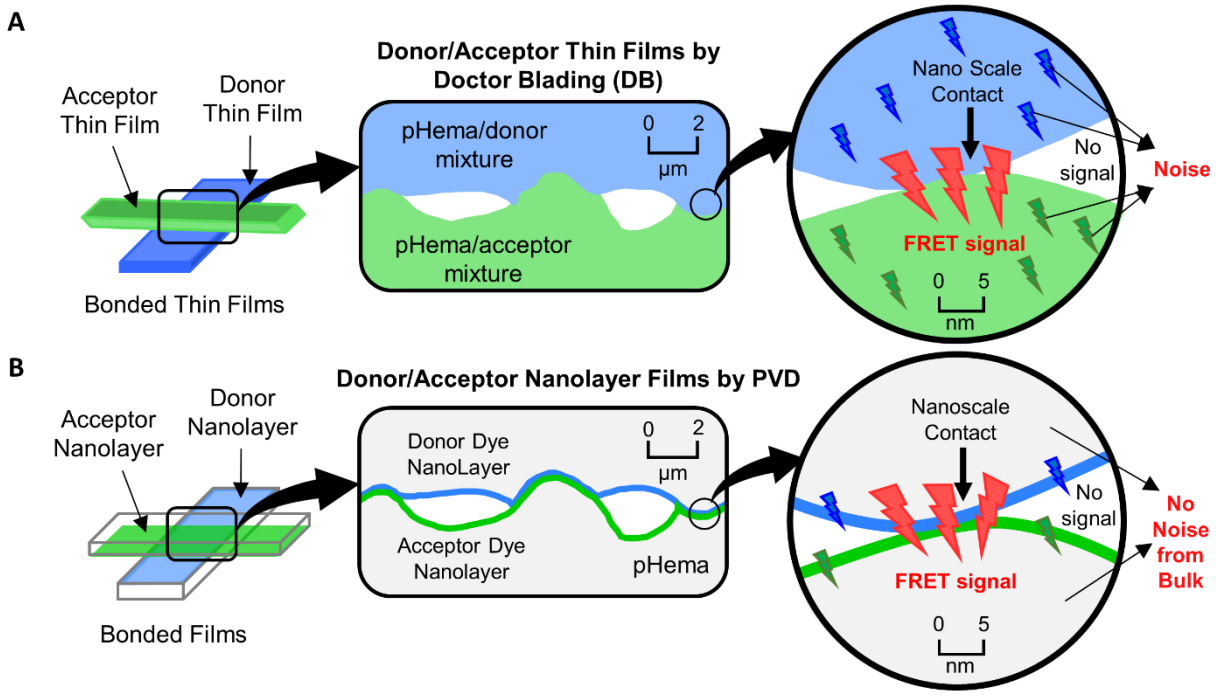

Figure 2 – Bonded films in close contact observed at micrometer and nanometer scale. Contact area decreases with increasing magnification. For areas in NSC, a FRET signal can be detected. Above the FRET distance range of the system, the transfer of energy does not occur. There is no FRET signal. (A) Donor and Acceptor bonded thin films prepared by DB, where the dyes were previously dissolved in the films. Donor and Acceptor molecules can be found through the entire bulk of the film (1.5 µm thickness) and excess fluorescence intensity (not FRET related noise) is detected during the FRET measurements; (B) Donor- and Acceptor nanolayer bonded films prepared by PVD, where the dyes can only be found in the material surface, where the NSC and FRET occur. No fluorescence noise from the bulk is detected.

RESULTS AND DISCUSSION

To apply our FRET method on arbitrary surfaces, a new FRET system based on dye-nanolayer films was developed. The dye nanolayers were prepared by PVD from the vaporization of the Donor and Acceptor molecules[20]. Any sufficiently transparent substrates can be functionalized with a dye-nanolayer of FRET dyes to evaluate NSC and surface adhesion.

The FRET dyes employed in this work present a high quantum yield and small spectral overlap, which results in a low Förster Radius (2.2 nm at 0.1mM) and FRET distance range (0.6-2.2 nm). This pair of FRET dyes was specifically designed to study interactions that occur at short nanometric distances, as is the case for the intermolecular forces responsible for adhesion. Another reason to choose C120 and CDCF as FRET dyes was a suitably low vapor pressure of the molecules that they could be vaporized in the PVD.

Here, were prepared bonded Donor-Acceptor nanolayer films under a series of different loads to measure FRET. With this, the main objective was to create different degrees of NSC and adhesion, since the nanometric distance between the soft/pressure-sensitive films is decreasing in the function of the applied load.

Later, the resulting FRET signals were compared with the energy necessary to separate the bonded dye-nanolayer films in Z-direction tensile tests. And therefore, validate the new system as an

appropriate FRET method for the measurement of NSC.

Dye Nanolayer Films

The dye-nanolayer films used in the FRET experiments consisted of a substrate (pHema thin film) and a dye (Donor or Acceptor) nanolayer. Accordantly, the films were prepared in two steps: (1) 1.5 µM pHema thin films were formed by doctor blading, and (2) the dye-nanolayers were deposited over the pHema thin films by PVD. For the deposition, the Donor and Acceptor molecules were vaporized using a combination of high temperatures and low pressure in a custom-built PVD chamber, as demonstrated in Figure 4. (all details in the Materials and Methods PDV section).

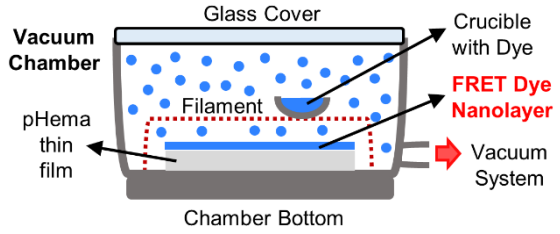

Figure 4 – Schematic representation the PVD chamber used for the preparation of the dye-nanolayers.

After the procedures, the surface of the untreated and treated films was analyzed by atomic force microscopy (AFM). Figure 5 shows the topography of the original pHema thin film (A) and the Donor-nanolayer (B) and Acceptor-nanolayer (C) films. The topography looks similar (Figure 5A-C), and their correspondent roughness (A: 25 ± 6 nm; B: 25 ± 6 nm and C: 23 ± 6 nm, values are average in the ± 95 % confidence interval, n=3), are equivalent, showing that the PVD procedure did not alter the surface morphology of the films; which indicates that the deposited dye-nanolayers are uniform and well distributed.

Moreover, the uniform deposition of the dye molecules can also be confirmed by the fluorescence spectra of the films. When comparing the spectra of C120 and CDCF dissolved in pHema (Figure 6A) with the PVD films spectra (Figure 6B), both present similar excitation and emission intensity peaks. The Donor fluorescence spectra are virtually the same, and only the Acceptor spectra show some wavelength shift (Figure 6A and 6B). In the Acceptor-nanolayer film, the excitation and emission spectra are closer to each other. Such changes between the same molecules in different environments, influenced by the medium, concentration and thickness (light path), are expected[25].

This may have been caused by the long exposure to high temperatures and low vacuum pressure during the PVD, which definitely can interfere with the substrate transparency and fluorescence spectra precision.

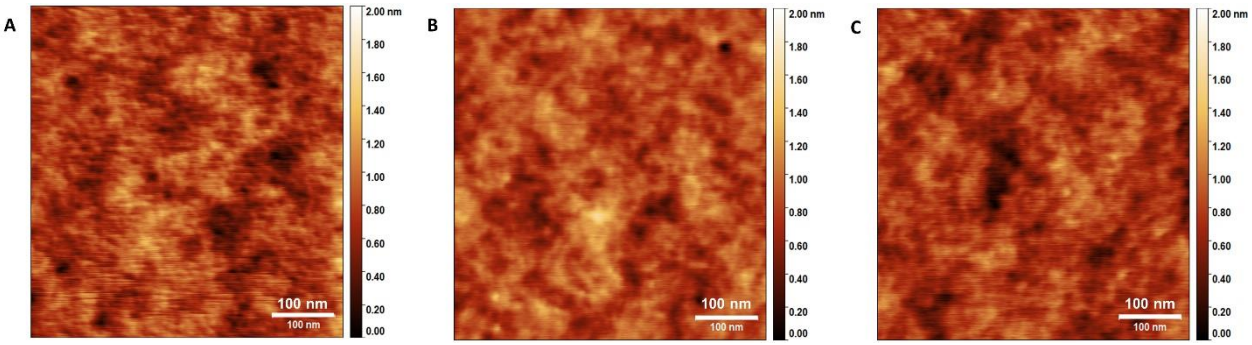

Figure 5 – AFM topography imagens of the (A) pHema, (B) Donor-nanolayer and (C) Acceptor-nanolayer films.

Another possible explanation is the large size of the Acceptor molecules, harder to vaporize and distribute than the Donor, complicating the formation of a smooth dye-nanolayer. Nevertheless, the AFM images demonstrate low and similar roughness for all films.

In addition, there is the possibility of some chemical interaction between the dyes and pHema and its eventual effects on the fluorescence spectra should not be discarded. During PVD no initiator or catalyzer was used to enhance the reactivity of the molecules. However, the C120 and CDCF molecules (Figure 3A-C) present several reactive groups (C120: $-CH_3$ and $-NH_2$; and CDCF: -Cl, -OH and -COOH) available to react with the pHema (containing -OH and -COOH reactive groups). In particular, the $-NH_2$ and -Cl in the C120 and CDCF, respectively, are located in the extremities of the molecules and are less stable/more reactive at higher temperatures and low pressure, as in the PVD procedure applied in this study. Therefore, we cannot confirm or deny any chemical bonding between the deposited nanolayer of dye molecules and the pHema surface. As well as its possible interference on the dye-nanolayer films, in particular, the Acceptor one.

Nevertheless, the dye-nanolayer films present a spectral overlap between the Donor emission and Acceptor excitation spectra (Figure 6B, marked in orange), on which FRET depends. That is identical to the one observed in the dye-dissolved pHema films (Figure 6A, marked in orange), demonstrating their equal capacity for FRET.

In summary, we have demonstrated that PVD is working for the functionalization of substrate surfaces with nanolayers of FRET dyes. Spectroscopic characterization revealed that the Donor and Acceptor-nanolayers fulfill the requirements to produce a FRET signal when being brought to a close distance around the estimated Förster Radius of 1 nm.

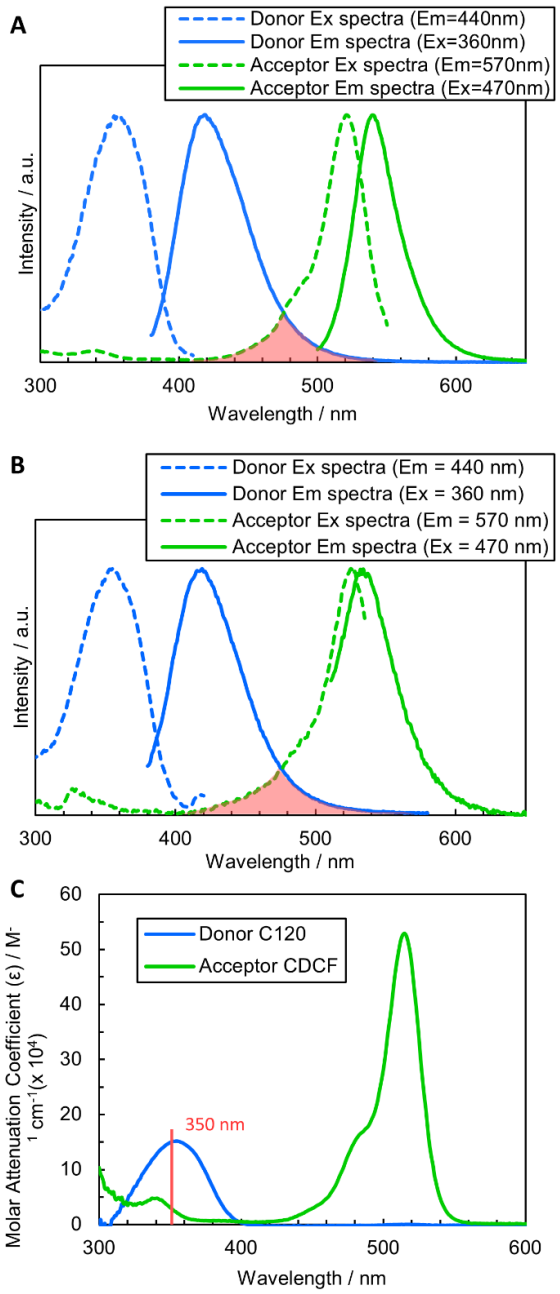

Figure 6 – Excitation and emission fluorescence spectra of the (A) Donor- and Acceptor-dissolved pHema thin films and (B) Donor- and Acceptor-nanolayer films. The spectral overlap between Donor emission and Acceptor excitation is marked in orange. (C) Molar attenuation coefficient (ε) spectra of the Donor- and Acceptor-dissolved pHema thin films. For FRET measurements, the samples were excited at 350 nm ($\varepsilon_A/\varepsilon_D$ = 0.21).

FRET measurements

The FRET nanolayer system was analyzed by FRET spectroscopy. For this, the Donor and Acceptor-nanolayer films were bonded together with several ascending loads, from 1.5 to 140 bar. Increasing pressure leads to an increase in the degree of NSC and a subsequent increase in adhesion. The samples were produced by bonding pure Donor-nanolayer (D), pure Acceptor-nanolayer (A), and no dye/clean pHema (H) films, as demonstrated in Figure 7. Where D/H, H/A and D/A are the Donor-pHema, Acceptor-pHema, and Donor-Acceptor thin films combinations, respectively (Figure 7). In the fluorescence spectrometer, all experiments were carried out keeping a consistent arrangement of the films, with Acceptor in the front and Donor in the back position in relation to the light source, which was in a 45º/45º configuration (Figure 7).

As the molar concentration of the dyes in the nanolayer films is unknown, for these FRET experiments we used the molar attenuation coefficients spectra (ε) of the Donor- and Acceptor thin films with dyes dissolved in pHema 0.1 mM (Figure 6C). The ε spectra are necessary to identify the wavelength intervals where both dye molecules can be excited using the same excitation wavelength, which is a FRET requirement[12,13]. Moreover, the ratio $\varepsilon_A/\varepsilon_D$ is later used to determine the FRET efficiency (FRETeff, Eq. 3, Materials and Methods section), which is the measure for the detected FRET signal and, hence, the degree of NSC[12,13]. The FRET excitation wavelength must be selected to have a high ε_D because the Donor molecules need enough light to be excited and transfer energy to the Acceptor. On the contrary, ε_A must be lower since the Acceptor will receive extra energy from the Donor. Still, ε_A cannot be too low since it also needs to be excited for the FRET. Accordantly, the fluorescence spectra for the dye-nanolayer films were collected at 350 nm excitation, where the ratio $\varepsilon_A/\varepsilon_D$ = 0.21 (see Figure 6C).

Figure 8A-F depicts the bonded Donor/Acceptor-nanolayer films emission spectra bonded together with pressures from 50 to 140 bar.

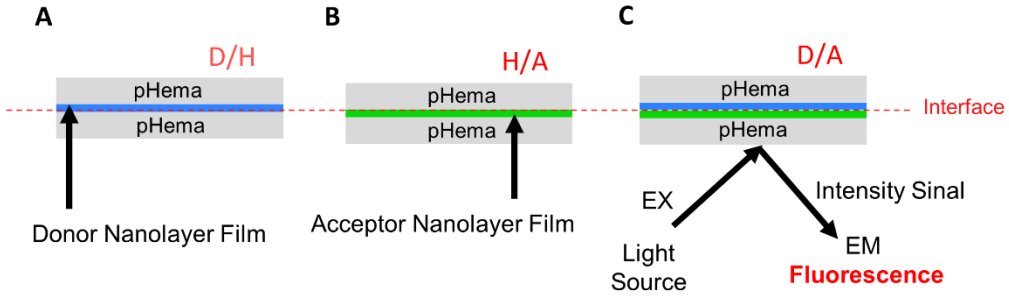

Figure 7 - Bonded dye-nanolayer films: (A) Donor/pHema (D/H), (B) pHema/Acceptor (H/A), and (C) Donor/Acceptor (D/A).

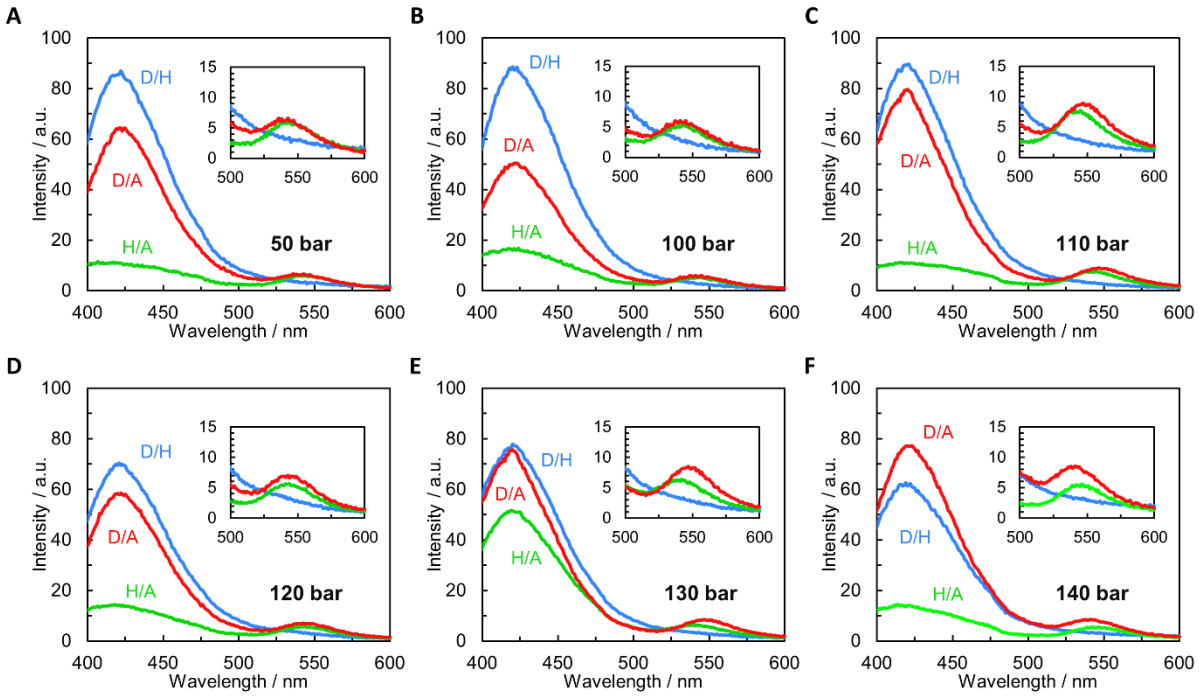

Figure 8 - Emission fluorescence spectra of the Donor- and Acceptor-nanolayer bonded thin films with increasing bonding pressure of (A) 50 bar, (B) 100 bar, (C) 110 bar, (D) 120 bar, (E) 130bar and (F) 140 bar (excited at 350 nm, $\varepsilon_A/\varepsilon_B = 0.21$).

From 50 to 130 bar (Figure 8A-E) a standard FRET performance, with Donor Quenching (from I_D to I_{DA}, Figure 1) and Acceptor Sensitization (from I_A to I_{AD}, Figure 1), can be observed. However, a shift from the normal Donor-FRET behavior can be noticed for a bonding pressure of 140 bar (Figure 8F). Here, the Donor intensity increases when in the presence of the Acceptor, against what is expected during FRET due to the Donor → Acceptor energy transfer (Figure 8F). This phenomenon can occur when the Donor and Acceptor molecules are too close to each other, below $0.5R_0$, it is called Dexter Transfer. Being so close there is a high chance of orbital overlapping, which can result in electron exchange between the Donor and Acceptor molecules, and energy transfer in both directions occurs: Donor ↔ Acceptor. Thus, instead of a traditional FRET Donor intensity decrease, caused by Donor quenching (Figure 8A-E) we have the Donor intensity rise as can be observed in Figure 8F.

The fact that we can observe Dexter transfer with this FRET system may be related to the dye-nanolayer films. Because in this new approach, the Donor and Acceptor molecules are no longer distributed through the entire polymeric matrix of the thin films (Figure 2A), but only on the pHema surface (Figure 2B). Thus, all the dye-nanolayer molecules are concentrated in the interface between the bonded films, accessible for FRET and physically closer, which can explain the presence of Dexter transfer (contact below $0.5R_0 = 0.6$ nm) within films boned under 140 bar (Figure 8F). This result confirms the sensitivity of the method due to the development of a FRET pair/system specially designed and optimized for the measurement of NSC. Considering that no dye migration or interdiffusion at these pressure conditions (room temperature) is observed, so the transfer of energy only occurs on the interface between the dye-nanolayer films, and the FRET signals derive exclusively from their proximity, i.e. NSC.

Nevertheless, from 1.5 to 130 bar a standard FRET performance, with Donor Quenching and Acceptor Sensitization, can be observed (Figure 8 and Table 1). The FRETeffs from 1.5 to 140 bar (Table 1), were calculated with the Acceptor sensitization method (Eq.4, see Materials and Methods section), which only relies on the Acceptor molecule's response to the nanometric presence and proximity of the Donor dye[10,26,27]. For 1.5 bar the measured FRETeff was 0 %, indicating no NSC within $0.5R_0$-$2R_0$. On the other hand, for 130 bar the FRETeff was ~ 6 % (Table 1), a high FRET signal intensity, especially considering that the molar concentration of the dyes is low (below 0.1 mM) and nonequal.

Table 1 – FRET signal intensity **(**FRETeff), maximum tensile force and separation energy per unit area of the bonded nanolayer films under different loads. Values are averages ± 95 % confidence interval (n=3 for FRET efficiency, and n=4 for tensile force and separation energy).

D/A bonding pressure (bar)	FRETeff (%)	Maximum Tensile Force (N)	Separation Energy per Unit Area (mJ/cm²)
1.5	0	10.3 ± 0.5	0.05 ± 0.00
50	2.5 ± 0.6	20.2 ± 2.8	0.13 ± 0.02
100	3.1 ± 0.8	30.0 ± 3.0	0.24 ± 0.03
110	3.3 ± 0.9	39.8 ± 3.6	0.35 ± 0.04
120	4.9 ± 0.7	47.8 ± 5.5	0.45 ± 0.07
130	5.9 ± 0.9	52.2 ± 0.7	0.51 ± 0.01
140	10.2 ± 1.2	76.3 ± 3.8	0.84 ± 0.05

Analyzing the fluorescence spectra, FRET signals and FRETeffs altogether (Figure 8 and Table 1), our experiments reveal that when the pressure to bond the Donor/Acceptor-nanolayer films increases, the FRET signals, and their relative FRETeffs also increase accordingly.

Correlation between NSC and adhesion

In order to validate the measurement of NSC using FRET, we measured the adhesion between the nanolayer films, which was created by the NSC between the surfaces, and correlate it to the measured FRET signals. Thus, the bonded films were separated by z-directional tensile testing to determine the separation energy and maximum adhesion force. The results showed that both parameters increase, with the increasing pressure applied to bonded dye-nanolayer films (Table 1), due to a higher degree of NSC and adhesion force. The separation energy per unit area was calculated by the integral of the tensile test force-displacement curves (Figure S2). The bonded surfaces FRETeffs and correspondent adhesion (separation energy per unit area) were plotted together in Figure 9. FRETeff linearly increases with the separation energy/adhesion (Figure 9). Demonstrating that by functionalization of surfaces with FRET dye-nanolayers the degree of NSC between these surfaces can indeed be measured using FRET spectroscopy.

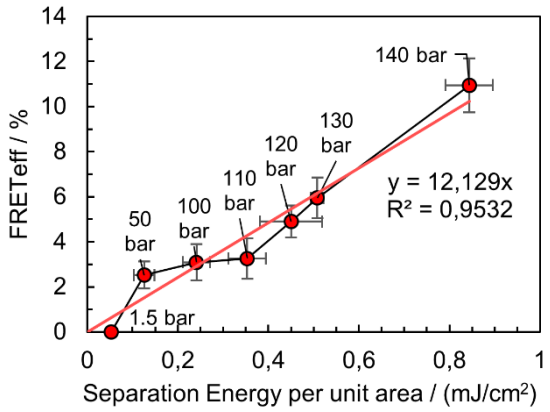

Figure 9 –FRETeff as a function of the adhesion (separation energy per unit area) between the Donor/Acceptor bonded nanolayer films pressed with 1.5 to 140 bar. Values are average ± 95 % confidence interval (n=3 for FRET efficiency, and n=4 for tensile force and separation energy). The high correlation confirms the relationship between the degree of NSC (represented by the adhesion) and the measured FRET signal (FRETeff).

CONCLUSIONS

In this work was presented a new FRET system based on dye-nanolayer films prepared by physical vapor deposition and developed for the measurement of NSC and its influence on adhesion. The dye-nanolayer films exhibit low roughness, uniform dye distribution, clear

fluorescence intensities, and a spectral overlap, suitable for FRET.

For the FRET experiments and tensile testing, the dye-nanolayer films were bonded with increasing pressure, to create different degrees of NSC and adhesion, corresponding to the applied load. The results showed that NSC measured by FRET and adhesion (separation energy per unit area) linearly increase with the employed pressure used to bond the dye-nanolayer films.

This validates the capacity of the new FRET system for measurement of the degree of NSC between solid materials and the reliable correlation that can be established between FRET and adhesion.

The key innovation of this experimental method is that it can, in principle, be applied to arbitrary surfaces of soft and hard materials. Functionalizing surfaces with FRET dye-nanolayers is an actively novel approach to study NSC using FRET spectroscopy. It can be applied on any sufficiently transparent substrate that can be used for the deposition of the Donor and Acceptor molecules. Or even, using other FRET pairs (low saturation pressure for PVD).

Our investigations provide a unique experimental approach for the measurement of NSC on large sample areas, particularly useful to study adhesion between solid materials that can be of interest in all fields of engineering, contact mechanics and tribology.

MATERIALS AND METHODS

pHema Thin Films Preparation. pHema (Sigma-Aldrich, Mw 20 000 Da, CAS:25249-16-5, USA) was dissolved to prepare a 10 % (m/v) ethanol/water-milliQ mixture 95:5 (v/v) solution. Then, 500 µL of pHema solution were doctor bladed over polyvinyl chloride substrates to form 1.5 µm thin films using a bar film applicator (3M BYK-Gardner GmbH, Geretsried, Germany) and left at room temperature for the evaporation of the solvents and consolidation of the films.

Donor and Acceptor Thin Films Preparation. The FRET pair (Figure 3A and 3B) of fluorescence molecules C120 (Sigma-Aldrich, CAS:26093-31-2, USA), and CDCF (Sigma-Aldrich, CAS:111843-78-8, Switzerland) were dissolved in ethanol to prepare 0.1 mM Donor and Acceptor (ratio of 1:1) solutions. Then, 100 µL of dye(s) solution was added to 500 µL of pHema solution (described before). The polymer-dye solutions were doctor bladed over polyvinyl chloride carrier substrates with a bar film applicator (3M BYK-Gardner GmbH, Geretsried, Germany) [17] to form 1.5 µm Donor and Acceptor thin films (Figure 2A). To protect the dyes from unwanted quenching mechanisms or any other kind of light degradation, the dye solutions and thin films were prepared and handled in the dark and later protected in aluminum foil during the entire process and experiments.

Dye-Nanolayer Film Preparation – Physical Vapor Deposition. Donor and Acceptor molecules were deposited individually on pHema, thin films in a custom-built PVD chamber. To deposit the dye nanolayer films, a vacuum chamber reactor equipped with a filament with temperature controller was utilized (Figure 4). The procedure was realized in four stages: (1) a pHema thin film was placed in the bottom of the reactor and a stainless-steel crucible, containing the dye (Donor or Acceptor) powder, positioned over the heating filament (Figure 4). (2) The PVD chamber was degassed overnight to reach high vacuum. (3) The next day, the chamber was closed in a batch configuration, meaning that after heating the crucible, the reactor was separated from the vacuum pump, and the filament was heated to vaporize the dye (Donor or Acceptor). (4) After the deposition time (Table 2) the heating was turned off, the chamber was opened and the dye-nanolayer film was collected (Figure 4). To protect the dyes from unwanted quenching mechanisms or any other kind of light degradation, the dyes powder and films were

prepared and handled in the dark and protected in aluminum foil.

Table 2 – PVD conditions used during the preparation of the dye nanolayer films.

Dye Molecule	Pressure (mtorr)	Time (h)	Temperature (ºC)	
			Substrate	Filament
C120	100	0.25	60	100
CDCF	100	6	60	120

Atomic Force Microscopy. The surface topography of the phema and dye-nanolayer films was investigated with AFM (Asylum Research MFP-3D, Santa Barbara, USA). The measurements were performed to scan 500 x 500 nm² topography images at ambient conditions (24°C and 45 % relative humidity). All measurements were obtained with Olympus AC 240 TS probes with a nominal tip radius of 7 nm and a cantilever spring constant of about 2 N/m. The open-source software Gwyddion was used to process the images (for all samples a second order polynomial background subtraction was performed) and determine the root mean square (RMS) roughness on at least three independent positions on each film.

Bonded Thin Films preparation. For FRET spectroscopy the bonding of the interface between the dye-nanolayer films was performed on 4 cm² of pure Donor (D), pure Acceptor (A) and/or pHema thin films without any dye (H), as demonstrated in Figure 7. The films were pressed at 1.5, 50, 100, 110, 120, 130 and 140 bar (hydraulic pressure PU30, V. Jessernigg & Urban, Graz, Austria) for 10 min.

FRET spectroscopy. Spectra measurements of bonded dye-nanolayer films (Figure 8) were recorded using a Fluorophotometer RF-5301PC (Shimadzu, Kyoto, Japan), at an excitation wavelength of 350 nm in a 45°/45° configuration as demonstrated in Figure 7.

FRET signals were detected from the bonded dye-nanolayer films and analyzed using Förster Theory[12]. The dye system presents a FRET working range distance that corresponds to $2R_0$ where R_0 is the Förster radius (nm). Following the instructions presented in the book FRET – Förster Resonance Energy Transfer: From Theory to Applications by Medintz and Hildebrandt (chapter 5, pages 106-122)[13], R_0 can be calculated via Eq. 1:

$$R_0 = \left(\frac{9\ln(10)\,k^2 QY_{\text{Donor}}\,J}{128\,\pi^5 N_A n^4}\right)^{1/6} \quad \text{(nm)} \qquad (1)$$

where N_A is Avogadro's constant (6.02 x 10^{20} $mmol^{-1}$), k^2 is the orientation factor (2/3), n is the refractive index (1.5 for the thin films), QY_{Donor} is the Donor quantum yield (measured by the absolute method, QY_{Donor} = 0.91) and J is the overlap integral calculated with Eq. 2:

$$J = \int f_D(\lambda)\,\epsilon_A(\lambda)\,\lambda^4\,d\lambda \ (\text{nm}^4.\text{M}^{-1}.\text{cm}^{-1}) \qquad (2)$$

where f_D is the area normalized fluorescence intensity of the Donor, ε_A is the attenuation coefficient of the Acceptor ($M^{-1}.cm^{-1}$) and λ is the wavelength (nm).

FRET efficiency (%) was calculated by the Acceptor Sensitization method[1] (Equation 3). It is the ratio of the Acceptor spectral intensity peak value in the presence (I_{AD}) and in the absence (I_A) of Donor (Figure 1).

To achieve appropriate FRET efficiency results, the direct luminescence of I_{AD} is subtracted from I_{AD}/I_A, and multiplied the correct luminescence ratio of the Acceptor and Donor molar attenuation coefficients (ε_A and ε_D) at the excitation wavelength used for the FRET experiments.

$$FRETeff = \left(\frac{I_{AD}-I_A}{I_A}\right)\left(\frac{\varepsilon_A}{\varepsilon_D}\right) \qquad (\%) \qquad (3)$$

The Donor and Acceptor molar attenuation coefficients (ε, $M^{-1}.cm^{-1}$) spectra are determined from the absorbance by Beer Lambert's Law (Eq. 4):

$$A = \varepsilon\, c\, l \qquad (4)$$

where A is the absorbance defined as the negative decadic logarithm of the measured transmittance, c is the concentration of the dye in the polymeric matrix (M) and l is the length of the light path, in this case, the thickness of the

thin films (cm). Pure Donor and pure Acceptor thin films absorbance was measured with a Varian Cary, UV-vis spectrophotometer (Agilent Technologies, California, USA). To minimize the inner filter effect and deviations from Beer-Lambert's law the optical density of the transmission measurements never exceeded 0.5 OD.

Thin film separation energy. Z-direction tensile tests were performed in a ZwickRoell Z010 multi-purpose tester (Georgia, USA) equipped with two steel bars, in which only the upper steel bar moves, driven by a linear motor. A double-sided adhesive tape is put on the upper and the lower steel bars. After the sample is placed on the lower steel bar, the linear motor moves the upper steel bar down until it touches the sample. To guarantee good attachment of the sample at the steel bars, a defined compression force of 1.5 bar is applied. Then, the sample is pulled apart in z-direction until it fails between the two polymer thin films. The force F with respect to the separation distance x is recorded. The two main values for interpreting the tensile tests are the maximum tensile force and the separation energy. The separation energy (J/cm^2) is the integral of the force-distance curves, divided by the bonded area of the thin films.

AUTHOR CONTRIBUTIONS

The manuscript was written through contributions of all authors. All authors have given approval to the final version of the manuscript.

FUNDING SOURCES

This research was funded by EU Horizon 2020 program under Marie Sklodowska-Curie Grant Agreement No. 764713, ITN Project FibreNet.

ACKNOWLEDGMENTS

The authors thank Caterina Czibula for the AFM measurements and image analysis.

REFERENCES

(1) Persson, B. N. J. On the Mechanism of Adhesion in Biological Systems. *J. Chem. Phys.* **2003**, *118* (16), 7614–7621. https://doi.org/10.1063/1.1562192.

(2) Busuttil, K.; Geoghegan, M.; Hunter, C. A.; Leggett, G. J. Contact Mechanics of Nanometer-Scale Molecular Contacts: Correlation between Adhesion, Friction, and Hydrogen Bond Thermodynamics. *J. Am. Chem. Soc.* **2011**, *133* (22), 8625–8632. https://doi.org/10.1021/ja2011143.

(3) Le Saux, G.; Wu, M. C.; Toledo, E.; Chen, Y. Q.; Fan, Y. J.; Kuo, J. C.; Schvartzman, M. Cell-Cell Adhesion-Driven Contact Guidance and Its Effect on Human Mesenchymal Stem Cell Differentiation. *ACS Appl. Mater. Interfaces* **2020**, *12* (20), 22399–22409. https://doi.org/10.1021/acsami.9b20939.

(4) Atkins, P.; de Paula, J. *Physical Chemistry for the Life Sciences*, 1st ed.; Oxford University Press: Oxford, 2006.

(5) Hirn, U.; Schennach, R. Comprehensive Analysis of Individual Pulp Fiber Bonds Quantifies the Mechanisms of Fiber Bonding in Paper. *Sci. Rep.* **2015**, *5* (July), 10503. https://doi.org/10.1038/srep10503.

(6) Gong, G.; Zhou, C.; Wu, J.; Jin, X.; Jiang, L. Nanofibrous Adhesion: The Twin of Gecko Adhesion. *ACS Nano* **2015**, *9* (4), 3721–3727. https://doi.org/10.1021/nn5063112.

(7) Yang, C.; Persson, B. N. J. Molecular Dynamics Study of Contact Mechanics: Contact Area and Interfacial Separation from Small to Full Contact. *Phys. Rev. Lett.* **2008**, *100* (2), 1–4. https://doi.org/10.1103/PhysRevLett.100.024303.

(8) Murphy, M. P.; Kim, S.; Sitti, M. Enhanced Adhesion by Gecko-Inspired Hierarchical Fibrillar Adhesives. *ACS Appl. Mater. Interfaces* **2009**, *1* (4), 849–855. https://doi.org/10.1021/am8002439.

(9) Ciavarella, M.; Joe, J.; Papangelo, A.; Barber, J. R. The Role of Adhesion in Contact Mechanics. *J. R. Soc. Interface* **2019**, *16* (151), 20180738. https://doi.org/http://dx.doi.org/10.1098/rsif.2018.0738.

(10) Simões, M. G.; Urstöger, G.; Schennach, R.; Hirn, U. Quantification and Imaging of Nanoscale Contact with Förster Resonance Energy Transfer. *ACS Appl. Mater. Interfaces* **2021**. https://doi.org/10.1021/acsami.1c04226.

(11) Sahoo, H. Förster Resonance Energy Transfer - A Spectroscopic Nanoruler: Principle and Applications. *J. Photochem. Photobiol. C Photochem. Rev.* **2011**, *12* (1), 20–30. https://doi.org/10.1016/j.jphotochemrev.2011.05.001.

(12) van der Meer, B. W. Förster Theory. In *FRET – Förster Resonance Energy Transfer*; John Wiley & Sons, Ltd, 2013; pp 23–62. https://doi.org/https://doi.org/10.1002/9783527656028.ch03.

(13) Hildebrandt, N. How to Apply FRET: From Experimental Design to Data Analysis. In *FRET – Förster Resonance Energy Transfer*; John Wiley & Sons, Ltd, 2013; pp 105–163. https://doi.org/https://doi.org/10.1002/9783527656028.ch05.

(14) Dexter, D. L. A Theory of Sensitized Luminescence in Solids. *J. Chem. Phys.* **1953**, *21* (5), 836–850. https://doi.org/10.1063/1.1699044.

(15) Persson, B. N. J.; Gorb, S. The Effect of Surface Roughness on the Adhesion of Elastic Plates with Application to Biological Systems. *J. Chem. Phys.* **2003**, *119* (21), 11437–11444. https://doi.org/10.1063/1.1621854.

(16) Benz, M.; Rosenberg, K. J.; Kramer, E. J.; Israelachvili, J. N. The Deformation and Adhesion of Randomly Rough and Patterned Surfaces. *J. Phys. Chem. B* **2006**, *110* (24), 11884–11893. https://doi.org/10.1021/jp0602880.

(17) Snell, N. E.; Rao, V. P.; Seckinger, K. M.; Liang, J.; Leser, J.; Mancini, A. E.; Rizzo, M. A. Homotransfer FRET Reporters for Live Cell Imaging. *Biosensors* **2018**, *8* (4). https://doi.org/10.3390/bios8040089.

(18) Christopoulos, T. K.; Diamandis, E. P. Chapter 14 - Fluorescence Immunoassays. In *Immunoassay*; Diamandis, E. P., Christopoulos, T. K., Eds.; Academic Press: San Diego, 1996; pp 309–335. https://doi.org/https://doi.org/10.1016/B978-012214730-2/50015-7.

(19) Shang, S. M.; Zeng, W. 4 - Conductive Nanofibres and Nanocoatings for Smart Textiles. In *Multidisciplinary Know-How for Smart-Textiles Developers*; Kirstein, T., Ed.; Woodhead Publishing Series in Textiles; Woodhead Publishing, 2013; pp 92–128. https://doi.org/https://doi.org/10.1533/9780857093530.1.92.

(20) Aliofkhazraei, M.; Ali, N. 7.04 - PVD Technology in Fabrication of Micro- and Nanostructured Coatings. In *Comprehensive Materials Processing*; Hashmi, S., Batalha, G. F., Van Tyne, C. J., Yilbas, B., Eds.; Elsevier: Oxford, 2014; pp 49–84. https://doi.org/https://doi.org/10.1016/B978-0-08-096532-1.00705-6.

(21) Danilov, D.; Hahn, H.; Gleiter, H.; Wenzel, W. Mechanisms of Nanoglass Ultrastability. *ACS Nano* **2016**, *10* (3), 3241–3247. https://doi.org/10.1021/acsnano.5b05897.

(22) Li, H.; Snow, P.; He, M.; Wang, P. I.; Wang, G. C.; Lu, T. M. Biaxially Textured Al Film Growth on CaF2 Nanostructures toward a Method of Preparing Single-Crystalline Si Film on Glass Substrates. *ACS Nano* **2010**, *4* (10), 5627–5632. https://doi.org/10.1021/nn1011978.

(23) Gong, C.; Huang, C.; Miller, J.; Cheng, L.; Hao, Y.; Cobden, D.; Kim, J.; Ruoff, R. S.; Wallace, R. M.; Cho, K.; Xu, X.; Chabal, Y. J. Metal Contacts on Physical Vapor Deposited Monolayer MoS2. *ACS Nano* **2013**, *7* (12), 11350–11357. https://doi.org/10.1021/nn4052138.

(24) Azizi, S.; Gholivand, M. B.; Amiri, M.; Manouchehri, I. DNA Biosensor Based on Surface Modification of ITO by Physical Vapor Deposition of Gold and Carbon Quantum Dots Modified with Neutral Red as an Electrochemical Redox Probe. *Microchem. J.* **2020**, *159* (September), 105523. https://doi.org/10.1016/j.microc.2020.105523.

(25) Urstöger, G.; Steinegger, A.; Schennach, R.; Hirn, U. Spectroscopic Investigation of DCCH and FTSC as a Potential Pair for Förster Resonance Energy Transfer in Different Solvents. *PLoS One* **2020**, *15* (2), 1–13. https://doi.org/10.1371/journal.pone.0228543.

(26) Medintz, I.; Hildebrandt, N. *FRET - Föster Resonace Energy Tranfer: From Theory to Applications*, 1st ed.; Medintz, I., Hildebrandt, N., Eds.; WILEY-VCH Verlag: Weinheim, Germany, 2014.

(27) Urstöger, G.; Simoes, M. G.; Steinegger, A.; Schennach, R.; Hirn, U. Evaluating the Degree of Molecular Contact between Cellulose Fiber Surfaces Using FRET Microscopy. *Cellulose* **2019**, *0123456789*, 7037–7050. https://doi.org/10.1007/s10570-019-02575-x.

SUPLEMENTARY INFORMATION

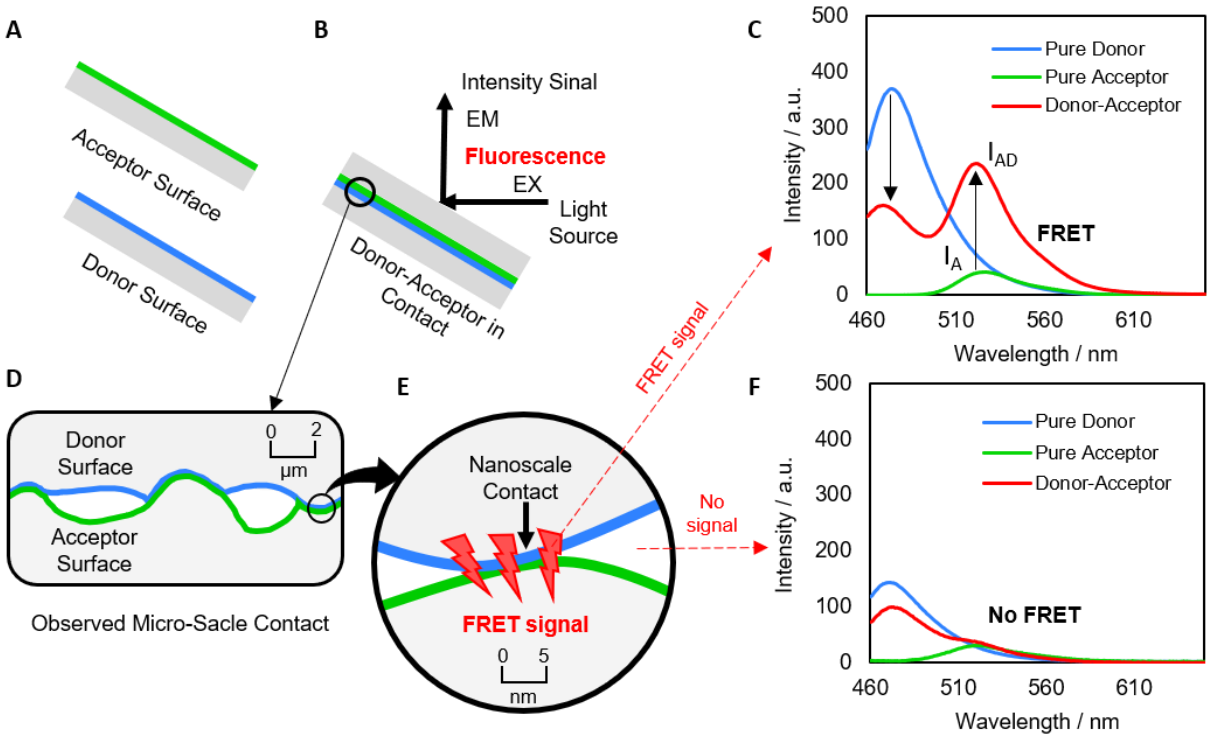

Figure S1 - FRET spectroscopy applied to surfaces in NSC: (A) Donor and Acceptor surfaces; (B) Donor and Acceptor surfaces in NSC; (C) FRET signal with the pure Donor, Acceptor, and Donor−Acceptor in NSC fluorescence spectra, where Donor intensity drops and Acceptor intensity rises (from I_A to I_{AD}, see arrows) due to the Donor-Acceptor energy transfer; (D) Donor and Acceptor surfaces in contact analyzed at micro- and (E) nanometer scales; (F) No FRET signal for areas above the FRET distance range of the system.

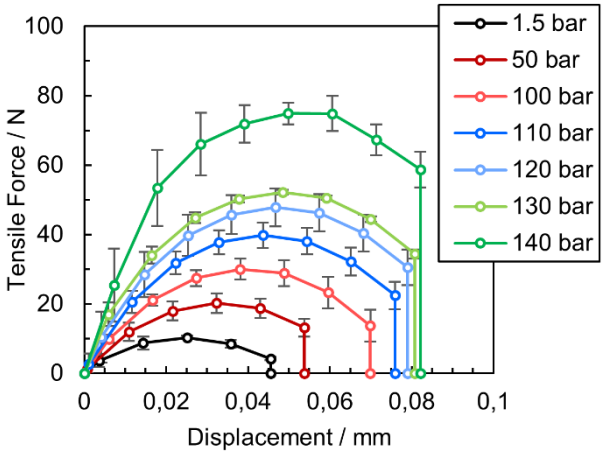

Figure S2 - Z-direction force-displacement curves of the Donor/Acceptor bonded nanolayer films pressed with 1.5 to 140 bar. Values are average ± 95 % confidence interval (n=3 for FRET efficiency, and n=4 for tensile force and separation energy).